— OSU-DOE-ER-01545-562

76

OSU DOE/ER-01545-562

# Bound state problem in light-front Tamm-Dancoff: A numerical study in 1+1 dimensions

ROUTE TO
NAME | LOCATION
RETURN TO FERMI LIBRARY

A. HARINDRANATH and Robert J. PERRY
Department of Physics
The Ohio State University
Columbus, OH 43210

J. SHIGEMITSU†
Physics Department, Boston University
590 Commonwealth Avenue
Boston, MA 02215
and
DESY, Theory Group
Notkestrasse 85
D-2000, Hamburg 52, Germany

FERMILAB
AUG 26 1991
LIBRARY

## ABSTRACT

Numerical solutions to the two-fermion bound state problem in the 1+1 dimensional Yukawa model are presented within the lowest order light-front Tamm-Dancoff approximation (*i.e.*, keeping only two-fermion and two- fermion/one-boson sectors). Our motivation is twofold: First, we want to understand the dynamics of the model from the very weak coupling domain where the system is governed by non-relativistic dynamics to moderate and strong coupling domains where retardation and self-energy effects become important. Second, we want to develop techniques for solving coupled Tamm-Dancoff integral equations, in particular methods that can be generalized to higher order Tamm-Dancoff approximations and/or higher dimensional theories. To achieve the first goal we first simplify the problem considerably (from a numerical point of view) by the explicit elimination of the higher Fock space sector. The resulting integral equation, whose kernel depends upon the invariant mass of the state, is solved for the coupling constant, for a given set of the invariant mass and fermion and boson mass parameters. To achieve the second goal we solve the coupled set of equations using both basis functions and direct discretization techniques. Results from these more general techniques are compared with the explicit elimination method.

August 12, 1991

† On sabbatical leave from The Ohio State University

## I. INTRODUCTION

The Light-Front Tamm-Dancoff (LFTD) approach[1,2] has been proposed recently to study relativistic bound state problems in both nuclear and particle physics. The main features of this approach are a) quantizing the theory on the light-front rather than the conventional equal-time surface, b) constructing a Fock space built on the bare vacuum state which is an *exact* eigenstate of the full light-front Hamiltonian, c) expanding the physical state under consideration in terms of bare states and truncating the expansion at some level, d) deriving coupled integral equations for the expansion coefficients which are the multi-particle amplitudes, e) carrying out renormalizations appropriate for the limited Fock space, and f) solving the coupled integral equations for the eigenvalues and eigenfunctions of the mass operator.

The Fock space truncation is forced upon us by practical considerations (unless one can find analytical solutions to the full set of coupled operator equations). This has nontrivial consequences for the renormalization program of the LFTD approach[2]. In theories where the constituents appear as physical particles in asymptotic states, we need to insure the appropriate threshold conditions on multi-particle amplitudes. This can be achieved by the introduction of *sector dependent* counterterms in the light-front Hamiltonian. It is worthwhile to emphasize that the introduction of counterterms is necessary whether or not the system of equations contains divergences.

We consider the bound state problem of two non-identical equal mass fermions in the two-dimensional Yukawa model presented in Ref. 2. Previously, Brooks and Frautschi[3], and Pauli and Brodsky[4] have investigated the two-dimensional Yukawa model using numerical methods. Brooks and Frautschi used a momentum space lattice in equal-time quantization whereas Pauli and Brodsky used a momentum space lattice in light-front quantization (Discretized Light Cone Quantization or DLCQ).

We have two main objectives. First, we wish to study the dynamics of the model for the entire range of couplings and mass parameters. Second, we want to develop and test methods that are more easily generalized to higher order Tamm-Dancoff approximations and/or higher dimensional theories. Note that the reliability of the Tamm-Dancoff approximation itself is not central to this work.

Our starting point is the coupled set of equations for the two-fermion and two-fermion, one-boson amplitudes. To achieve the first goal, it is most efficient numerically to eliminate the three particle amplitude in terms of the two-particle amplitude and arrive at an integral equation for the two-particle amplitude. The kernel of this equation depends on the eigenvalue $M^2$. We convert this integral equation into a matrix equation via Gauss-Legendre quadrature and solve for the coupling constant for a given value of the invariant mass. We investigate the weak-coupling limit and the effect of self-energies in the strong coupling domain.

Once we have a quantitative picture of the dynamics we return to the coupled integral equations to carry out our second objective. When we include higher Fock sectors it will not be possible to eliminate the higher Fock sectors analytically and arrive at an effective equation for the lowest sector. Hence for the very success of the LFTD program it is extremely important to develop various numerical methods to solve coupled integral equations. In this initial investigation, we employ two methods: a) expansion in basis

functions and b) direct discretization. In method a) a 'Basis Function' subtraction scheme is developed to handle the renormalization program while in method b) one must employ a subtraction scheme that depends on the discretization. We investigate merits and weaknesses of the two techniques.

The plan of this paper is as follows. In Section II we present the bound state spectrum and wave functions found by the explicit elimination method. The basis function method is presented in Section III. Section IV deals with the direct discretization method. Our conclusions are presented in Section V. Appendix A deals with the analytic solution of the Schrödinger equation for the Yukawa potential in one dimension.

## II. EXPLICIT ELIMINATION METHOD

The two dimensional Yukawa model under investigation is characterized by the Lagrangian density;

$$\begin{aligned} L = & \frac{1}{2}\partial_\mu\phi\,\partial^\mu\phi - \frac{m_B^2}{2}\phi^2 \\ & + \sum_j \bar{\psi}_j\,(i\gamma^\mu\partial_\mu - m_j)\,\psi_j - \lambda\,\phi\,\sum_j \bar{\psi}_j\,\psi_j \end{aligned} \tag{2.1}$$

where $\sum_j$ is over different fermion types. Light-front quantization of this Lagrangian and the derivation of the light-front Hamiltonian $P^-$ has been discussed for instance in reference 2. Here we only write down the simplified Hamiltonian relevant for our two-fermion bound state problem. It is given by

$$P^- = P^-_{free} \quad + P^-_{int} \quad , \tag{2.2}$$

where

$$\begin{aligned} P^-_{free} = & \int_0^\infty \frac{dk}{2\pi k}\,\frac{1}{2k} \\ & \Big[b^\dagger(k)b(k)(m_f^2 + \frac{\lambda^2}{4\pi}\beta(k)) \;+ B^\dagger(k)B(k)(M_F^2 + \frac{\lambda^2}{4\pi}\beta(k)) + \frac{1}{2}m_B^2 a^\dagger(k)a(k)\Big] \;, \end{aligned} \tag{2.3a}$$

$$\begin{aligned} P^-_{int} = & \frac{\lambda}{4\pi}\int_0^\infty \frac{dk_1}{k_1}\int_0^\infty \frac{dk_2}{2\pi 2k_2}\int_0^\infty \frac{dk_3}{k_3}\delta(k_1 - k_2 - k_3) \\ & \Big[b^\dagger(k_1)b(k_3)a(k_2)\;\; \bar{u}(k_1)u(k_3) + b^\dagger(k_3)b(k_1)a^\dagger(k_2)\;\; \bar{u}(k_3)u(k_1) \\ & + B^\dagger(k_1)B(k_3)a(k_2)\;\; \bar{U}(k_1)U(k_3) \\ & + B^\dagger(k_3)B(k_1)a^\dagger(k_2)\;\; \bar{U}(k_3)U(k_1)\Big] \;. \end{aligned} \tag{2.3b}$$

The self-inertia

$$\beta(k) = \mathcal{P}\;\int_0^\infty \frac{dk_1}{k_1}\;\frac{k}{k-k_1} \tag{2.4}$$

with $\mathcal{P}$ being the principal value. Here $m_1 = m_f$ and $m_2 = M_F$ are the fermion masses, $m_B$ is the boson mass and $\lambda$ is the coupling constant. The fermion and boson creation and annihilation operators obey the quantization conditions

$$\begin{aligned}
\{b(k_1), b^\dagger(k_2)\} &= 2\pi k_1 \ \ \delta(k_1 - k_2) \ , \\
\{B(k_1), B^\dagger(k_2)\} &= 2\pi k_1 \ \ \delta(k_1 - k_2) \ , \\
[a(k_1), a^\dagger(k_2)] &= 2\pi 2k_1 \ \ \delta(k_1 - k_2) \ .
\end{aligned}$$

We choose the spinor normalization so that

$$\bar{u}(k_1)\, u(k_2) = m_f \frac{k_1 + k_2}{\sqrt{k_1 k_2}} \ , \bar{U}(k_1)\, U(k_2) = M_F \frac{k_1 + k_2}{\sqrt{k_1 k_2}} \ .$$

The fermion number 2 state $\mid \Psi >$ is expanded as

$$\begin{aligned}
&\mid \Psi(P) > = \\
&\int \frac{dk_1}{\sqrt{2\pi k_1}} \int \frac{dk_2}{\sqrt{2\pi k_2}} \phi_2(k_1, k_2) b^\dagger(k_1) B^\dagger(k_2) \mid 0 > \delta(P - k_1 - k_2) \ + \\
&\int \frac{dk_1}{\sqrt{2\pi k_1}} \int \frac{dk_2}{\sqrt{2\pi k_2}} \int \frac{dk_3}{\sqrt{2\pi 2k_3}} \phi_3(k_1, k_2, k_3) b^\dagger(k_1) B^\dagger(k_2) a^\dagger(k_3) \mid 0 > \delta(P - k_1 - k_2 - k_3)
\end{aligned} \tag{2.5}$$

in the first Tamm-Dancoff approximation, where $\phi_2$ is the two-particle amplitude and $\phi_3$ is the three particle amplitude. Introduce the amplitudes

$$\phi_2(k_1, k_2) \to \phi_2(k_1) \to \psi_2(x) \ , \qquad \text{with} \quad x = \frac{k_1}{P} \ ,$$

and

$$\phi_3(k_1, k_2, k_3) \to \phi_3(k_1, k_2) \to \psi_3(x, y) \ , \qquad \text{with} \quad x = \frac{k_1}{P}, \ \ y = \frac{k_2}{P},$$

since momentum conservation implies $k_1 + k_2 = P$, $k_1 + k_2 + k_3 = P$. By projecting the equation of motion

$$2P^+ P^- \mid \Psi >= M^2 \mid \Psi > \tag{2.6}$$

on to a set of free states we arrive at the coupled system of equations :

$$\begin{aligned}
M^2 \ \psi_2(x) = &\left( (\frac{m_f^2}{x} + \frac{M_F^2}{1-x}) \ + \ C.T. \right) \ \ \psi_2(x) \\
&+ g M_F \int_{y_{min}}^{y_{max}} dy \, \frac{\psi_3(x, y)}{\sqrt{1 - x - y}} \, (\frac{1}{1-x} + \frac{1}{y}) \Theta(1 - x - y) \\
&+ g m_f \int_{y_{min}}^{y_{max}} dy \, \frac{\psi_3(1-y, 1-x)}{\sqrt{x + y - 1}} \, (\frac{1}{x} + \frac{1}{1-y}) \Theta(x + y - 1) \ ,
\end{aligned}$$

$$(2.7a)$$

$$M^2\psi_3(x,y) = \left(\frac{m_f^2}{x} + \frac{M_F^2}{y} + \frac{m_B^2}{1-x-y}\right)\psi_3(x,y)$$
$$+ gM_F\frac{1}{\sqrt{1-x-y}}\left(\frac{1}{y} + \frac{1}{1-x}\right)\psi_2(x)$$
$$+ gm_f\frac{1}{\sqrt{1-x-y}}\left(\frac{1}{x} + \frac{1}{1-y}\right)\psi_2(1-y) \ . \qquad (2.7b)$$

Here $g = \frac{\lambda}{\sqrt{4\pi}}$ , $C.T.$ denotes the counterterms and $x$ and $y$ are light-front momentum fractions. Note that we have absorbed the self-inertias into the counterterms in this expression.

Normalization requires

$$\int_0^1 dx\ \psi_2^2(x) \ + \ \int_0^1 dx \int_0^1 dy\ \theta(1-x-y)\psi_3^2(x,y) \ = 1 \ . \qquad (2.8)$$

It is worthwhile to make one observation before we proceed. There is an instantaneous interaction term in the light-front Hamiltonian (Ref. 2), which connects $\psi_3$ to itself via an integral operator. Such terms, which are absent in the equal-time Hamiltonian, arise in the light-front formulation as a result of the elimination of constrained variables. This contribution may or may not be included in the lowest order approximation. However, if we include this interaction, the explicit elimination of $\psi_3$ becomes impossible and we must solve the explicit $\psi_2$ plus $\psi_3$ problem to find the spectrum and wavefunctions. Since our major motivation here is to develop and critically evaluate methods for the coupled problem, we found it useful to have the solutions in an independent and numerically much simpler method. This is a major reason for dropping the contribution from the instantaneous term. There is no reason to keep or drop it at this order of LFTD. We mention that the system of equations is covariant, whether we keep the contribution from the instantaneous interaction or not. Thus even after the Tamm-Dancoff truncation we have a covariant equation.

Below boson production threshold, equation (2.7b) is used to eliminate $\psi_3$ from equation (2.7a) and we arrive at an integral equation for $\psi_2$ where the kernel depends on the eigenvalue $M^2$:

$$M^2\ \psi_2(x) = \left(\left(\frac{m_f^2}{x} + \frac{M_F^2}{1-x}\right) + C.T.\right)\psi_2(x)$$
$$+ g^2 m_f M_F \int_\epsilon^{x-\epsilon} \frac{dy}{x-y}\psi_2(y)\frac{\left(\frac{1}{x}+\frac{1}{y}\right)\left(\frac{1}{1-x}+\frac{1}{1-y}\right)}{M^2 - \frac{m_f^2}{y} - \frac{M_F^2}{1-x} - \frac{m_B^2}{x-y}}$$
$$+ g^2 m_f M_F \int_\epsilon^{1-x-\epsilon} \frac{dy}{1-x-y}\psi_2(1-y)\frac{\left(\frac{1}{1-x}+\frac{1}{y}\right)\left(\frac{1}{x}+\frac{1}{1-y}\right)}{M^2 - \frac{m_f^2}{x} - \frac{M_F^2}{y} - \frac{m_B^2}{1-x-y}}$$

$$+ g^2 m_f^2 \ \psi_2(x) \int_{\epsilon}^{x-\epsilon} \frac{dy}{x-y} \frac{(\frac{1}{x}+\frac{1}{y})^2}{M^2 - \frac{m_f^2}{y} - \frac{M_F^2}{1-x} - \frac{m_B^2}{x-y}}$$

$$+ g^2 M_F^2 \ \psi_2(x) \int_{\epsilon}^{1-x-\epsilon} \frac{dy}{1-x-y} \frac{(\frac{1}{1-x}+\frac{1}{y})^2}{M^2 - \frac{m_f^2}{x} - \frac{M_F^2}{y} - \frac{m_B^2}{1-x-y}}. \tag{2.9}$$

Here the second and third terms on the right-hand side of the equation represent one-boson exchange, and the fourth and fifth terms represent self-mass correction. We have introduced a cutoff $\epsilon$ on the loop variable $y$. Note that in the limit $\epsilon \to 0$ boson exchange terms are finite but self-mass correction terms diverge like $log\ \epsilon$.

Next we specify the counterterms. They are fixed by the renormalization condition that above the scattering threshold, free asymptotic fermions should propagate with their physical masses. This threshold is given by the zeroes of the complete coefficient of $\psi_2$; *i.e.*, above threshold

$$M^2 = \frac{m_f^2}{\chi} + \frac{M_F^2}{1-\chi}. \tag{2.10}$$

The counterterms are then given by

$$C.T. =$$

$$g^2 \frac{m_f^2}{x} \int_{\epsilon}^{x-\epsilon} \frac{dy}{y} \frac{(x+y)^2}{m_f^2(x-y)^2 + m_B^2 xy}$$

$$+ g^2 \frac{M_F^2}{1-x} \int_{\epsilon}^{1-x-\epsilon} dy \leq very \frac{(1-x+y)^2}{M_F^2(1-x-y)^2 + m_B^2(1-x)y}. \tag{2.11}$$

Note that the counterterms also diverge like $log\ \epsilon$ as $\epsilon \to 0$, which cancels the $log\ \epsilon$ divergence of self-mass correction terms.

We now proceed to the analysis of the renormalized two-body bound state equation given by equation (2.9) along with equation (2.11). For simplicity we set the two fermion masses to be equal. All dimensionful quantities, $M$, $m_B$ and $g$ are measured in units of the fermion mass. To begin the process of building physical intuition in terms of light-front variables and LFTD we start with the weak binding limit. It is shown in Ref. 2 that in the extreme weak-coupling limit (binding energy $\bar{B} << m_F$) the above equation reduces to the momentum space Schrödinger equation with a Yukawa potential. Next we drop the self-mass corrections and counterterms from equation (2.9) and analyze the resulting equation, which is called the light-front ladder approximation. This provides a quantitative

picture of the effects of retardation and relativistic kinematics. Finally we study the full equation (2.9) without further approximations. Using the counterterm of equation (2.11), self-mass corrections are now taken into account.

### A. Schrödinger equation

In the limit of extremely weak coupling, the integral equation reduces to the Schrödinger equation in momentum space[2]

$$[q^2/m_F + \bar{B}]\psi(q) = \frac{\lambda^2}{2\pi}\int_{-\infty}^{+\infty} dq' \frac{\psi(q')}{(q-q')^2 + m_B^2} \quad . \tag{2.12}$$

Here $q$ is the relative momentum. In light-front variables, this equation is

$$[\frac{m_f^2}{x(1-x)} - M^2]\psi(x) = \frac{\lambda^2}{2\pi}\int_0^1 \frac{dy}{(y(1-y))^{3/2}}\psi(y)\frac{1}{m_f^2[\frac{2x-1}{\sqrt{4x(1-x)}} - \frac{2y-1}{\sqrt{4y(1-y)}}]^2 + m_B^2} \quad . \tag{2.13}$$

Here the variable $x$ is the light-front momentum fraction. The variables $x$ and $q$ are related by $x = \frac{1}{2}(1 - \frac{q}{\sqrt{m_f^2+q^2}})$. The analytic solution to equation (2.12) in coordinate space is given in Appendix A. We also solved equations (2.12) and (2.13) numerically via Gauss-Legendre quadrature. We studied the solutions for three values of the boson mass squared: $m_B^2 = 0.05, 0.5$, and 3.5. The invariant mass of the lowest bound state ($M^2 = 4m_F[m_F - \bar{B}]$) for the three choices of boson masses are given in Fig. 1. We note that the invariant mass of the bound state approaches zero faster, the smaller the boson mass. Of course, the solution of the Schrödinger equation is not to be trusted when the invariant mass deviates considerably from the threshold value (in the present case $4m_F^2$). For a given value of the coupling constant, the number of bound states increases as the boson mass decreases. The ground state wavefunction for $m_B^2 = .5$ obtained from the solution of equation (2.13) is plotted in Fig. 2 for $g = .1$ and $g = .4$. For weak coupling the wavefunction is strongly peaked about light-front momentum fraction $x \approx \frac{1}{2}$ but as the coupling strengthens, medium to high momentum components build up indicating a possible breakdown of the non-relativistic approximation. To get a quantitative picture of this breakdown, we turn to the study of relativistic effects.

### B. Light-front ladder approximation

We start from equations (2.9) and (2.11) and drop self-mass corrections and counterterms. The resulting equation is called the light-front ladder approximation, or LFLA. Here one takes into account relativistic kinematic corrections and retardation effects (indicated by the presence of the invariant mass $M^2$ in the kernel). The equation was discretized using Gauss-Legendre quadrature. We have solved this equation to find the coupling constant for each given value of $M^2$, for boson masses $m_B^2 = 0.05, 0.5$, and 3.5. The convergence of results with respect to the order of the quadrature was found to be slower as the boson mass became lighter. In all cases the relativistic effects are found to be repulsive, *i.e.*, for a given value of the invariant mass LFLA requires a larger coupling constant compared

to the Schrödinger equation. In this case also the invariant mass decreases and eventually becomes negative as the coupling strength increases (see Fig. 3).

Once again the question is in what domain of the coupling constant can one trust the results. To get a quantitative picture we return to equations (2.9) and (2.11).

### C. Lowest order Light-Front Tamm-Dancoff: Explicit elimination

Once we include the self-mass effects, the renormalized equation which we call first light-front Tamm-Dancoff, or FLFTD has the same structure as LFLA. Hence we again solve for the coupling constant for various values of mass parameters after discretization via Gauss-Legendre quadrature. In Figs. 3a, 3b and 3c we present the invariant mass versus the coupling constant for Schrödinger equation, LFLA, and FLFTD.

We observe that the three approximations are fairly close to each other in the weak coupling domain. In the strong coupling domain two effects are observed. First, the self-mass effects are more repulsive than retardation effects. Second, the invariant mass initially decreases but eventually becomes independent of the coupling constant as the coupling constant increases. It can be shown that after the introduction of counterterms, the eigenvalue $M^2$ depends only on an effective coupling constant $\tilde{g}^2 = f(g^2)$ where $f(g^2)$ approaches an invariant function of momentum fractions as $g$ becomes large.

The two-particle amplitude $\psi_2$ of the ground state is presented in Figs. 4a, 4b and 4c. The spread of $\psi_2$ as the coupling increases is clearly visible.

Although we are analyzing a covariant approximation to the full Tamm-Dancoff problem, the question arises concerning the reliability of the lowest order approximation. An obvious method is to include higher Fock space states and study the convergence of the invariant mass. An alternative is however available in the present approximation scheme. The explicit elimination method gives us the two particle piece $\psi_2$ of the full state $\psi$. Since we know the invariant mass of this state and the coupling constant we can utilize equation (2.7b) to explicitly calculate the three particle amplitude $\mid \psi_3 >$. By normalizing the full state $\mid \Psi >$ we evaluate the contributions to the norm, NORM2 and NORM3, from the two-particle and three-particle states respectively; *i.e.,*

$$NORM2 = \int_0^1 dx \quad \mid \psi_2(x) \mid^2 \quad , \tag{2.14}$$

and

$$NORM3 = \int_0^1 dx \int_0^{1-x} dy \quad \mid \psi_3(x,y) \mid^2 \quad . \tag{2.15}$$

We plot these norms versus the coupling constant in Figs. 5a, 5b, and 5c. We can probably trust the lowest order approximation only in the region where NORM2 > NORM3. From the figures it is clear that the region where the self-mass effects become important is also the region where the approximation (*i.e.,* the truncation of Fock space to the lowest two sectors) starts to break down. Thus in the strong coupling region, even though the invariant mass stabilizes, (*i.e.,* becomes independent of the coupling strength), the state is mainly a three-particle state. Thus the lowest order approximation is questionable in the region where the self-mass corrections become important. In the present work, however,

this is of little concern to us since our major motivation is to develop techniques for solving coupled integral equations.

## III. SOLVING THE COUPLED TAMM-DANCOFF EQUATIONS USING BASIS FUNCTIONS

In the previous section the coupled Tamm-Dancoff equations, equations (2.7a) and (2.7b), were analyzed by first eliminating the three-particle wave function $\psi_3$ in the second equation and plugging back into the first equation for $\psi_2$. In this way the full solution to lowest order Tamm-Dancoff in the charge two sector was obtained. In this and the next section we experiment with other methods for solving equations (2.7a) and (2.7b). In particular, we will retain both $\psi_3$ and $\psi_2$ and reduce the problem to a linear eigenvalue problem for $M^2$. The main goal here is to develop methods that are more easily generalized to higher order Tamm-Dancoff and/or higher dimensional theories. One must keep in mind that it will not always be possible to eliminate all but one of the amplitudes and end up with a single integral equation such as equation (2.9). In fact, in general it is not even possible to eliminate one amplitude. We will have to learn to work directly with the coupled equations. In this section we discuss a method in which both $\psi_2$ and $\psi_3$ are expanded in terms of basis functions. In the next section we report on results obtained by direct discretization of equation (2.7). Since in this simple 1+1 dimensional model results obtained via other methods (e.g. from the previous section) are available, we have an ideal laboratory in which to gain familiarity with and test these more general approaches.

Basis functions have been used for several decades in quantum chemistry to solve many-body Schrödinger equations[5]. The wavefunctions are expanded in terms of a finite number of basis functions (e.g. Gaussians) and one ends up with a finite matrix diagonalization problem. One important objective of the present work is to investigate whether basis functions can also be applied to the Tamm-Dancoff equations. A major difference between quantum chemistry and the current field theory applications is that the latter involves renormalization and the elimination of infinities via counterterms. Can renormalization be implemented with only a small number of basis functions ? We have expended considerable time trying to come up with a practical renormalization scheme within the context of using basis functions and a finite matrix representation of complex field theoretic bound state equations.

There is a wide range of different basis sets that one could contemplate testing. Given that there is almost no data on basis functions in field theory, we decided to rely initially on the experience of quantum chemists and try Gaussians. We have also worked with sines, a basis set that has the advantage that all integrals can be carried out analytically. Generically, the amplitudes $\psi_2$ and $\psi_3$ are represented as;

$$\psi_2(x) = \sum_i a_i h_i(x) \ , \tag{3.1a}$$

$$\begin{aligned} \psi_3(x,y) &= \sum_k b_k F_k(x,y) \\ &= \sum_{(ij)} b_{(ij)} \phi_i(x) \phi_j(y) \ , \end{aligned} \tag{3.1b}$$

with

$$h_k(x) \;\; or \;\; \phi_k(x) = exp[-u_k(x-v_k)^2] \;\; , \tag{3.2a}$$

or

$$h_k(x) \;\; or \;\; \phi_k(x) = sin(k\pi x) \;\; . \tag{3.2b}$$

Note that we do not require our basis functions to form an orthonormal set; however, we do require that the three-body basis functions be products.

After inserting the above expansion into (2.7), one has;

$$\begin{aligned} M^2 \sum_j a_j h_j(x) = \sum_j a_j \left( \frac{m_f^2}{x} + \frac{M_F^2}{1-x} + \; C.T. \right) h_j(x) \\ + gM_F \sum_{(ij)} b_{(ij)} \int_{y_{min}}^{y_{max}} dy \, \frac{\phi_i(x)\phi_j(y)}{\sqrt{1-x-y}} \left(\frac{1}{1-x} + \frac{1}{y}\right) \Theta(1-x-y) \\ + gm_f \sum_{(ij)} b_{(ij)} \int_{y_{min}}^{y_{max}} dy \, \frac{\phi_i(1-y)\phi_j(1-x)}{\sqrt{x+y-1}} \left(\frac{1}{x} + \frac{1}{1-y}\right) \Theta(x+y-1) \;\; , \end{aligned} \tag{3.3a}$$

$$\begin{aligned} M^2 \sum_{(ij)} b_{(ij)} \phi_i(x)\phi_j(y) = \sum_{(ij)} b_{(ij)} \left(\frac{m_f^2}{x} + \frac{M_F^2}{y} + \frac{m_B^2}{1-x-y}\right) \phi_i(x)\phi_j(y) \\ + gM_F \sum_j a_j \frac{1}{\sqrt{1-x-y}} \left(\frac{1}{y} + \frac{1}{1-x}\right) h_j(x) \\ + gm_f \sum_j a_j \frac{1}{\sqrt{1-x-y}} \left(\frac{1}{x} + \frac{1}{1-y}\right) h_j(1-y) \;\; . \end{aligned} \tag{3.3b}$$

We have left the counterterm (C.T.) unspecified for the time being.
To convert equation (3.3) into a matrix equation one operates with $\int dx \, h_k(x)$ on (3.3a) and with $\int dx \int dy \, \Theta(1-x-y) \, \phi_k(x)\phi_l(y)$ on (3.3b) . Suppose one uses $N_2$ basis functions for $\psi_2$ and $N_3$ total number of products for $\psi_3$ ($N_3 = n_3 \times n_3$, where the indices i and j in (3.1b) run from 1 to $n_3$). One then ends up with matrices of size $N \times N$ , where $N = N_2 + N_3$ . The eigenvalue equation becomes

$$M^2 \sum_{b=1}^{N} A_{ab} X_b = \sum_{b=1}^{N} (B + B^{C.T.})_{ab} X_b \;\; , \tag{3.4}$$

where $X_b = a_j$ or $b_{(ij)}$. When $1 \leq a, b \leq N_2$ , we have

$$A_{ab} = \int_0^1 dx\, h_a(x) h_b(x) \ , \tag{3.5a}$$

$$B_{ab} = \int_\epsilon^{1-\epsilon} dx\, h_a(x) \left(\frac{m_f^2}{x} + \frac{M_F^2}{1-x}\right) h_b(x) \ , \tag{3.5b}$$

$$B_{ab}^{(C.T.)} = \int_\epsilon^{1-\epsilon} dx\, h_a(x) \, (C.T.) \, h_b(x) \ . \tag{3.5c}$$

When $N_2 + 1 \leq a, b \leq N$ and $a \simeq (kl) \rightarrow (k_a l_a)$ , $b \simeq (ij) \rightarrow (i_b j_b)$ we have

$$A_{ab} = \int_0^1 dx \int_0^1 dy\, \Theta(1-x-y) \phi_{k_a}(x) \phi_{l_a}(y) \phi_{i_b}(x) \phi_{j_b}(y) \ , \tag{3.6a}$$

$$B_{ab} = \int_{x_{min}}^{x_{max}} dx \int_{y_{min}}^{y_{max}} dy\, \Theta(1-x-y)$$
$$\phi_{k_a}(x) \phi_{l_a}(y) \left(\frac{m_f^2}{x} + \frac{M_F^2}{y} + \frac{m_B^2}{1-x-y}\right) \phi_{i_b}(x) \phi_{j_b}(y) \ . \tag{3.6b}$$

When $1 \leq a \leq N_2$ and $N_2 + 1 \leq b \leq N$ , we have

$$B_{ab} = C_{ab}^{(1)} + C_{ab}^{(2)} \ , \tag{3.7}$$

$$C_{ab}^{(1)} = g\, M_F \int_{x_{min}}^{x_{max}} dx \int_{y_{min}}^{y_{max}} dy\, \Theta(1-x-y) \frac{h_a(x)}{\sqrt{1-x-y}} \left(\frac{1}{1-x} + \frac{1}{y}\right) \phi_{i_b}(x) \phi_{j_b}(y) \ , \tag{3.8a}$$

$$C_{ab}^{(2)} = g\, m_f \int_{x_{min}}^{x_{max}} dx \int_{y_{min}}^{y_{max}} dy\, \Theta(x+y-1) \frac{h_a(x)}{\sqrt{x+y-1}} \left(\frac{1}{x} + \frac{1}{1-y}\right) \phi_{i_b}(1-y) \phi_{j_b}(1-x) \ . \tag{3.8b}$$

Finally, for $N_2 + 1 \leq a \leq N$ and $1 \leq b \leq N_2$, we use

$$B_{ab} = B_{ba} \ . \tag{3.9}$$

All other matrix elements vanish. In principle, one now just has to carry out the integrals in equations (3.5) through (3.8) to evaluate all matrix elements and then diagonalize to obtain eigenvalues and eigenfunctions. There are however some subtle points that need to be emphasized. First of all one must choose the limits of integration carefully, so that not only the $\Theta$-function constraints are satisfied, but also so that singularities of the integrands are avoided. For instance, in (3.5b) and (3.5c) $\epsilon$'s have already been inserted to avoid end-point singularities at $x = 0$ and $x = 1$. The dependence on this type of $\epsilon$ disappears in the final answers for eigenvalues, since upon diagonalization the bound state wave functions are such that they vanish around $x = 0$ and $x = 1$. For sine basis functions (equation (3.2b)) expressions such as $h_j(x)/x$ are also finite everywhere from the beginning. However, for Gaussian basis functions one needs to retain a nonzero $\epsilon$ at intermediate stages of the calculation.

The cutoff dependence of some of the other matrix elements, equations (3.6) through (3.8), is more subtle. We know from the previous section that without the 'counterterm' , one will have *log* $\epsilon$ singularities in general. So in the present formalism a similar *log* $\epsilon$ dependence must show up upon diagonalization through an interplay of matrix elements in (3.6) and (3.8), if the basis is sufficiently large. In our calculations with Gaussian basis functions all our integrals were done using an 'Adaptive Gauss Quadrature' routine from the Quadpack[6] Library. The CPU time required was sometimes fairly large making this method impractical for larger calculations without some modifications. After some experimenting, we found it most convenient to introduce cutoffs into equations (3.6) and (3.8) in the following way;

$$\int_{x_{min}}^{x_{max}} dx \int_{y_{min}}^{y_{max}} dy\, \Theta(1-x-y) \longrightarrow \int_{\epsilon}^{1-\epsilon} dy \int_{\epsilon_1}^{1-y-\epsilon_1} dx$$

$$\int_{x_{min}}^{x_{max}} dx \int_{y_{min}}^{y_{max}} dy\, \Theta(x+y-1) \longrightarrow \int_{\epsilon}^{1-\epsilon} dy \int_{1-y+\epsilon_1}^{1-\epsilon_1} dx \tag{3.10}$$

$\epsilon_1$ was taken to be $\epsilon/10$ (the relative factor of ten is arbitrary; the only requirement being $\epsilon > 2\epsilon_1$). We will show below that for a wide range of $\epsilon$'s a *log* $\epsilon$ dependence in the eigenvalues can be reproduced approximately when the counterterm is omitted. To further optimize the numerics (both in terms of CPU time and proper $\epsilon$ dependence) we have taken the following steps. First, we include the square root factors appearing in (3.8) into our definition of $\psi_3$; that is instead of (3.1b) one has;

$$\frac{\psi_3(x,y)}{\sqrt{1-x-y}} = \sum_{(ij)} b_{(ij)} f_i(x)\, f_j(y) \tag{3.1b'}$$

with $f_i(x)$ given again by the left-hand-side of (3.2a) or (3.2b). Equations (3.6) and (3.8)

are then modified to;

$$A_{ab} = \int_{\epsilon}^{1-\epsilon} dy \int_{\epsilon_1}^{1-y-\epsilon_1} dx\,(1-x-y)\, f_{k_a}(x) f_{l_a}(y) f_{i_b}(x) f_{j_b}(y)\ , \tag{3.6a'}$$

$$B_{ab} = \int_{\epsilon}^{1-\epsilon} dy \int_{\epsilon_1}^{1-y-\epsilon_1} dx\,(1-x-y)$$

$$f_{k_a}(x) f_{l_a}(y) \left(\frac{m_f^2}{x} + \frac{M_F^2}{y} + \frac{m_B^2}{1-x-y}\right) f_{i_b}(x) f_{j_b}(y)\ , \tag{3.6b'}$$

$$C_{ab}^{(1)} = g\, M_F \int_{\epsilon}^{1-\epsilon} dy \int_{\epsilon_1}^{1-y-\epsilon_1} dx\, h_a(x) \left(\frac{1}{1-x} + \frac{1}{y}\right) f_{i_b}(x) f_{j_b}(y)\ , \tag{3.8a'}$$

$$C_{ab}^{(2)} = g\, m_f \int_{\epsilon}^{1-\epsilon} dy \int_{1-y+\epsilon_1}^{1-\epsilon_1} dx\, h_a(x) \left(\frac{1}{x} + \frac{1}{1-y}\right) f_{i_b}(1-y) f_{j_b}(1-x)\ . \tag{3.8b'}$$

Most of our calculations were done using equations (3.6′) and (3.8′). Another advantage of this form is that for sine basis functions all integrals can be carried out analytically. As a final step to save on CPU time, for Gaussians we have carried out some partial integrations analytically (e.g. in (3.6$b'$)) to isolate singular parts.

As a next step one must specify the 'counterterm', $B^{(C.T.)}$. Our renormalization prescription is the same as in the previous section. When $\psi_3$ is eliminated explicitly in favor of $\psi_2$ as in section 2, one has an analytic form for the 'self-mass' contribution (equation (2.9)); and it is straightforward to read off what the appropriate counterterm should be. In the approach of this section, the analogue of 'self-mass' corrections emerges only upon diagonalizing and solving equation (3.4). Should one in this case nevertheless use the same 'counterterm' as in equation (2.11) ? Will 'counterterm' plus 'self-energy produced after diagonalization' lead to the correct finite correction to the binding energy ? If one uses a complete ( and hence in principle infinite) set of basis functions for $\psi_3$ the answer to these two questions is yes. The whole purpose of using basis functions however is to choose them cleverly so that one can reproduce the correct physics with only a small number of them. It is very probable that a much smaller number is needed to get the finite contributions accurately, than is necessary for the singular parts that will be eventually canceled. So one would like to come up with a subtraction scheme that is capable of canceling basis function dependent singular parts, but still leads to correct finite parts consistent with our renormalization prescription. The need for a general basis dependent subtraction scheme becomes clear if one considers using sine basis functions. In that case all integrals in (3.6′)

and (3.8′) are finite and no $log\ \epsilon$ terms will show up . Obviously, one should not introduce a counterterm like that in equation (2.11) which has a $log\ \epsilon$ divergence. On the other hand even in this case one needs a finite renormalization to ensure correct threshold behavior, so one cannot ignore the counterterm altogether. We describe below a so-called 'Basis Function' (BF-) subtraction scheme which can be applied to any set of basis functions, in particular to both the Gaussian and the sine basis functions. Regardless of whether a $log\ (\epsilon)$ dependent or just a finite counterterm is called for, the BF-subtraction scheme is set up to satisfy our renormalization prescription described in Sec. II and lead to the correct binding energy. What is still required, however, is that the set of basis functions be sufficiently clever and complete so as to get the finite parts to reasonable accuracy. Let us rewrite equation (3.4) as

$$M^2 \begin{pmatrix} \hat{A}_2 & 0 \\ 0 & \hat{A}_3 \end{pmatrix} \begin{pmatrix} X_2 \\ X_3 \end{pmatrix} = \begin{pmatrix} \hat{B}_2 + \hat{B}^{(C.T.)} & \hat{C}^{(1)} + \hat{C}^{(2)} \\ (\hat{C}^{(1)} + \hat{C}^{(2)})^T & \hat{B}_3 \end{pmatrix} \begin{pmatrix} X_2 \\ X_3 \end{pmatrix} . \tag{3.11}$$

$\hat{A}_{2,3}$ and $\hat{B}_{2,3}$ are the $N_{2,3} \times N_{2,3}$ matrices corresponding to equations (3.5) or (3.6′), and the $\hat{C}^{(i)}$'s are the $N_2 \times N_3$ matrices given in (3.8′). One can now proceed with the analogue of eliminating $\psi_3$. One first expresses $X_3$ in terms of $X_2$ and then inserts the result into the equation for $X_2$,

$$X_3 = (M^2\, \hat{A}_3 - \hat{B}_3)^{-1} (\hat{C}^{(1)} + \hat{C}^{(2)})^T X_2, \tag{3.12}$$

$$\begin{aligned} M^2\, \hat{A}_2\, X_2 = {} & (\hat{B}_2 + \hat{B}^{(C.T.)})\, X_2 \\ & + (\hat{C}^{(1)} + \hat{C}^{(2)})\, (M^2\, \hat{A}_3 - \hat{B}_3)^{-1} (\hat{C}^{(1)} + \hat{C}^{(2)})^T X_2 \end{aligned} \tag{3.13}$$

where $T$ denotes transpose.

The analogue of the self-mass graphs are given in this formalism by,

$$\hat{S}(M^2) = \hat{C}^{(1)}\, \hat{D}^{-1}\, (\hat{C}^{(1)})^T + \hat{C}^{(2)}\, \hat{D}^{-1}\, (\hat{C}^{(2)})^T\ , \tag{3.14}$$

where;

$$\hat{D} = M^2\, \hat{A}_3 - \hat{B}_3\ . \tag{3.15}$$

The boson exchange graphs are given by

$$\hat{E}(M^2) = \hat{C}^{(1)}\, \hat{D}^{-1}\, (\hat{C}^{(2)})^T + \hat{C}^{(2)}\, \hat{D}^{-1}\, (\hat{C}^{(1)})^T\ . \tag{3.16}$$

Let us first see what would happen if $\hat{B}^{(C.T.)}$ in equation (3.13) were replaced by $-\hat{S}$, for some fixed value $M^2 = M_0^2$ . Such a counterterm would ensure that self-mass

contributions vanish identically for that one particular value of $M^2$. For any other value the infinite parts would still cancel (one can argue that the infinite parts are independent of $M^2$), however a finite part which depends on the arbitrary value $M_0^2$ would remain. So this procedure does not yet quite lead to our desired renormalization prescription. One needs a further finite subtraction to go from fixed $M^2$ to $M^2$ satisfying the renormalization prescription of section 2. This finite correction can be obtained by taking the difference of the expression for the self-mass equation (2.9) evaluated once for $M^2 = m_f^2/x + M_F^2/(1-x)$ and the second time for $M^2 = M_0^2$. The full counterterm then becomes;

$$\hat{B}^{(C.T.)} = \hat{B}^{(C.T.a)}(M_0^2) + \hat{B}^{(C.T.b)}(M_0^2) \tag{3.17}$$

$$\hat{B}^{(C.T.a)}(M_0^2) = -\hat{S}(M_0^2) \tag{3.18a}$$

$$B_{ab}^{(C.T.b)}(M_0^2) = g^2 \int_{\epsilon}^{1-\epsilon} dx\, h_a(x)\, h_b(x) \int_{\epsilon_1}^{1-\epsilon_1} dz\, \frac{(1+z)^2}{z} \{\frac{m_f^2}{x}(G_1 - G_2) - \frac{M_F^2}{1-x}(G_3 - G_4)\} \tag{3.18b}$$

where,

$$G_1 = \frac{1}{m_f^2\,(1-z)^2 + m_B^2\, z}\,, \tag{3.19a}$$

$$G_2 = \frac{1-x}{m_f^2\,(1-x)(1-z) + M_F^2\, z\, x\,(1-z) + m_B^2\,(1-x)\, z - M_0^2\, z\, x\,(1-z)(1-x)}\,, \tag{3.19b}$$

$$G_3 = \frac{1}{M_F^2\,(1-z)^2 + m_B^2\, z}\,, \tag{3.19c}$$

$$G_4 = \frac{x}{m_f^2\,(1-x)\, z\,(1-z) + M_F^2\, x\,(1-z) + m_B^2\, x\, z - M_0^2\, z\, x\,(1-z)(1-x)}\,. \tag{3.19d}$$

The left hand side of (3.17) should be independent of $M_0^2$. In most of our calculations we have used $M_0^2 = (m_f + M_F)^2$. We have checked that changes in $M_0^2$ of 10% lead to differences in eigenvalues comparable to our other systematic errors (usually less than 1 % ). Note that $\hat{B}^{(C.T.b)}$ and the difference $\hat{S}(M^2) - \hat{S}(M_0^2)$ , which is the combination relevant for equation (3.13), are both finite. For Gaussians, $\hat{B}^{(C.T.a)} = \hat{S}(M_0^2)$ is used first to get rid of infinities, and $\hat{B}^{(C.T.b)}$ then makes finite corrections to eliminate $M_0^2$ dependence and implement our renormalization prescription. This procedure also works for sine basis

functions, for which $\hat{S}(M^2)$ and $\hat{S}(M_0^2)$ are individually finite. All this assumes that the basis functions are representing $\psi_2$ and $\psi_3$ sufficiently well so that the finite parts of all integrals are accurately reproduced. The main goal of the present investigation is to gather data on the number and types of basis functions required to achieve this. So we turn now to some of our actual numerical results.

To get some feeling for how to expand a typical wave function in terms of Gaussians of type (3.2a) one can try to fit some of our results for $\psi_2$ of the previous sections. There is a huge amount of freedom in choosing the centers of the Gaussians (the $v_k$'s) and the width (the $u_k$'s). One can decide to work with only a small number of different $v_k$'s ($0 \leq v_k \leq 1$ ) and many different $u_k$'s or vice versa. We have found that good fits to $\psi_2$ can be obtained with 6 Gaussians (two widths each at three different centers). The optimal choices for the parameters does depend on the coupling and masses. The question is whether the same $\psi_2$ and the corresponding $\psi_3$ consistent with equations (2.9) and (2.11) will follow automatically from direct diagonalization and what the criteria for a good choice of basis functions will be when the exact results are not known.

When we started playing with Gaussian basis functions we were immediately faced with the problem that due to the infinity of possibilities there is no systematic way to build up larger and larger sets and test convergence; that is there is no obvious initial minimal set to start with, to which one can add new Gaussians in a well-motivated manner. The situation is different with sine basis functions where one can just let the parameter $k$ in (3.2b) take on larger and larger integer values. It will not be possible to describe the entire history of how we ended up using the Gaussians that we chose. In many cases it was just 'trial and error' until the, in the present situation, known eigenvalues were well approximated. Some of the sets used are tabulated in Table 1, and are denoted 'set A', 'set B' etc.

In the first round of calculations we kept the same set of basis functions for fixed $m_f$,$M_F$ and $m_B$ and tried to reproduce the correct eigenvalues for a range of couplings g. In Fig. 6a, 6b, and 6c we show the lowest eigenvalue versus g for three different values of $m_B$ for sets A and D, and compare with the results from section 2. As in the previous section all masses are measured in units of the fermion mass (also $m_f = M_F$ as before). One sees that even with a small number of Gaussians reasonable agreement is found with the known results especially for the two smaller values of $m_B^2$. This gives us some confidence that the subtraction scheme described above is implementing our renormalization prescription correctly. To check on the $\epsilon$ independence we plot in Fig. 7 the lowest eigenvalue versus $\epsilon_1$ for one particular choice of masses and basis set. We also show what happens if no counterterm is included and verify an approximate $log\ \epsilon$ behavior. Finally in Figs. 8a, 8b, and 8c we present results for sine basis functions together with the exact results. Again agreement is good except for large $m_B$ and large g. We recall that the singularity structure of matrix elements are very different for sines compared to Gaussians and are encouraged that both types of basis functions give the same finite physical results.

To summarize the data presented so far, it appears that a small number of suitable basis functions reproduce the eigenvalues well. This is true even if we do not choose to optimize by using different basis functions for different couplings. Before going on to discuss wavefunctions we mention some of the problems that emerge when the calculations

are scrutinized in more detail. The first issue becomes apparent when we ask ourselves the question, how would one choose one set of basis functions over another if one did not know the true results. The problem is a serious one since, as can be seen in Fig. 6 and Fig. 8, the eigenvalues do not necessarily approach their correct values monotonically from above. We believe that due to nonlinearities in our complicated subtraction scheme a variational principle is lacking in our calculations. We describe below one consistency requirement which tells us how close we are to the true result, but there is certainly room for better ideas to get around this problem. The second issue has to do with our experience that adding more basis functions does not necessarily improve things. This phenomenon is well known to quantum chemists and can be traced back to numerical instabilities from using nonorthogonal basis functions (sines are also not 'orthogonal' for $\psi_3$ due to the $\Theta$-function in (3.6a)). The left-hand-side of (3.11) is not proportional to a unit matrix, so one is dealing here with a generalized eigenvalue problem. Denoting the matrix on the left-hand-side by $\hat{A}$, one sees that instabilities could arise if $\hat{A}$ has very small eigenvalues, or in other words if near 'linear dependencies' occur among the basis functions. Attempts to date to construct appropriate linear combinations of basis functions which do not suffer from linear dependency problems, have not proved to be useful. To solve the generalized eigenvalue problem we used the Eispack[7] routine RSG which uses a Cholesky decomposition[8] of the matrix $\hat{A}$ . This routine is able to handle situations where the determinant of $\hat{A}$ is fairly small. However, for large basis sets, eventually one ran into numerical problems and the whole method collapses. Because of this we did not attempt to expand $\psi_3$ with more than $n_3 \times n_3 = 6 \times 6$ basis functions. Fortunately in most cases it was not necessary to go to larger sets, since $n_3 \times n_3 = 4 \times 4$ or even $2 \times 2$ already gave respectable answers. It is mainly for large $m_B^2$ and large coupling that we would have liked to test larger basis sets. Having the ability to go to larger basis sets also gives us more leverage in choosing our initial minimal set. The way things now stand, it is crucial that one come close to the correct result right away before the method breaks down. So the two major problems, the lack of a variational principle and the 'almost linear dependence' problem ( it is not excluded that the two problems are related ), could present a bottleneck for applications of basis functions in the future. Clearly a lot more work needs to be done on these issues and perhaps more sophisticated numerical techniques developed.

We now look at wave functions in more detail for two values of couplings $g = 0.110$ and $g = 0.517$ and for $m_B^2 = 0.5$ . After diagonalization the coefficients $a_j$ and $b_{ij}$ are known and one can reconstruct $\psi_2$ and $\psi_3$ from (3.1a) and (3.1$b'$) . To come up with quantitative estimates of how well the wave functions are doing we have looked at several quantities. First one can check whether the relative normalizations of $\psi_2$ and $\psi_3$ come out correctly. We calculate NORM2 and NORM3 defined in (2.14) and (2.15) and compare with results for the amplitudes from the previous section (called 'exact' results in the Tables). Other measures include;

$$DEVWF2 = \int_0^1 dx \left(|\psi_2^{exact}(x)| - |\psi_2(x)|\right)^2 ,$$

$$DEVWF3 = \int_0^1 dx \int_0^1 dy\, \Theta(1-x-y)\left(|\psi_3^{exact}(x,y)| - |\psi_3(x,y)|\right)^2 . \qquad (3.20)$$

Finally, if the 'exact' results are not available one can still check how well the relationship between $\psi_2$ and $\psi_3$ as given in equation (2.7b) is satisfied. One can take the $\psi_2$ that came out of diagonalization and use equation (2.7b) to construct a $\psi_3(x,y)$ which we will denote $\tilde{\psi}_3$ . This $\tilde{\psi}_3$ can then be compared with the actual $\psi_3$ obtained through diagonalization, giving

$$DEVWF = \int_0^1 dx \int_0^1 dy\, \Theta(1-x-y)\left(|\tilde{\psi}_3(x,y)| - |\psi_3(x,y)|\right)^2 . \qquad (3.21)$$

In Tables 2a and 2b we tabulate various quantities for g = 0.110 and g = 0.517 respectively, for several basis sets listed in Table 1. For the g = 0.110 data one sees that the [6 + 2 × 2] basis sets get the eigenvalue to about 1% and the [6 + 4 × 4] sets to better than 0.1%. NORM2 is also respectably reproduced. We note that for this weak coupling most of the wave function resides in $\psi_2$ with minimal contribution from $\psi_3$. Hence NORM2 and DEVWF2 are more important than NORM3 and DEVWF3 . In Figs. 9a and 9b we plot $\psi_2^2(x)$ for the basis set L (the worst DEVWF2) and for set J (the best DEVWF2) together with the exact $\psi_2^2$.

Turning to the g = 0.517 data, again the [6 + 4 ×4] sets do better in terms of $M^2$ and NORM2 and NORM3. For DEVWF2 one notices that sometimes by going to larger basis sets this quantity gets worse although $DEVWF2 + DEVWF3$ improves. For this larger coupling feedback from $\psi_3$ onto $\psi_2$ is important ( this is also evident from the relative sizes of NORM2 and NORM3). When comparing the four [6 +4 × 4] sets (A,C,D and E) we see that the latter two have significantly better DEVWF2, although their eigenvalues are worse. Here by worse we mean by about 1% and for this coupling we certainly do not claim to have things under control to better than 1% or 2%. In Figs. 10a, 10b and 10c we show $\psi_2^2(x)$ for sets A, D and F. These plots visualize the same information contained in DEVWF2 . Of course when NORM3 is comparable to or larger than NORM2, doing well in $\psi_2$ is not the only criterion for a good wave function. In Table 3 we list DEVWF of equation (3.21). If one did not know the exact result the only information available would be $M^2$ and DEVWF. One sees that DEVWF does not differentiate between the four [6 + 4 × 4] sets and one would have to quote something like the average and standard deviation of the four $M^2$ values as ones best estimate. DEVWF does seem to see the difference between the [6 + 4 × 4] and [6 + 2 ×2] basis sets and in particular to disfavor the low eigenvalue of set H . In the future it is worthwhile trying to come up with other criteria for choosing one basis set over another. At the moment we do not have a systematic way to test convergence. We can only give some statistical estimate from among basis sets with reasonable DEVWF values. If a large number of basis sets with small DEVWF give similar eigenvalues one has some confidence that one is close to the true $M^2$ .

Finally we discuss the wavefunctions using sine basis functions. In Figs. 11a and 11b we plot $\psi_2^2(x)$ using 12+ 4 × 4 sine basis for $m_B^2 = .5$ and $g = .110$ and .517 respectively. In

the two particle sector we have used only the sine functions which are symmetric under the interchange of $x$ and $1-x$. We recall that using sine basis functions the convergence of the eigenvalue was generally from above as the number of basis functions were increased. The exception was the case $m_B^2 = 3.5$ in the strong coupling domain where the convergence was from below. The sine basis functions do not have the problem, that the Gaussians have, of not telling us how to choose one basis set over another or how to add basis functions. In addition the sine basis functions allow us to compute matrix elements analytically.

## IV. SOLVING THE COUPLED TAMM-DANCOFF EQUATIONS USING DIRECT DISCRETIZATION

There are many ways to develop discretized versions of the coupled integral equations found in any Tamm-Dancoff approximation. Generically one tries to utilize quadrature rules to replace the integrals occurring both in the LFTD equations and the normalization condition with discrete sums. It is possible to discretize the equations of motion directly, or to discretize the expectation value of $P^2$ for fixed $P^+$. In both cases one replaces the original problem of finding the full amplitudes by a problem of finding the value of the amplitudes at a prescribed set of points. This last quantity then forms a vector, and the equations of motion become a matrix equation. Just as quadrature rules are often related to basis functions, such discretization techniques are related to basis function techniques; however, we will not explore this relationship. We begin by briefly discussing the general problem of choosing quadrature rules, and then rapidly turn to the simple choices that we have investigated. As discussed in the last section, any numerical algorithm must include a prescription for computing counterterms. In this section we again take advantage of the simplicity of the first Tamm-Dancoff approximation to analytically determine the mass counterterm appropriate for each discretized equation of motion, and completely avoid the larger issue of how one should determine these counterterms in higher Tamm-Dancoff approximations.

Having decided to employ quadrature rules, we still have an infinite number of options. We must decide on a multi-dimensional grid, and we must select weights to associate with each point on the grid in each integral. Obviously the grid and weights should be chosen to provide accurate estimates of the integrals occurring in the normalization condition and in the expectation value of $P^2$. Since these integrals depend on the unknown amplitudes, quadrature rules must be chosen that are accurate for a wide range of functions. We are forced to employ the same grid in all integrals, but we are free to use different weights in each integral. Ideally we would like to choose a formula that is suited to adaptive quadrature, because we may not know anything about the shape or strength of the amplitudes a priori. This means that we would like to have the freedom to set down an initial grid and then improve the resolution in any given region depending on the initial solution of the LFTD equations. Putting these considerations together we have decided to examine relatively simple few-point quadrature formulae. A major difficulty in the development of accurate formulae is the fact that we are faced with multi-dimensional quadrature.

We have investigated only the simplest quadrature rules. First, we always use the same weights in all integrations. Second, we assume a product rule for the weights in

multi-dimensional integrals, and this is probably one of the largest sources of error in our calculations. A product of one-dimensional weights leads to errors in multi-dimensional integrals that fall off less rapidly than the one-dimensional errors, regardless of the one-dimensional quadrature formula employed. This problem is exacerbated by the fact that some integrands diverge along the edges and in the corners, as discussed below. As a result we usually found little benefit to using anything more sophisticated than a trapezoidal rule. In fact we have never observed significant improvement in any result from using quadrature rules more complicated than the trapezoidal rule. We will briefly discuss improvements resulting from using grids in which the end-points are not simply removed.

In order to choose a grid, consider the discretization of the LFTD equations, equations (2.7a) and (2.7b). For every grid point $x = x_n$ we choose for $\psi_2(x)$, we must include the grid points $(x, y) = (x_n, y)$ and $(x, y) = (x, 1 - x_n)$ for $\psi_3(x, y)$ and vice versa. In other words, we must include the points $(x, y) = (x_n, 1 - x_m)$ for all allowed $n$ and $m$. The implications of these constraints are readily seen by examining the triangular region of momentum space in which the three-body amplitude lives. For fermion momenta $x$ and $y$, and boson momentum $z$, momentum conservation implies $x + y + z = 1$. This constraint leads to an equilateral triangular surface in momentum space, as shown in Fig. 12. Note that when one moves parallel to any boundary, the variable that vanishes on the boundary stays constant. The constraint $x + y = 1$ is met only on the bottom boundary of the triangle, and we construct the grid for $\psi_2$ on this boundary. Given a set of grid points for $\psi_2(x)$ on this boundary, it is easy to see that the above constraints imply that the grid for $\psi_3(x, y)$ is obtained by drawing lines parallel to the other two boundaries from each such point, and using the points where these lines intersect as the grid for $\psi_3(x, y)$. This procedure is easily generalized to arbitrarily large many-body spaces, where one must draw hypersurfaces through each point $x_n$, parallel to all hypersurfaces on which one momentum vanishes and construct a grid using the points at which these hypersurfaces intersect within a hyperpyramid.

We have now constructed the most general grid we can use, and it is specified once we choose the grid points for $\psi_2$. Before proceeding to the next step of determining weights, note that one of the major disadvantages of using grids is now apparent. The number of grid points one *must* employ to obtain a given resolution in the two-body space, $N$, grows like $N^{m-1}$ where $m$ is the maximum number of particles allowed by the Tamm-Dancoff truncation. We will consider cases where $N$ is of order $10^2$, so that the number of grid points is of order $10^4$ in our extremely simple example. This already leads to a potentially difficult matrix problem, so we use the Lanczos algorithm to generate low-lying eigenvalues and eigenstates.[9,10] The advantage of grid methods is that the matrix elements of $P^2$ are easily found and can be expressed in analytic form. We saw in the last section that this need not be the case for many choices of basis states, and when we use Gaussian basis states we must use numerical quadrature to compute matrix elements. An additional advantage is the obvious check on convergence provided by increasing the number of grid points. We have found no instability in the method as the number of grid points is increased. To the contrary, the most efficient method for computing accurate eigenvalues with a grid is to extrapolate the eigenvalues that would be obtained in the continuum from a series of results on small grids.

The simplest grids are equal-spaced, and an obvious choice is to divide the line $0 < x < 1$ into $N+2$ equal segments, discarding the end-points. Once one has chosen a grid, it is next necessary to choose weights. The simplest choice is to use equal weights; i.e., the trapezoidal rule. We will refer to the combination of equal spaced points with end points removed and equal weights as a *basic grid.* A promising method for choosing weights is to adjust them so that the quadrature formulae yield exact results for amplitudes that are piece-wise polynomial. In addition to the basic grid, we have studied one and three panel equal-spaced grids, using the trapezoidal rule and Simpson's rule; and we have studied one and three panel Gauss-Legendre grids. In each case, the quadrature rule was chosen for the two-fermion momentum, after which the three-body grid was constructed following the procedure outlined above. Given a three-body grid point $(x, y)$, the weight for this point was chosen to be the product of the weights for the points $x$ and $1-y$ on the two-body grid. This completely specifies all grid points and weights.

Perhaps the most tedious step in the development of numerical algorithms is assigning indices to each point on the grid. For the two-body grid this is trivial, and one has an index $i$ which runs from 1 to $N$. On the three-body grid we need a vector index $l$ that runs from 1 to $N(N-1)/2$, so that we can treat all quantities with arguments in this domain as vectors. This is necessary both for efficient storage and to allow the code to be vectorized. However, there is no natural way to sequence the points on this grid, making $l$ an awkward index for most purposes, as will become all too clear below. Consider the momenta $x$ and $y$. For a given point $l$ on the grid, we can find $x$ by drawing a line parallel to the left side of the triangle in Fig. 12 and determining its intercept on the lower boundary. This means we would like to be able to use an identity of the type $x_l = x_i$. To find $y$ we would draw a line parallel to the right side, and try to use an identity such as $y_l = y_j = 1 - x_j$. We will assume that every point on the three-body grid is specified by an index $l$ with which we also associate these indices $i$ and $j$, and we show this relationship where necessary by writing $l_{ij}$, $i_l$ and $j_l$. In order to avoid confusion we will use the letters $i$ and $j$ to refer to indices that run from 1 to $N$, and the letter $l$ to refer to indices that run from 1 to $N(N-1)/2$.

After discretization, the normalization condition, equation (2.8), becomes

$$1 = \sum_{i=1}^{N} w(i)\Big(\psi_2(x_i)\Big)^2 + \sum_{l=1}^{N(N-1)/2} w(i_l)w(j_l)\Big(\psi_3(x(i_l), 1 - x(j_l))\Big)^2. \tag{4.1}$$

Our aim is to convert the original coupled integral equations into a single matrix equation, so we want to work with vectors that have a unit norm. We restrict ourselves to positive weights and define the vectors $c_2(i)$ and $c_3(l)$ so that

$$c_2(i) = \sqrt{w(i)}\,\psi_2(x(i)), \tag{4.2}$$

and

$$c_3(l) = \sqrt{w(i_l)w(j_l)}\,\psi_3(x(i_l), 1 - x(j_l)). \tag{4.3}$$

Given a grid, weights and state vectors, it is relatively straightforward to determine the discretized LFTD equations that result from equations (2.7a) and (2.7b). They are

$$
\begin{aligned}
M^2 c_2(i) = & \left(\frac{m_f^2}{x_i} + \delta(i) + \frac{M_F^2}{1-x_i} + \Delta(i)\right) c_2(i) \\
& + g m_f \sum_{j=1}^{i-1} \sqrt{\frac{w(j)}{x_i - x_j}} \left(\frac{1}{x_i} + \frac{1}{x_j}\right) c_3(l_{ji}) \\
& + g M_F \sum_{j=i+1}^{N} \sqrt{\frac{w(j)}{x_j - x_i}} \left(\frac{1}{1-x_i} + \frac{1}{1-x_j}\right) c_3(l_{ij}),
\end{aligned} \tag{4.4a}
$$

$$
\begin{aligned}
M^2 c_3(l_{ij}) = & \left(\frac{m_f^2}{x_i} + \frac{M_F^2}{1-x_j} + \frac{m_B^2}{x_j - x_i}\right) c_3(l_{ij}) \\
& + g m_f \sqrt{\frac{w(i)}{x_j - x_i}} \left(\frac{1}{x_i} + \frac{1}{x_j}\right) c_2(j) \\
& + g M_F \sqrt{\frac{w(j)}{x_j - x_i}} \left(\frac{1}{1-x_j} + \frac{1}{1-x_i}\right) c_2(i) \ .
\end{aligned} \tag{4.4b}
$$

Note that in the first sum to occur in equation (4.4a) the indices on $l$ have been reversed. In the first sum as $j$ increases one moves parallel to the right side of the triangle in Fig. 12, while in the second sum one moves parallel to the left side. We have dropped the subscripts on $i$ and $j$ in equation (4.4b), but their values are specified by $l$. We have introduced the counterterms $\delta(i)$ and $\Delta(i)$, which are adjusted so that self-mass corrections vanish when $M^2 = m_f^2/x_i + M_F^2/(1-x_i)$. This is accomplished using

$$
\delta(i) = g^2 m_f^2 \sum_{j=1}^{i-1} \frac{w(j)}{x_i - x_j} \left(\frac{1}{x_i} + \frac{1}{x_j}\right)^2 \left(\frac{m_f^2}{x_j} + \frac{m_B^2}{x_i - x_j} - \frac{m_f^2}{x_i}\right)^{-1}, \tag{4.5a}
$$

$$
\Delta(i) = g^2 M_F^2 \sum_{j=i+1}^{N} \frac{w(j)}{x_j - x_i} \left(\frac{1}{1-x_i} + \frac{1}{1-x_j}\right)^2 \left(\frac{M_F^2}{1-x_j} + \frac{m_B^2}{x_j - x_i} - \frac{M_F^2}{1-x_i}\right)^{-1}. \tag{4.5b}
$$

When one goes to the continuum limit these counterterms insure that the mass of all two-fermion scattering states is correct regardless of their relative momentum. This in turn allows one to construct well separated wave packets that propagate as free fermion packets with the correct mass.[1,2] In the continuum limit equation (4.5) amounts to an infinite number of renormalization conditions that require one to determine a complete function. On the grid one cannot construct states in which two fermions are separated by an arbitrarily large distance, and these counterterms do not fix the discrete masses at which scattering state eigenvalues occur. Rather, they fix the limits approached by the discrete eigenvalues as the continuum limit is approached (i.e., as the number of grid points is taken

to infinity). We should note that this counterterm includes the self-inertia. Typically one would not be able to analytically determine the counterterm that properly fixes the mass for all scattering states. This is accomplished by a function of the momentum fraction $x$, and not by a simple constant, and only in the lowest order Tamm-Dancoff approximation is it possible to analytically compute the self-mass correction as a function of momentum fraction. We do not address this central point in this article.

We should note that renormalization requires delicate cancellations that directly involve the eigenstates. For the Yukawa model in 1+1 dimensions on the light front, a logarithmically divergent self-mass counterterm cancels an interaction between the two-body and three-body sectors. Numerical calculations may need to accurately determine the eigenstates near the edges of momentum space, where small errors in the eigenstates might leave large counterterms uncancelled. This point is clarified by considering the expectation value of the invariant mass,

$$\begin{aligned}\left\langle M^2 \right\rangle = & \sum_{i=1}^{N}\left(\frac{m_f^2}{x_i} + \delta(i) + \frac{M_F^2}{1-x_i} + \Delta(i)\right)\Big(c_2(i)\Big)^2 \\ & + \sum_{i=1}^{N}\sum_{j=i+1}^{N}\left(\frac{m_f^2}{x_i} + \frac{M_F^2}{1-x_j} + \frac{m_B^2}{x_j - x_i}\right)\Big(c_3(l_{ij})\Big)^2 \\ & + 2gm_f \sum_{i=1}^{N}\sum_{j=1}^{i-1}\sqrt{\frac{w(j)}{x_i - x_j}}\left(\frac{1}{x_i} + \frac{1}{x_j}\right)c_2(i)c_3(l_{ji}) \\ & + 2gM_F \sum_{i=1}^{N}\sum_{j=i+1}^{N}\sqrt{\frac{w(j)}{x_j - x_i}}\left(\frac{1}{1-x_i} + \frac{1}{1-x_j}\right)c_2(i)c_3(l_{ij}) \ . \end{aligned} \tag{4.6}$$

If we consider a state in which $c_2(i) = c_2\delta_{in}$, and let $n$ be near the middle of the grid where we expect the two-body wave function to peak, we find that the mass counterterms contribute $\big(\delta(n) + \Delta(n)\big)\big(c_2\big)^2$ to the mass. As $N \to \infty$, both $\delta(n)$ and $\Delta(n)$ diverge logarithmically. The terms that cancel these divergences come from the last two terms in equation (4.6), and the cancellation is entirely the result of $c_3(l_{nj})$ and $c_3(l_{jn})$ falling off in the 'correct' manner near the edges of the grid. The eigenvalue problem is equivalent to minimizing the mass. Regardless of how well one chooses weights in order to obtain an accurate estimate of the mass for a given trial state, the mass of the trial state is sensitive to its value near the edges of the grid as we let $N \to \infty$. This is a potentially large source of error for many numerical algorithms, and the problem will be worse when one deals with quadratic divergences in 3+1 dimensions.

The severity of the renormalization problem in 1+1 dimensions depends on how important the eigenstate at the edges is for an accurate determination of the mass and other observables *after* the cancellation of the mass counterterms. For example, when the coupling constant is weak the eigenstates peak sharply in the central regions of momentum space and the edges do little *except* cancel the mass counterterm. In this case, one can simply use cutoffs that remove the edges and still compute observables to high accuracy

after incorporating the dependence on the cutoffs in the counterterms. In these simple cases it is easy to see that the exact eigenstate is accurately approximated by its perturbative form near the edges of the grid. However, as the coupling is strengthened, the binding energy increases and the eigenstates develop non-perturbative components near the edges of the grid. Here one is forced to move cutoffs near the edges, and more accurately compute the eigenstate throughout the entire allowed momentum space. Similar effects can be seen in the basis function calculations. When the edges begin to become important, it may become necessary to employ quadrature rules that are accurate for logarithmically divergent integrals, since it is only the finite remainder after removing this divergence that is important to the observables. As a result one begins to see increasing errors in all the simple quadrature rules that we have employed; however, as we will see below these errors are not unmanageable.

At this point we have completely specified a Hamiltonian matrix of dimension $N(N+1)/2$, and we need to evaluate its lowest eigenvalues and eigenstates. This matrix is not sparse, and we want to allow $N$ to become relatively large. While these matrices are not so large that we must adopt special methods to study them, in anticipation of future work in which additional Fock space sectors are included and/or 3+1 dimensional theories are studied, we have chosen to use the Lanczos algorithm.[9,10] This algorithm is useful when one wants to find only the lowest eigenvalues and eigenstates of a large matrix, and the matrix elements are easily computed. This is exactly the kind of problem we have.

We will briefly describe the Lanczos algorithm and refer the reader to the literature for more extensive discussion. Given a $M \times M$ Hamiltonian, $H$, one first chooses an initial state, $|\phi_1>$. A second state is generated by applying the Hamiltonian and orthogonalizing with respect to the first state,

$$|\phi_2\rangle = N_2\Big(H|\phi_1\rangle - H_{1,1}|\phi_1\rangle\Big), \tag{4.7}$$

where

$$H_{i,j} = \langle\phi_i|H|\phi_j\rangle.$$

$N_2$ is a normalization constant. One next generates additional states by repetitive application of the formula

$$|\phi_{i+1}\rangle = N_{i+1}\Big(H|\phi_i\rangle - H_{i,i}|\phi_i\rangle - H_{i,i-1}|\phi_{i-1}\rangle\Big). \tag{4.8}$$

It is readily shown that in this basis the original Hamiltonian is tridiagonal, and one computes the matrix elements in the process of generating the states. The main advantage of the algorithm is that one can stop this process at some value of $i = i_{max} \ll M$, and diagonalizing the resultant $i_{max} \times i_{max}$ tridiagonal matrix yields an approximation to the lowest eigenvalues and eigenstates of the original matrix. One can improve these approximations by generating a new guess from the resultant eigenstates and starting the process over again. We iterate this process until a specified accuracy is obtained, as signalled by the change of a specified eigenvalue.

Let us turn to the results. We discuss only the basic grid, for which

$$x_i = \frac{i}{N+1}, \qquad w(i) = \frac{1}{N+1}, \qquad i = 1, 2, ..., N. \tag{4.9}$$

With few exceptions the results from other simple grids are qualitatively identical to those obtained with the basic grid. In Figs. 13a, 13b, and 13c we show the lowest eigenvalue versus $g$ for the same three values of $m_B^2$ used in Figs. 7a, 7b and 7c, and compare to the results from Section II. In each case, we show the results of using $N = 15$ and $N = 45$ grid points for $\psi_2$. There is no simple way to study the accuracy of 'comparable' basis function and grid calculations, because at this early stage of investigation we have no good way to decide which calculations are comparable. We will elaborate this slightly in the conclusion, but in this section we will simply avoid any comparison. The first thing to note is that for sufficiently large $N$ the grid results converge to the exact result with a well-defined leading error that is order $1/N$. To see this we show in Figs. 14a, 14b, and 14c the grid results for the last points in Figs. 13a, 13b and 13c, as a function of the number of grid points used, $N$. In addition we show the result of using Richardson extrapolation to remove the leading $1/N$ and the $1/N^2$ error in the grid results. It is clear that in all cases, for sufficiently large $N$ this extrapolation significantly improves the mass estimate. We have also investigated the use of higher order extrapolations and found that one can readily remove $1/N^3$ and higher order errors, subject to the constraint that the mass eigenvalue must be computed to sufficient accuracy. Results can easily be obtained to four or more significant figures using this technique. We have not shown extrapolated results in Figs. 13a, 13b and 13c because they lie on top of the exact results. These conclusions hold for all grids that we have investigated. One can employ a trapezoidal rule and keep a point near the edge of momentum space, or use Gauss-Legendre points and weights, and the error still goes like $1/N$.

An examination of Figs. 13a, 13b and 13c shows that the error for a given grid size tends to grow as the coupling constant increases, just as we saw in the basis function calculations. The grid results continue to approach the exact results as a power series in $1/N$; however, as the coupling grows this series converges more slowly for a given $N$. We have not shown this, but the behavior one sees as a function of $g$ is somewhat like that seen in going from Fig. 14a to Fig. 14b. In Fig. 14a one can see that the grid calculations converge rapidly towards the exact result even near $N = 5$; whereas in Fig. 14b one must go to grid sizes around $N = 40$ before the results even begin to move towards the correct answer as the number of grid points is increased. We have not fully understood this behavior, but several clues are provided by an examination of the eigenstates.

As $g$ increases, the binding energy increases, the eigenstates are increasingly dominated by the three-body component, and the eigenstates begin to spread evenly through momentum space except at the edges where the states are *supposed* to go to zero. This behavior is readily seen in Figs. 4a, 4b and 4c. In Figs. 15a, 15b and 15c we show $\psi_2(x)$ from the above grid calculations and compare to the exact results, for several sets of parameters. These figures reveal that the grid states closely resemble the exact states when they are strongly peaked near $x = 1/2$. However, as the states spread and develop significant strength near the edge of momentum space one begins to notice that the grid states either do not approach zero at the edges of momentum space at the proper rate or do not

approach zero at all. This problem is not due to the use of the Lanczos algorithm. It may be due to errors in the quadrature estimates of the contribution to the invariant mass from the edges of momentum space. In Fig. 15d we show the result of using the trapezoidal rule but keeping one of the grid points very near the edge of momentum space, with the same parameters as the state shown in Fig. 15c. Clearly this improves the behavior of the state near the edge of momentum space in this case, but there are other parameter sets for which all grids that we have studied lead to states with some form of spurious behavior near the edge of the grid. Even in these cases one can obtain accurate estimates of the eigenvalues, but it is likely that these edge problems increase the coefficients of each term in the $1/N$ expansion of the error.

To complete our discussion of the grid calculations we show in Figs. 16a and 16b a comparison of exact and grid calculations of $\psi_2^2(x)$ for the same sets of parameters used in Figs. 9 and 10 respectively. One sees that even on relatively small grids it is possible to obtain reasonable approximations to the wave functions when they peak near $x = 1/2$.

To summarize, simple quadrature rules provide discretized versions of the LFTD equations that yield accurate, systematically improvable eigenvalues and eigenstates. One can use relatively small grids and Richardson extrapolation to obtain accurate results, with increasing errors when NORM2 becomes small and the eigenstate develops an important component along the edge of the grid. The program is easily vectorized because 85% of the computer time is spent generating new states, as in equation (4.8). The primary limitation for these methods in more difficult calculations comes from the exponential growth of the number of grid points as the dimension of the Fock space is increased either to allow additional particles or additional spatial dimensions. A second source of difficulty comes from the need to set up increasingly complicated grids in higher dimensional spaces while referring to all quantities as vectors.

## SUMMARY AND CONCLUSIONS

In this work we study the two-fermion bound state problem of the 1+1 dimensional Yukawa model in a truncated Fock space which consists of two-fermion and two-fermion/one-boson sectors. First, by the explicit elimination of the three body state, we arrive at an integral equation for the two body state which contains one-boson exchange and logarithmically divergent self-mass corrections. This equation is renormalized using sector dependent counterterms. For various mass parameters we study the non-relativistic limit (Schrödinger equation), light-front ladder approximation, and the full integral equation. We find relativistic effects to be very important in the strong coupling domain, where the invariant mass becomes independent of the coupling constant due to self-mass corrections and counterterms. The results of this method of calculation serve as a testing ground for more elaborate methods to solve the coupled set of equations.

To solve the coupled set of equations, we employ two methods: a) expansion in basis functions and b) direct discretization. In the following we illustrate the distinct features of these two methods of solution.

Let us first summarize the aspects of basis function expansions. This method has been in use for several decades in fields employing non-relativistic many-body techniques, for example, quantum chemistry. In this method many-body amplitudes are expanded

in basis functions and the coupled set of integral equations are converted into a matrix equation which is then solved for the eigenvalues using standard techniques. Let us first emphasize the essential complications that arise in the field theory calculation. In a typical non-relativistic many-body problem, after the elimination of center of mass motion, the problem is set up in terms of relative momentum variables which are unconstrained. In the present field theoretic problem, the light-front approach enables us to perform frame independent calculations; however, the momentum fraction variables that appear have to add up to one, which poses severe constraints. As a result, multi-dimensional integrals do not factorize into products of one dimensional integrals. A second major problem is that of renormalization. Our familiarity with divergent diagrams of field theory is in the basis of plane wave states. In the present work divergent diagrams arise as a result of matrix diagonalization and they are generated in a non-plane wave basis. Thus the counterterms generated via conventional perturbation theory are inappropriate in our context. We use sines and Gaussians as two sets of basis functions and end up with finite and divergent self-mass contributions respectively. To be efficient, the renormalization is to be carried out with a small number of basis functions. We introduce and implement a 'Basis counterterm' renormalization program towards this goal. As a result both types of basis functions, even though drastically different in characteristics, give the same finite physical results within numerical accuracy.

Since the basis counterterms naturally involve the basis functions, the Hamiltonian depends on the basis functions. As a result we lack a variational principle and the ground state eigenvalue is not guaranteed to be above the true value. Thus the convergence to the true result is sometimes from above and sometimes from below.

Let us now compare and contrast sine and Gaussian basis set calculations. Using sine basis functions, after performing a few tricks, all integrals except those involving some parts of the counterterms can be evaluated analytically. Further, all integrands are free of singularities. The matrix dimensions are also very small. Thus the CPU time needed for the whole calculation is relatively very low. With sine basis sets, improved eigenvalues are obtained by merely increasing the number of basis functions. Our choice for the basis is not orthogonal in the three particle sector and numerical inaccuracies due to non-orthogonality set in quickly as the number of basis functions increases. With Gaussian basis functions, at most only one integration may be performed analytically due to finite limits of integration. Thus most matrix elements involve two-dimensional numerical integration with singular integrands. To save CPU time we found it necessary to redefine amplitudes and perform some partial integrations. For the choice of Gaussians we are faced with infinite possibilities and have to resort to a 'trial and error' method. We find that even with a small number of Gaussians one can obtain eigenvalues accurate to a few percent. Here also we are faced with non-orthogonality problems for large basis sets. Since there is no simple rule for adding more basis functions to improve results, we have performed consistency checks on the wavefunctions.

There are two major problems that need to be investigated further. One is the non-orthogonality issue. In the present work we have used a product ansatz for the three body sector. One may study alternatives. The other problem is consistency criteria when the choice of basis states offers infinite possibilities as is the case of Gaussians.

We have also directly discretized the LFTD integral equations, and studied the dependence of the masses and eigenstates on the grid and quadrature weights employed. When one uses a product rule to determine the weights for multi-dimensional integrals, there is no apparent advantage to using a quadrature rule more complicated than trapezoidal. Errors always behave as $1/N$ for $N$-point grids and one can easily use Richardson extrapolation to improve results. The counterterms depend on the grid employed, but for our simple calculations it was possible to analytically determine this dependence. In principle the mass counterterm is a vector that must be determined a posteriori by fitting observables. In our calculation we have adjusted the mass counterterm to properly fix the masses of well-separated fermions; however, such scattering observables are not easily computed using the methods we have studied and may be of little use in future calculations. Our calculations are most successful when the coupling is not too large, and there is some hope that one can use analytic techniques to determine counterterms for small coupling even in more complicated calculations.

The primary limitation of direct discretization is the rapid growth in the number of grid points, and thereby in the dimension of the mass matrix, as the number of Fock states or spatial dimensions is increased. If one sets up a grid in the manner we use, the Fock space sector with the most particles automatically contains the largest number of grid points, even though one would like to include such states with low resolution. This is possible using basis functions, where one can arbitrarily choose the number of functions employed in any sector. Beyond this significant limitation, direct discretization offers many important advantages. The mass matrix elements can all be computed analytically, allowing one to employ the Lanczos algorithm and extremely large matrices. The resultant code is readily vectorized, allowing one to efficiently use supercomputers. Errors are well-behaved as the number of grid points is increased, allowing one to use extrapolation and effectively compute with extremely large matrices.

In conclusion, we have performed a preliminary investigation of the numerical program to solve coupled integral equations in the light-front Tamm-Dancoff approach to field theory. In this work we have just scratched the surface of an enormous and unexplored field. We have utilized two vastly different basis functions to investigate various issues, as well as a variety of grids. We have also indicated possible avenues of future investigation for improvements.

## ACKNOWLEDGMENTS

We are indebted to Isaiah Shavitt and Ken Wilson for enlightening discussions on the basis function approach. We also acknowledge helpful conversations with Charlotte Elster, Stan Głazek, Daniel Mustaki, Steve Pinsky and Dave Wasson, and the contributions of Chad Mohler to the numerical study of direct discretization. One of us (J.S) would like to thank the members of the theory groups at the Boston University Physics Department and at DESY for their hospitality during the time in which this project was being completed. This work is supported in part by the Department of Energy under Grant No. DE-AC02ER01545 and DE-AC02-89ER40509 (J.S) and the National Science Foundation under Grant No. PHY-8719526 and the Presidential Young Investigator program through Grant

No. PHY-8858250 (R.J.P) and by a grant from Cray Research, Inc. The computational support of the Ohio Supercomputer Center is also gratefully acknowledged.

## Appendix A. Analytic solution of the Schrödinger equation

We start from the Schrödinger equation in momentum space:

$$[\frac{q^2}{2m_f} + \bar{B}]\psi(q) = \frac{\lambda^2}{2\pi}\int_{-\infty}^{+\infty} dq' \frac{\psi(q')}{(q-q')^2 + m_B^2} \quad . \tag{A.1}$$

In one dimension the Fourier transform of the one-boson exchange potential is

$$V(x) = -\frac{\lambda^2}{2m_B} e^{-m_B|x|} \; . \tag{A.2}$$

Thus the Schrödinger equation in coordinate space is

$$(\frac{-1}{m_f}\frac{d^2}{dx^2} - \frac{\lambda^2}{2m_B} e^{-m_B|x|})\psi(x) = -\bar{B}\psi(x) \; . \tag{A.3}$$

Introducing the variables, $\mu = \frac{2m_B}{m_f}$, $a = \frac{\lambda^2}{\mu}$, $\eta = m_f\bar{B}$, $k^2 = \frac{4a}{m_B^2}$ , and $\nu^2 = \frac{4\eta}{m_B^2}$, the equation after the change of variable $y = e^{\frac{-m_B x}{2}}$ for $x > 0$ is

$$[y^2\frac{d^2}{dy^2} + y\frac{d}{dy} + k^2y^2 - \nu^2]\psi(y) = 0 \quad . \tag{A.4}$$

Thus the solution for $x > 0$ is

$$\psi(x) = \mathcal{N} J_\nu(ke^{-\frac{m_B x}{2}}), \tag{A.5}$$

and the solution for $x < 0$ is

$$\psi(x) = \mathcal{N} J_\nu(ke^{\frac{m_B x}{2}}). \tag{A.5}$$

Here $\mathcal{N}$ is a normalization factor and $J_\nu$ is the Bessel function of fractional order. Thus the solution is

$$\psi(x) = \mathcal{N} J_\nu(ke^{\frac{m_B|x|}{2}}). \tag{A.5}$$

Since

$$\lim_{x\to\infty} \psi(x) \quad \to 0,$$

$J_\nu(0) = 0$. Since the ground state wavefunction is an even parity state we have $\psi(x) = \psi(-x)$. For $\psi(x)$ to be continuous this implies $\frac{d\psi}{dx}\,|_{x=0} = 0$. Thus for the ground state we have

$$J_{\nu-1}\Big(\sqrt{\frac{2\lambda^2 m_f}{m_B^3}}\Big) = J_{\nu+1}\Big(\sqrt{\frac{2\lambda^2 m_f}{m_B^3}}\Big) \quad . \tag{A.6}$$

Since the first excited state is an odd parity state we have, for the first excited state $J_\nu(k) = 0$.

The eigenvalues can be determined by either graphical methods or numerical procedures.

## REFERENCES


1. R. J. Perry, A. Harindranath, and K. G. Wilson, Phys. Rev. Lett. 65 (1990) 2950.
2. R. J. Perry and A. Harindranath, Phys. Rev. D43 (1991) 4051.
3. E. D. Brooks and S. C. Frautschi, Z. Phys. C23 (1984) 263.
4. H. C. Pauli and S. J. Brodsky, Phys. Rev. D32 (1985) 1993; D32 (1985) 2001.
5. For example, see I. Shavitt, in Methods in Computational Physics, Vol. II, B. Alder, S. Fernbach, and M. Rotenberg (eds.) (Academic Press, New York, 1963), p.1 ; J. D. Morgan III, in Numerical Determination of the Electronic Structure of Atoms, Diatomic and Polyatomic Molecules, M. Defranceschi and J. Delhalle (eds.) (Kluwer Academic Publishers, 1989), p.49; K. G. Wilson, "Gaussian Bases", unpublished.
6. R. Piessens *et. al.,* Quadpack: A Subroutine Package for Automatic Integration (Springer-Verlag, New York, 1983).
7. B. T. Smith, *et. al.,* Matrix Eigensystem Routines - EISPACK Guide (Springer-Verlag, New York, 1976).
8. R. S. Martin and J. H. Wilkinson, in Handbook for Automatic Computation, Vol. II, Linear Algebra, J. H. Wilkinson and C. Reinsch (eds.) (Springer-Verlag, New York, 1971), p. 304.
9. C. Lanczos, J. Res. Natl. Bur. Stand. 45 (1950) 255.
10. For an application of the Lanczos method to light-front field theory, and for extensive references, see J. R. Hiller, "Application of discretized light-cone quantization to a theory of charged and neutral bosons in 1+1 dimensions", University of Minnesota preprint TPI-MINN-90/67-T (1990).

## TABLE CAPTIONS

1. Examples of basis sets.
2. a) Eigenvalues and characteristics of wave functions for $m_B^2 = 0.5$ and $g = 0.110$. b) Eigenvalues and characteristics of wave functions for $m_B^2 = 0.5$ and $g = 0.517$.
3. $M^2$ and $DEVWF$ for $m_B^2 = 0.5$ and $g = 0.517$ .

## FIGURE CAPTIONS

1. The ground state eigenvalue of the Schrödinger equation $M^2$ versus the coupling constant for $m_B^2 = 0.05$ (dashed), 0.5 (dot-dashed), and 3.5 (solid).
2. The Schrödinger wave function $\psi(x)$ versus the momentum fraction $x$ for $m_B^2 = 0.5$ and coupling constant $g = .1$ (solid) and $g = .4$ (dashed).
3. a) The ground state eigenvalue $M^2$ versus the coupling constant for $m_B^2 = 0.05$ for Schrödinger equation (dashed), LFLA (dot-dashed), and FLFTD (solid). b) Same as in 3 a) but for $m_B^2 = 0.5$ . c) Same as in 3 a) but for $m_B^2 = 3.5$.
4. a) The two-particle amplitude $\psi_2(x)$ for $m_B^2 = 0.05$ and $g = .042$ (dotted), .084 (dashed),
   .22 (dot-dashed), .4 (solid), and .71 (dotted) in FLFTD. b) Same as in 4 a) but for $m_B^2 = .5$ and $g = .110$ (dotted), .183 (dashed),
   .375 (dot-dashed), .517 (solid), .842 (dotted), and 1.31 (dashed). c) Same as in 4 a) but for $m_B^2 = 3.5$ and $g = .269$ (dotted), .412 (dashed), .773 (dot-dashed), 1.06 (solid), 1.56 (dotted), and 2.02 (dashed).
5. a) Two-particle and three-particle norms NORM2 (solid) and NORM3 (dashed) respectively for FLFTD for $m_B^2 = .05$ versus the coupling constant. b) Same as in 5 a) but for $m_B^2 = 0.5$. c) Same as in 5 a) but for $m_B^2 = 3.5$.
6. a) Ground state eigenvalue $M^2$ versus coupling constant for basis states A (cross) and D (diamond) compared with exact result (solid) for $m_B^2 = .05$. b) Same as in a) but for $m_B^2 = 0.5$. c) Same as in a) but for $m_B^2 = 3.5$.
7. Ground state eigenvalue versus the smaller cutoff $\epsilon_1$ for basis set D without counterterms (dashed) and with counterterms (solid) for $g = .2$ .
8. a) Ground state eigenvalue $M^2$ versus the coupling constant for sine basis sets $[12+4\times 4]$ (cross) and $[12+6\times 6]$ (diamond) compared with exact result (solid) for $m_B^2 = 0.05$. b) Same as in a) but for $m_B^2 = 0.5$. c) Same as in a) but for $m_B^2 = 3.5$.
9. a) $\psi_2^2(x)$ for basis set L (solid) compared with the exact result (dashed) for $g = 0.110$ and $m_B^2 = .5$ . b) Same as in a) but for the basis set J.
10. a) $\psi_2^2(x)$ for basis set A (solid) compared with the exact result (dashed) for $g = .517$ and $m_B^2 = .5$ . b) Same as in a) but for the basis set D. c) Same as in a) but for basis set F.
11. a) $\psi_2^2(x)$ for sine basis functions $[12 + 4 \times 4]$ (solid) and comparison with the exact result (dashed) for $g = .110$ and $m_B^2 = .5$ . b) Same as in a) but for $g = .517$ .
12. Typical momentum space grid. $\psi_2(x)$ is discretized along the lower boundary, while the grid for $\psi_3(x, y)$ is the set of points inside the triangle where lines of constant $x$ and lines of constant $y$ intersect.
13. a) Ground state eigenvalue $M^2$ versus coupling constant for a 15 point (cross) and 45 point (diamond) basic grid compared with exact result (solid) for $m_B^2 = .05$. b) Same as in a) but for $m_B^2 = 0.5$. c) Same as in a) but for $m_B^2 = 3.5$.
14. a) Ground state eigenvalue $M^2$ versus the number of grid points (dotted), along with the first (dashed) and second (solid) Richardson extrapolation, for $m_B^2 = 0.05$ and $g = 0.71$. b) Same as in a) but for $m_B^2 = 0.5$ and $g = 6.37$. c) Same as in a) but for $m_B^2 = 3.5$ and $g = 2.16$.

15. a) The two-particle amplitude $\psi_2(x)$ for $m_B^2 = 0.05$ and $g = 0.71$, computed on a 15 point basic grid (dotted), a 45 point grid (dashed), a 75 point grid (dot-dashed) and using explicit elimination (solid). b) Same as in a) but for $m_B^2 = 0.5$ and $g = 1.31$. c) Same as in a) but for $m_B^2 = 3.5$ and $g = 2.16$. d) Same as in c) but using a grid with an end-point very near the edge of momentum space.
16. a) $\psi_2^2(x)$ for a 15 point basic grid (dotted) and a 45 point basic grid (dashed) compared with the exact result (solid) for $g = 0.110$ and $m_B^2$=.5 . b) Same as in a) but for $g = .517$ and $m_B^2$ =.5 .

TABLE 1 Examples of Basis Sets

| *SET* | *SIZE* | $\Psi_2$ | | | $\Psi_3$ | | |
|---|---|---|---|---|---|---|---|
| | | *center* | *width* | | *center* | *width* | |
| *A* | $6+4\times4$ | 0.0 | 10 | 50 | 0.3 | 10 | 50 |
| | | 0.5 | 10 | 50 | 0.6 | 10 | 50 |
| | | 1.0 | 10 | 50 | | | |
| *B* | $6+4\times4$ | same | | | 0.0 | 10 | 50 |
| | | | | | 0.6 | 10 | 50 |
| *C* | $6+4\times4$ | same | | | 0.3 | 10 | 25 |
| | | | | | 0.6 | 10 | 25 |
| *D* | $6+4\times4$ | same | | | 0.0 | 50 | |
| | | | | | 0.3 | 10 | |
| | | | | | 0.45 | 50 | |
| | | | | | 0.6 | 10 | |
| *E* | $6+4\times4$ | same | | | 0.0 | 50 | |
| | | | | | 0.3 | 25 | |
| | | | | | 0.45 | 50 | |
| | | | | | 0.6 | 25 | |
| *F* | $6+2\times2$ | same | | | 0.3 | 10 | |
| | | | | | 0.6 | 10 | |
| *G* | $6+2\times2$ | same | | | 0.3 | 25 | |
| | | | | | 0.6 | 25 | |
| *H* | $6+2\times2$ | same | | | 0.3 | 50 | |
| | | | | | 0.6 | 50 | |
| *J* | $6+4\times4$ | 0.4 | 150 | 300 | 0.0 | 10 | 25 |
| | | 0.5 | 150 | 300 | 0.6 | 10 | 25 |
| | | 0.6 | 150 | 300 | | | |

| | | | | |
|---|---|---|---|---|
| $K$ | $6+4\times4$ | same | 0.0 | 10 50 |
| | | | 0.6 | 10 50 |
| $L$ | $6+2\times2$ | same | 0.0 | 10 |
| | | | 0.6 | 10 |
| $M$ | $6+2\times2$ | same | 0.0 | 25 |
| | | | 0.6 | 25 |

TABLE 2a Eigenvalues and Characteristics of Wave Functions for $m_B^2 = 0.5$ and $g = 0.110$

| *SET* | $M^2$ | *NORM2* | *NORM3* | *DEVWF2* | *DEVWF3* |
|---|---|---|---|---|---|
| *Exact* | 3.950 | 0.925 | 0.075 | | |
| *J* $[6 + 4 \times 4]$ | 3.949 | 0.950 | 0.050 | 0.042 | 0.051 |
| *K* $[6 + 4 \times 4]$ | 3.947 | 0.951 | 0.049 | 0.050 | 0.054 |
| *L* $[6 + 2 \times 2]$ | 3.901 | 0.941 | 0.059 | 0.177 | 0.060 |
| *M* $[6 + 2 \times 2]$ | 3.904 | 0.966 | 0.034 | 0.083 | 0.052 |

TABLE 2b Eigenvalues and Characteristics of Wave Functions for $m_B^2 = 0.5$ and $g = 0.517$

| $SET$ | $M^2$ | $NORM2$ | $NORM3$ | $DEVWF2$ | $DEVWF3$ |
|---|---|---|---|---|---|
| $Exact$ | 2.800 | 0.411 | 0.589 | | |
| $A$ $[6+4\times4]$ | 2.792 | 0.418 | 0.582 | 0.115 | 0.108 |
| $B$ $[6+4\times4]$ | 2.804 | 0.415 | 0.585 | 0.098 | 0.087 |
| $C$ $[6+4\times4]$ | 2.798 | 0.416 | 0.584 | 0.103 | 0.092 |
| $D$ $[6+4\times4]$ | 2.827 | 0.403 | 0.597 | 0.012 | 0.077 |
| $E$ $[6+4\times4]$ | 2.819 | 0.406 | 0.594 | 0.014 | 0.106 |
| $F$ $[6+2\times2]$ | 2.837 | 0.390 | 0.610 | 0.077 | 0.170 |
| $G$ $[6+2\times2]$ | 2.761 | 0.368 | 0.632 | 0.141 | 0.239 |
| $H$ $[6+2\times2]$ | 2.626 | 0.437 | 0.563 | 0.079 | 0.334 |

TABLE 3 $M^2$ and $DEVWF$ for $m_B^2 = 0.5$ and $g = 0.517$

| $SET$ | $M^2$ | $DEVWF$ |
|---|---|---|
| $A$ $[6+4\times4]$ | 2.792 | 0.068 |
| $B$ $[6+4\times4]$ | 2.804 | 0.081 |
| $C$ $[6+4\times4]$ | 2.798 | 0.075 |
| $D$ $[6+4\times4]$ | 2.827 | 0.078 |
| $E$ $[6+4\times4]$ | 2.819 | 0.100 |
| $F$ $[6+2\times2]$ | 2.837 | 0.168 |
| $G$ $[6+2\times2]$ | 2.761 | 0.269 |
| $H$ $[6+2\times2]$ | 2.626 | 0.338 |

Figure 1

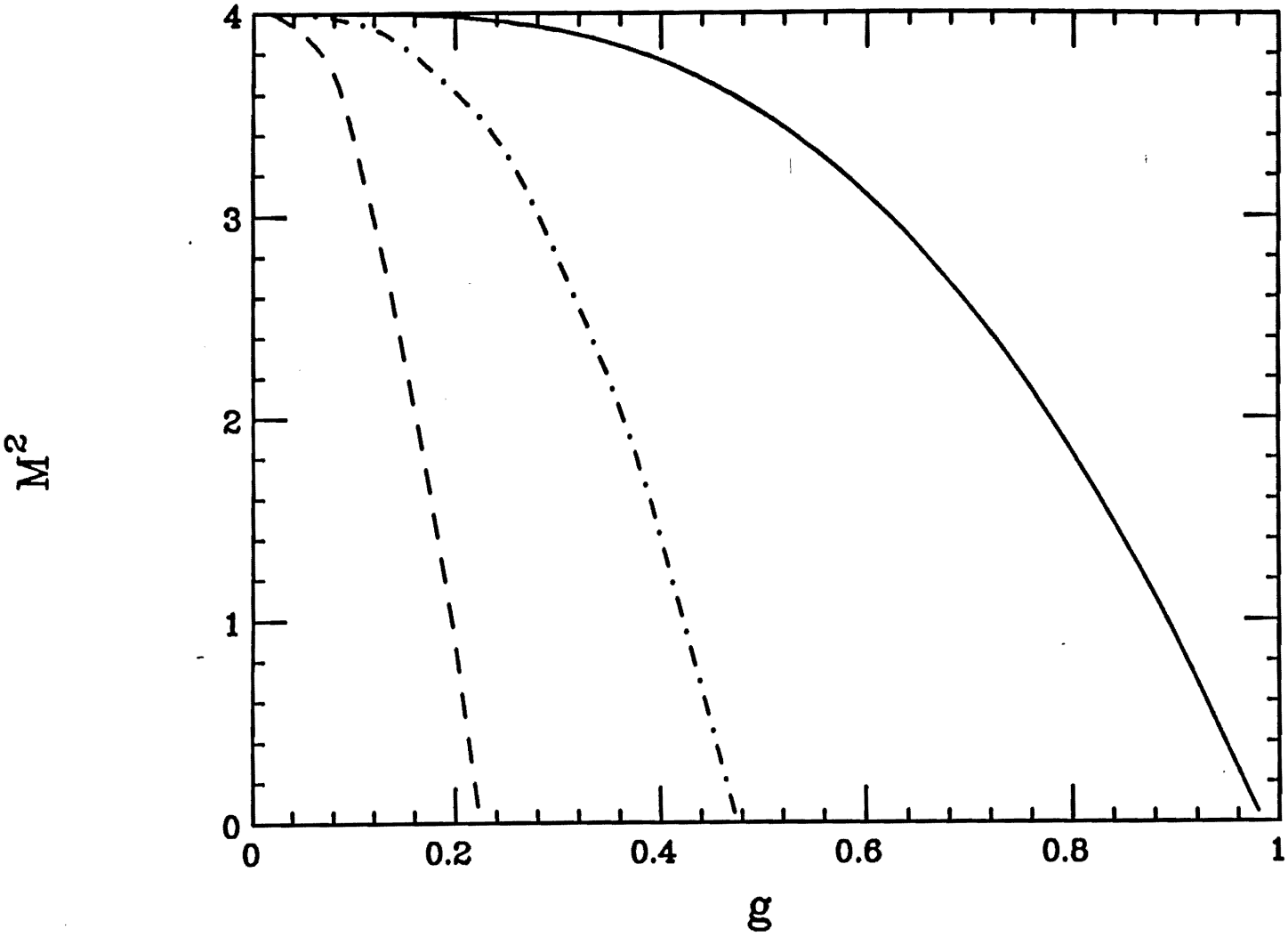

Figure 2

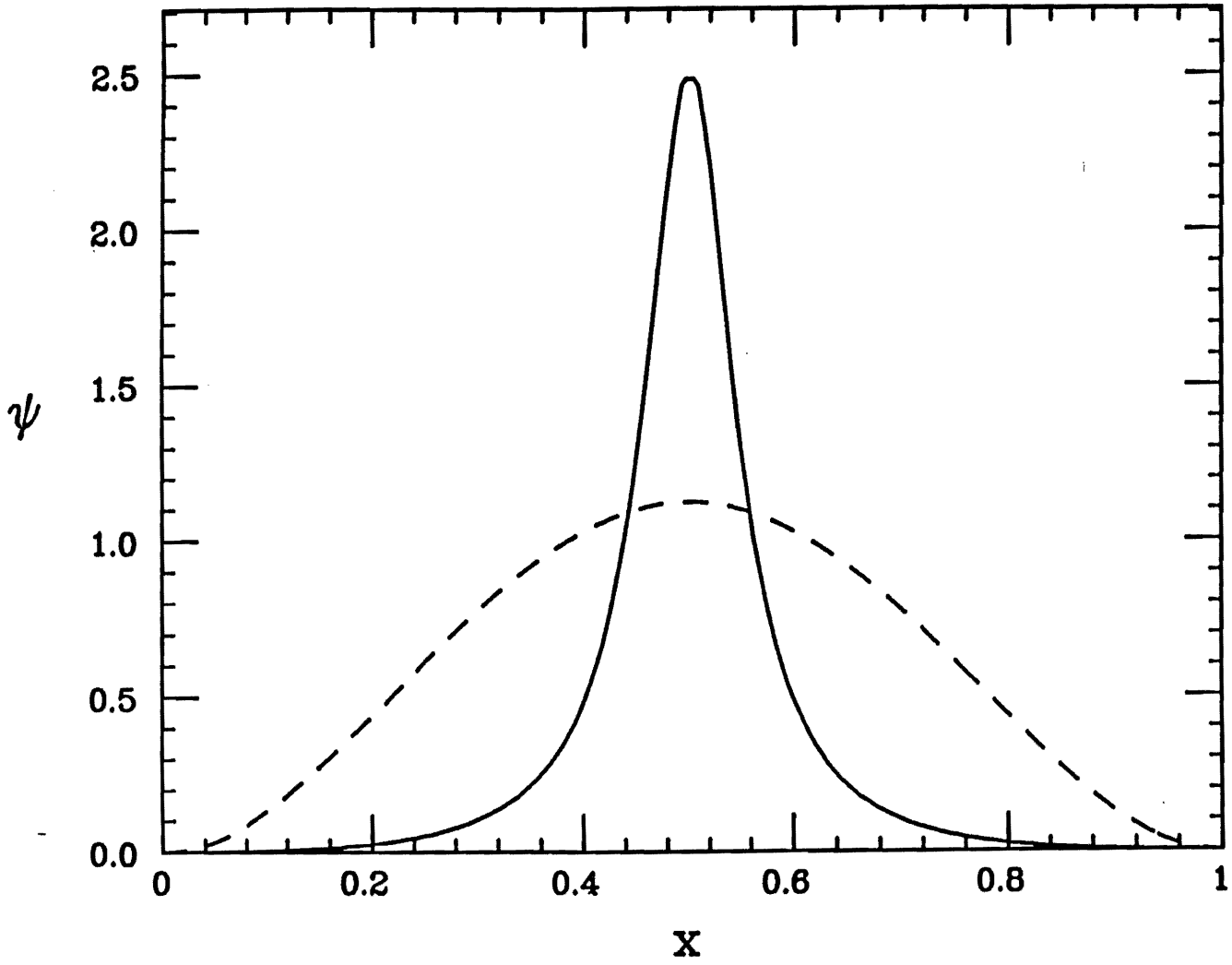

Figure 3a

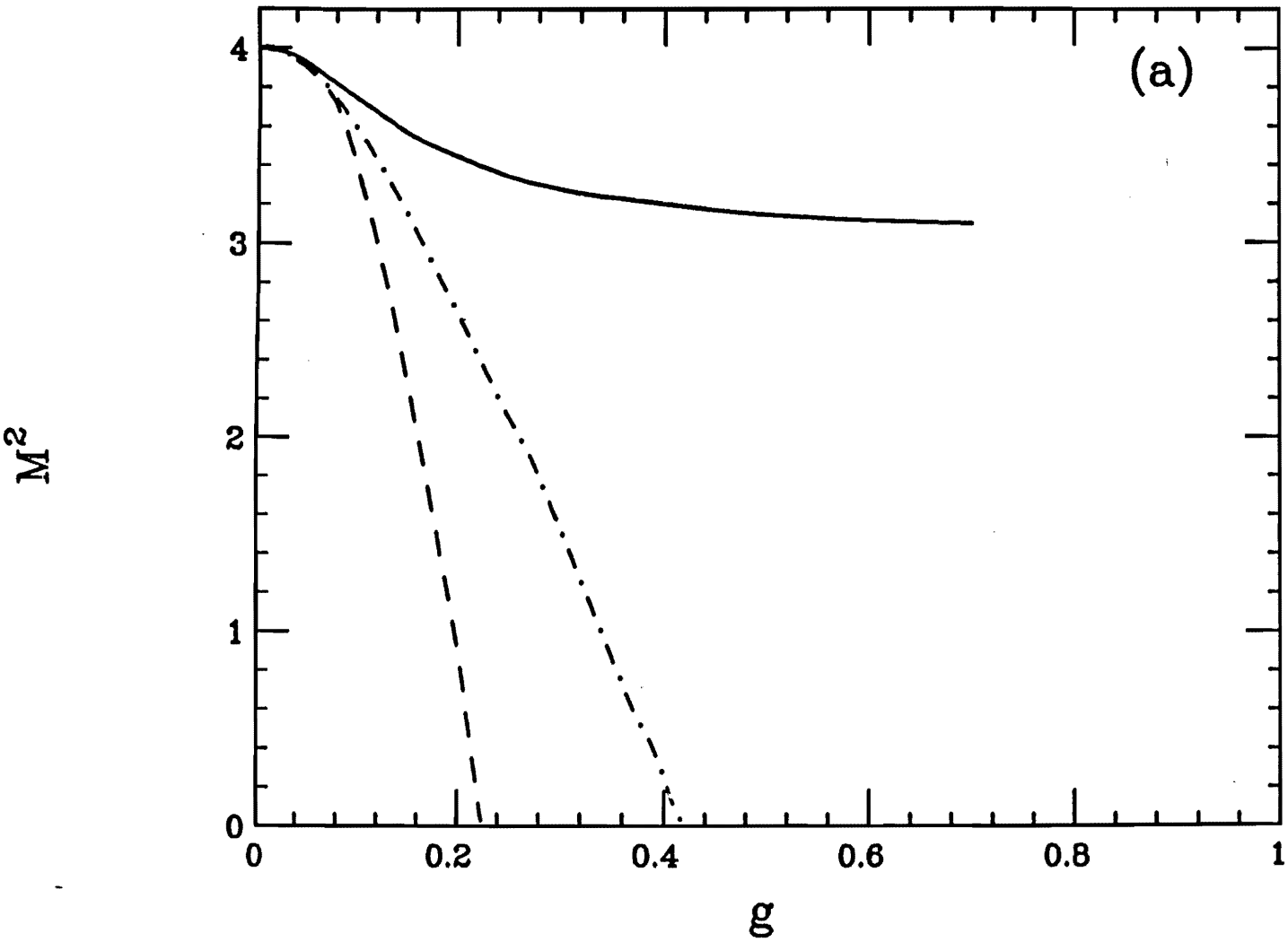

Figure 3b

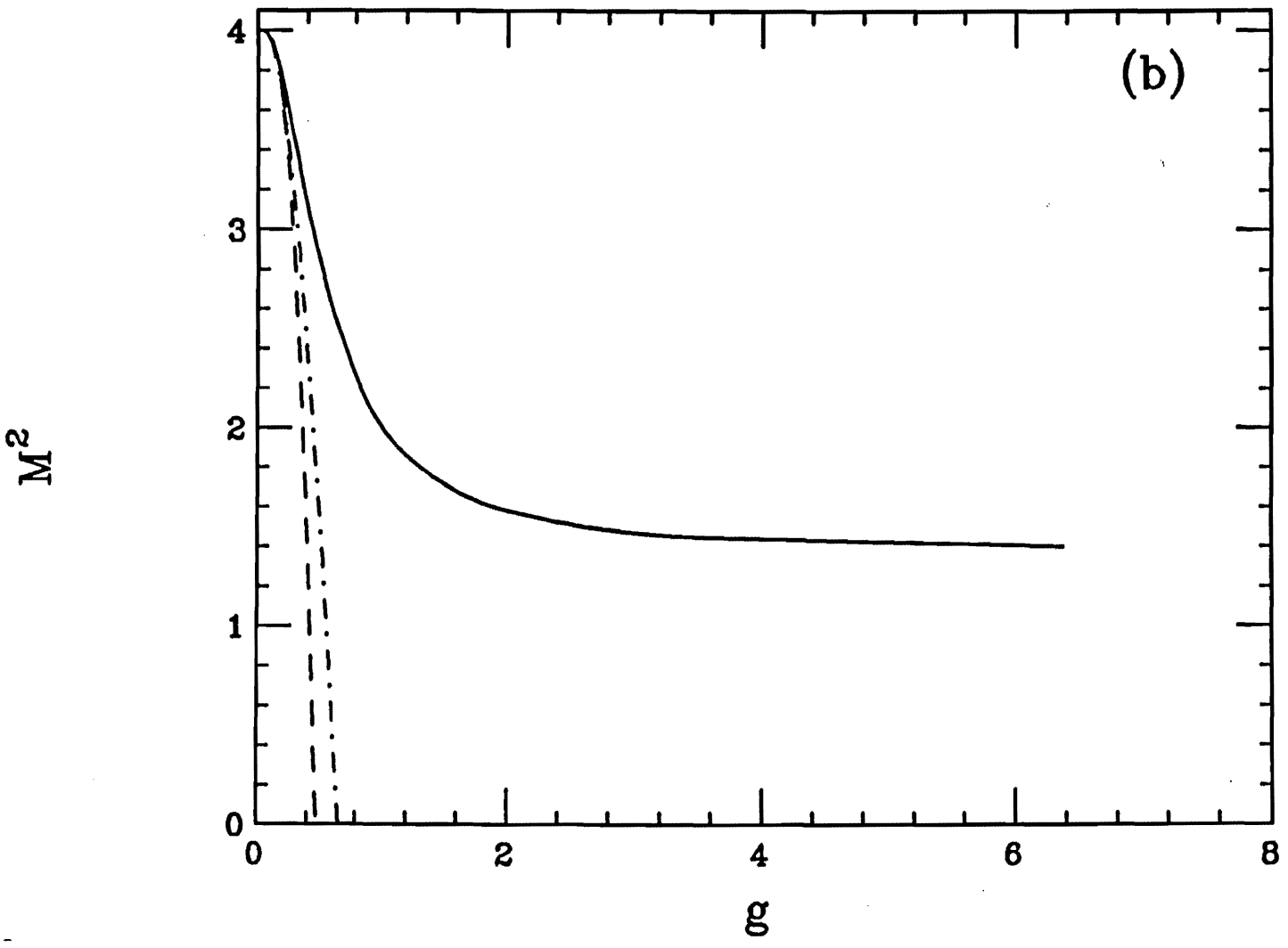

Figure 3c

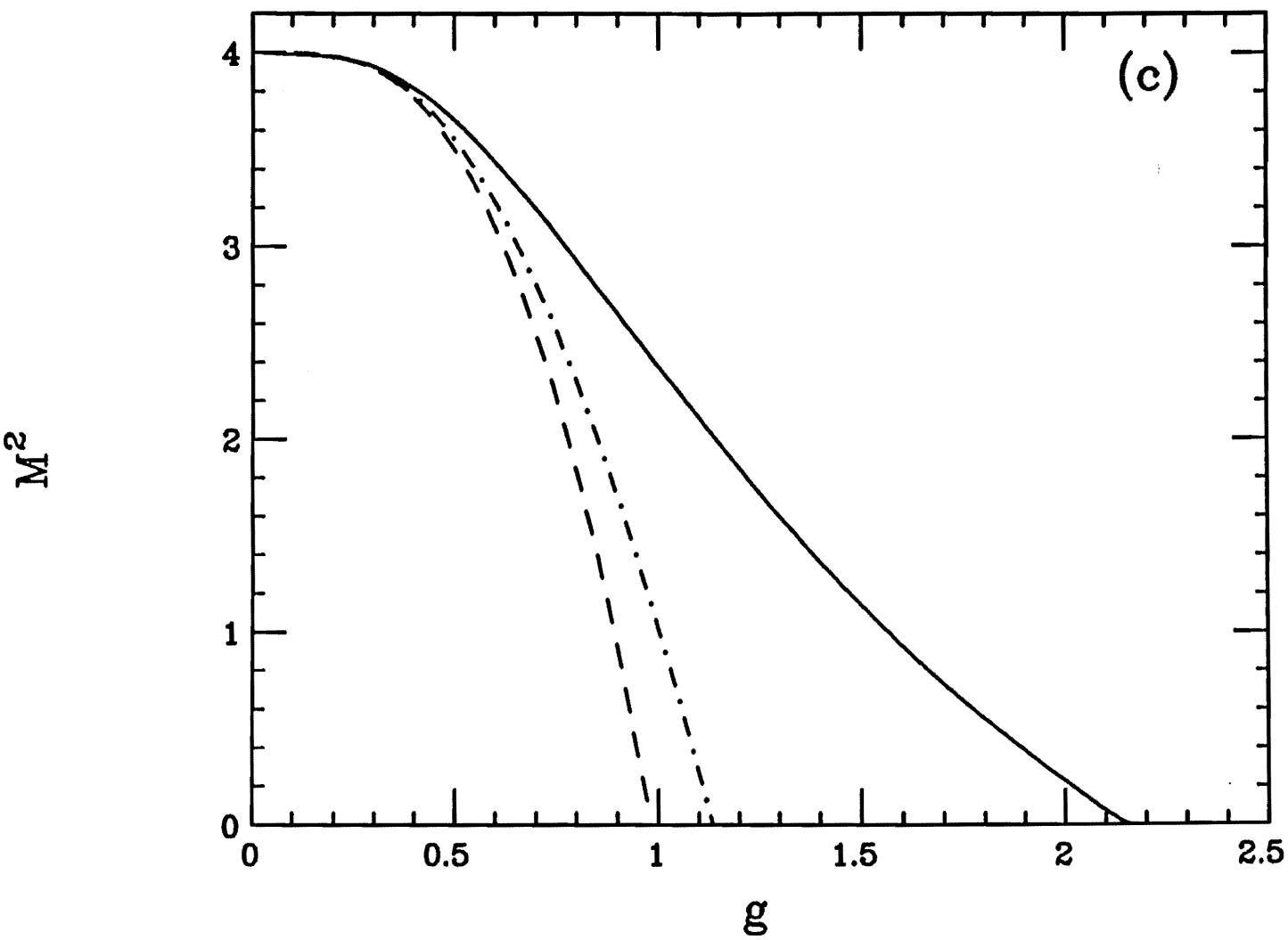

Figure 4a

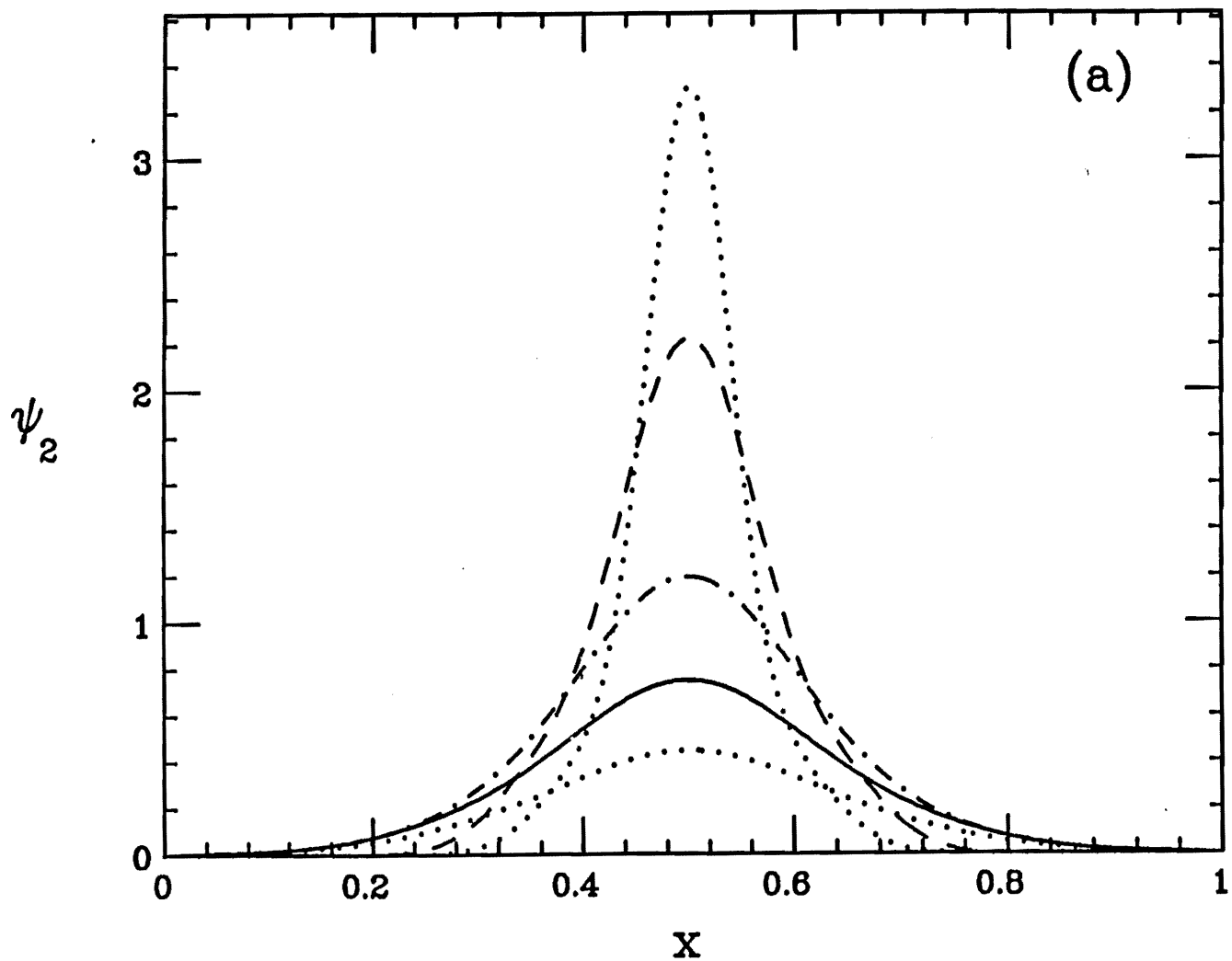

Figure 4b

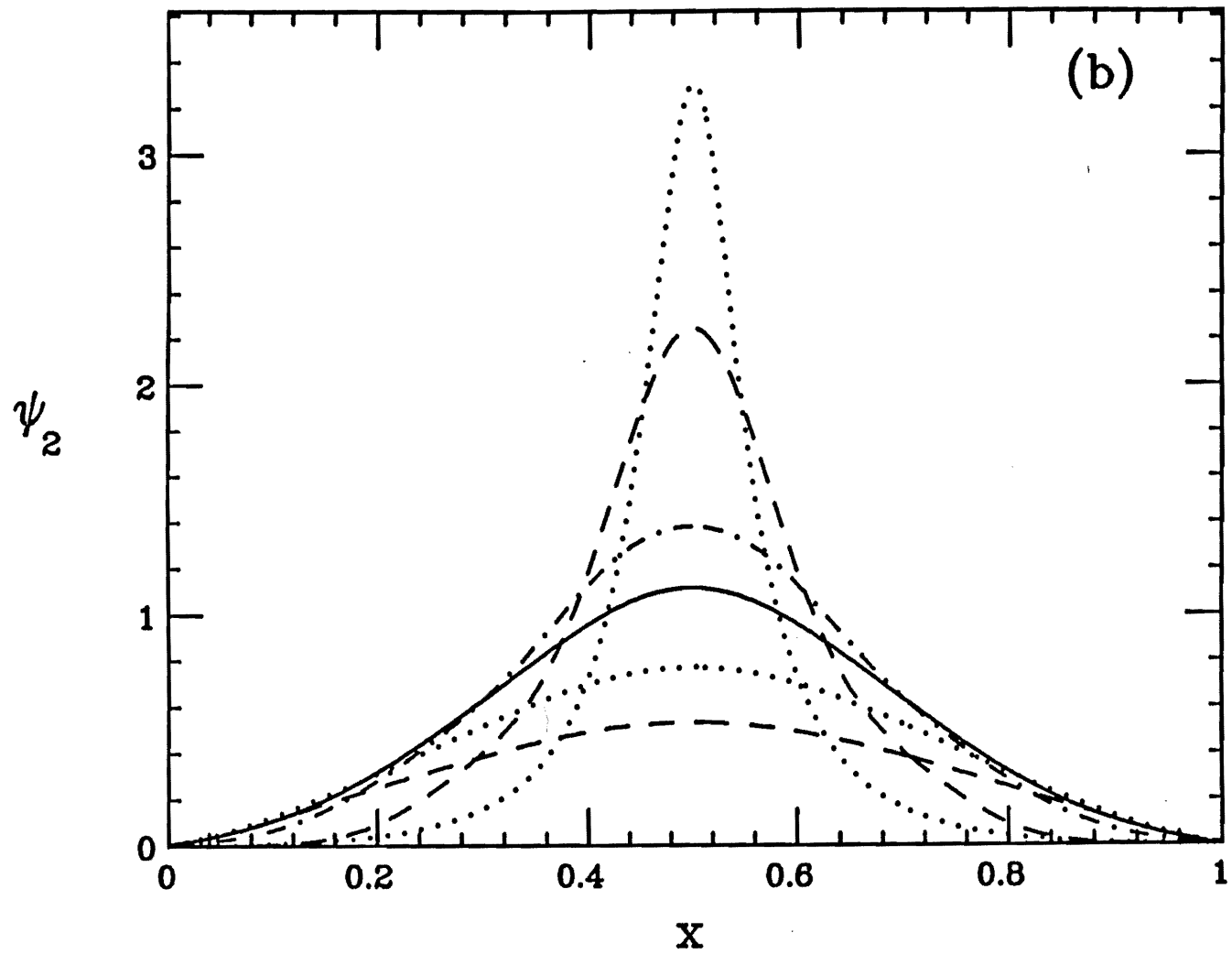

Figure 4c

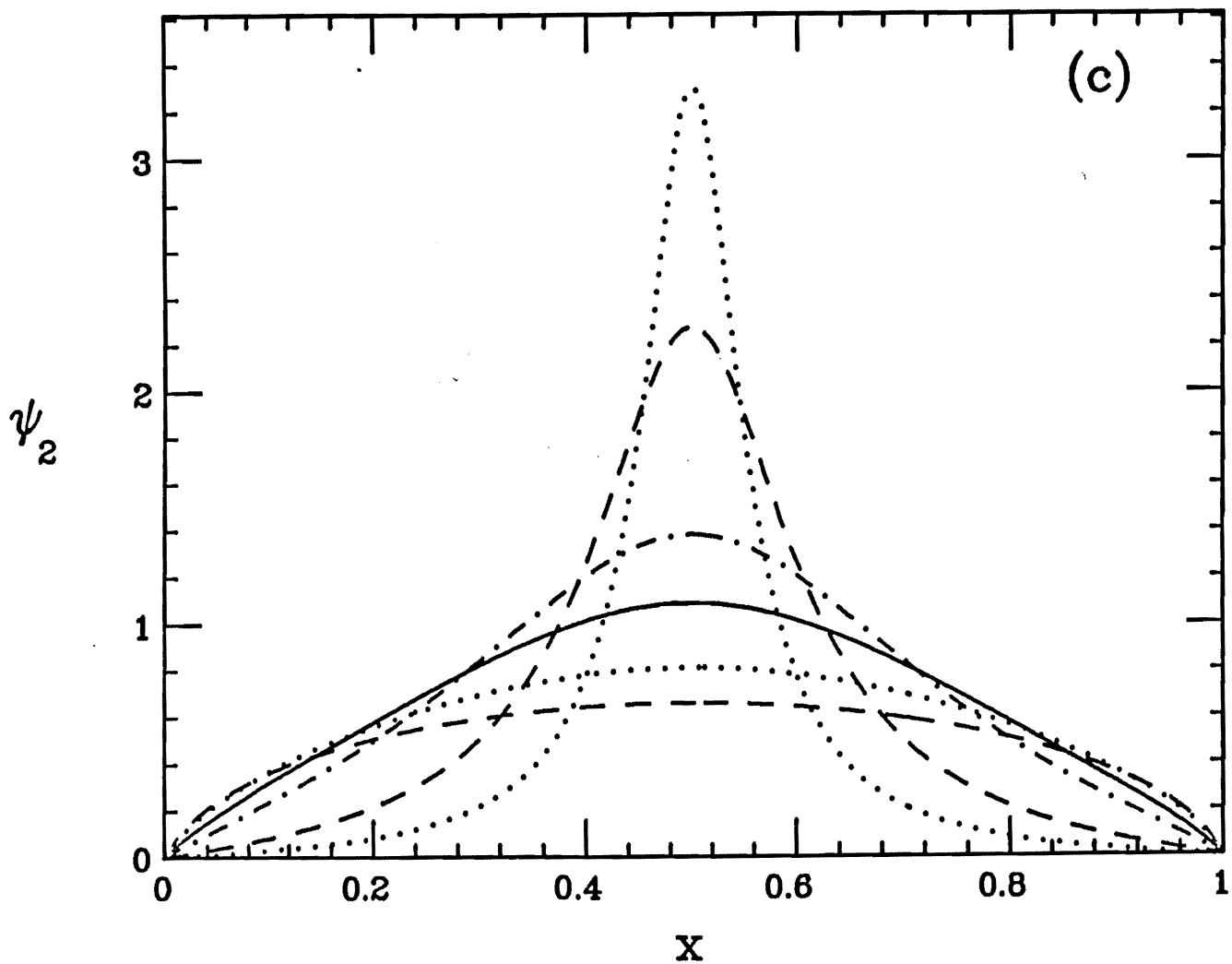

Figure 5a

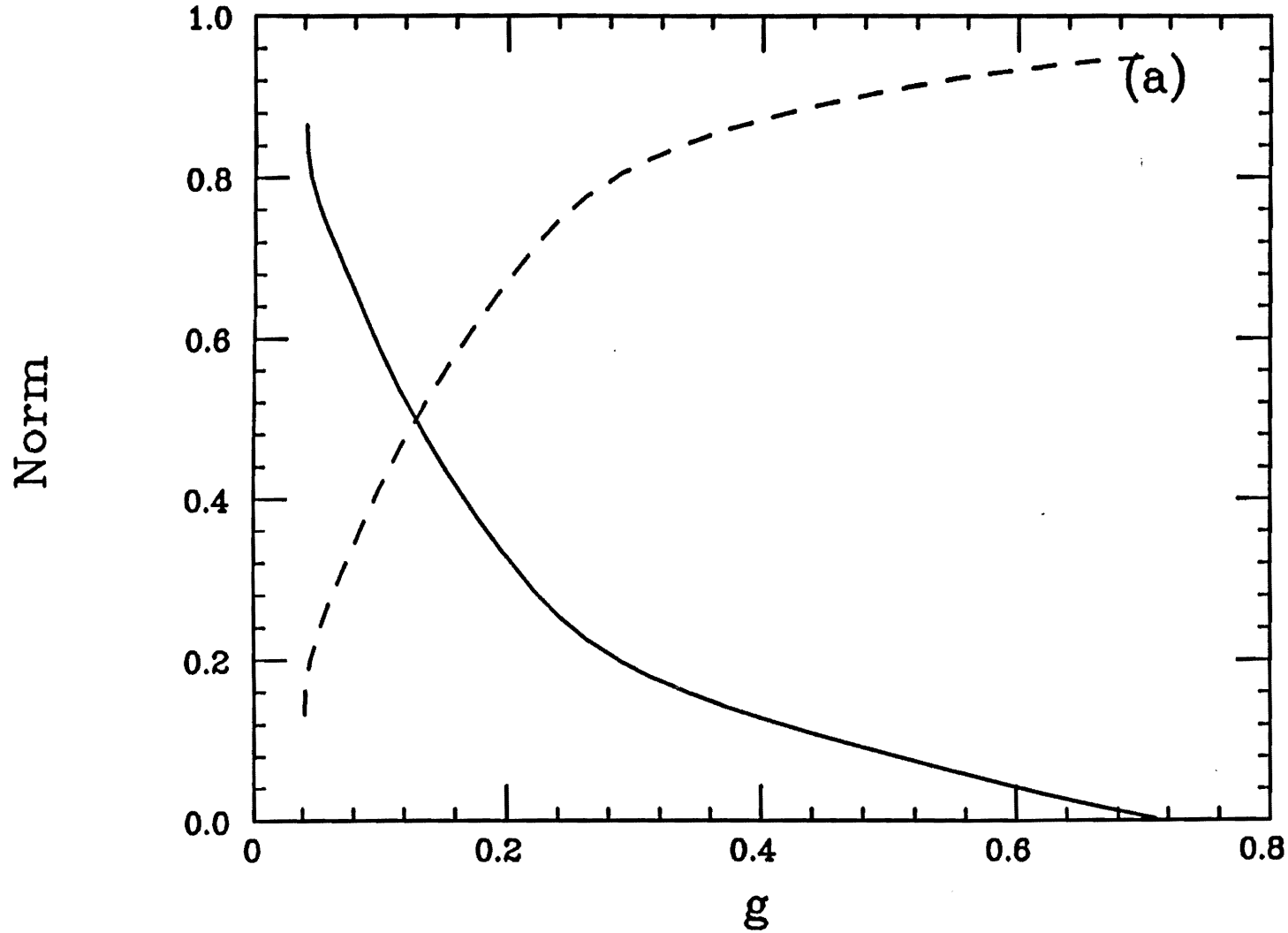

Figure 5b

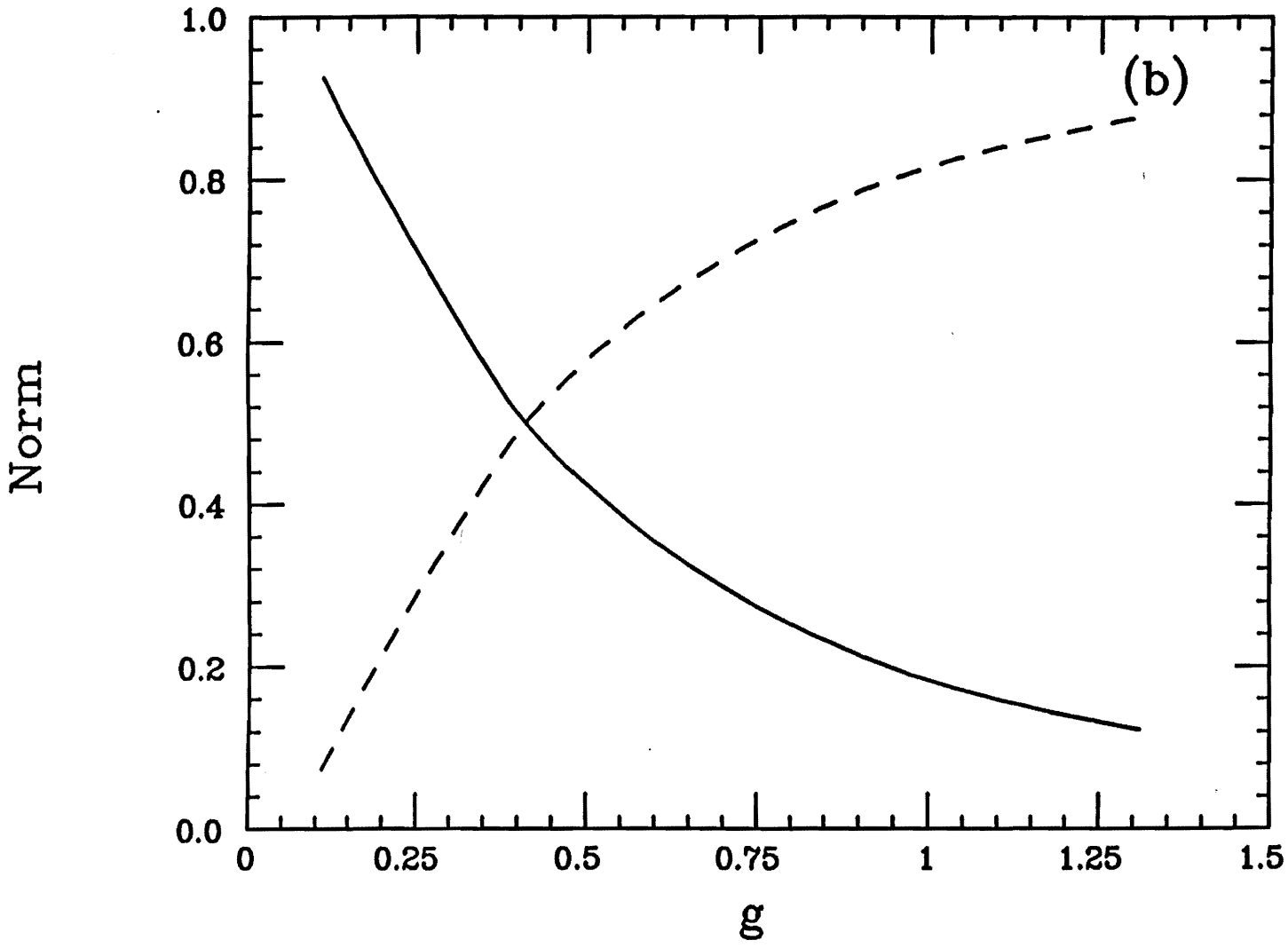

Figure 5c

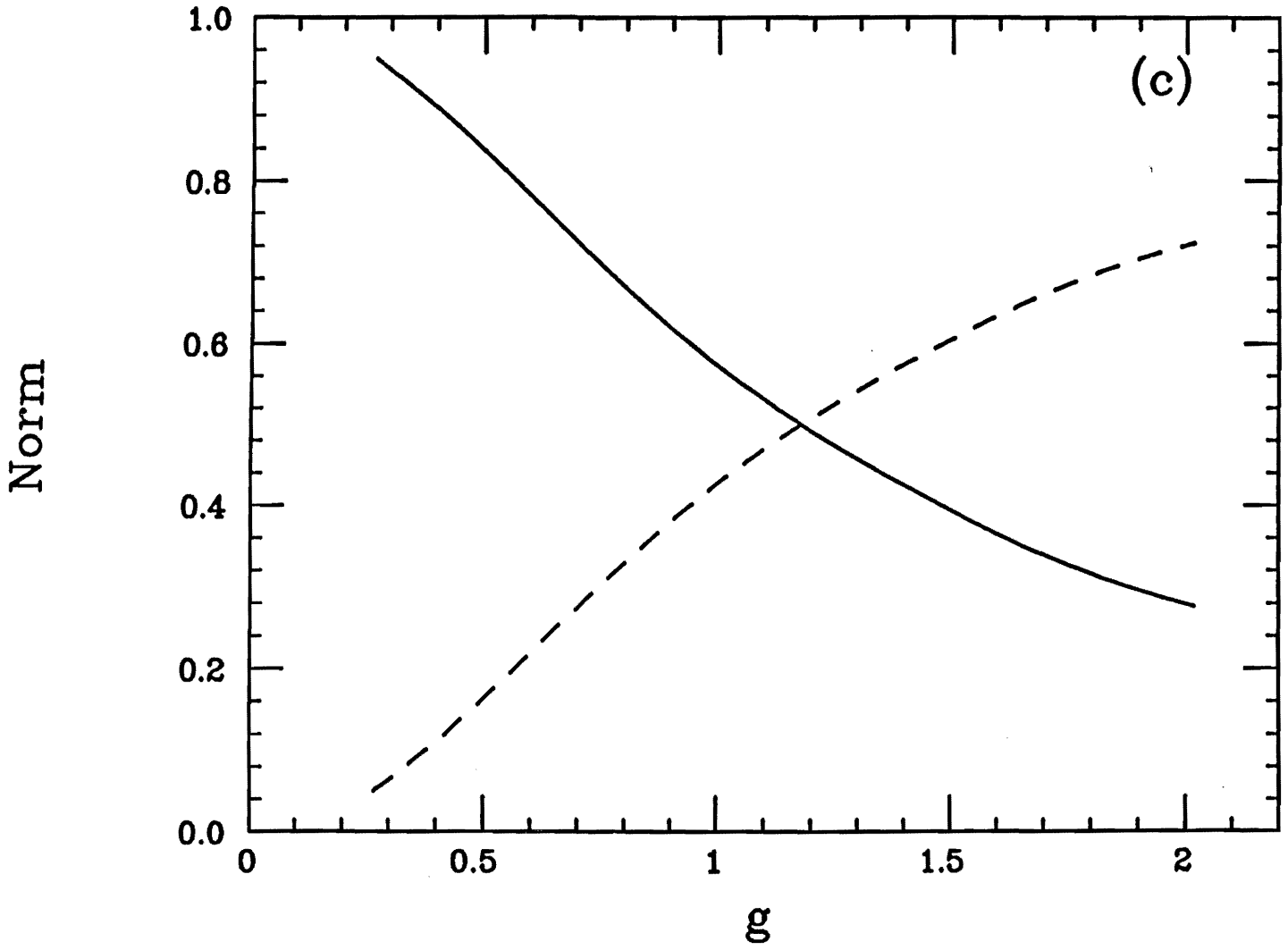

Figure 6a

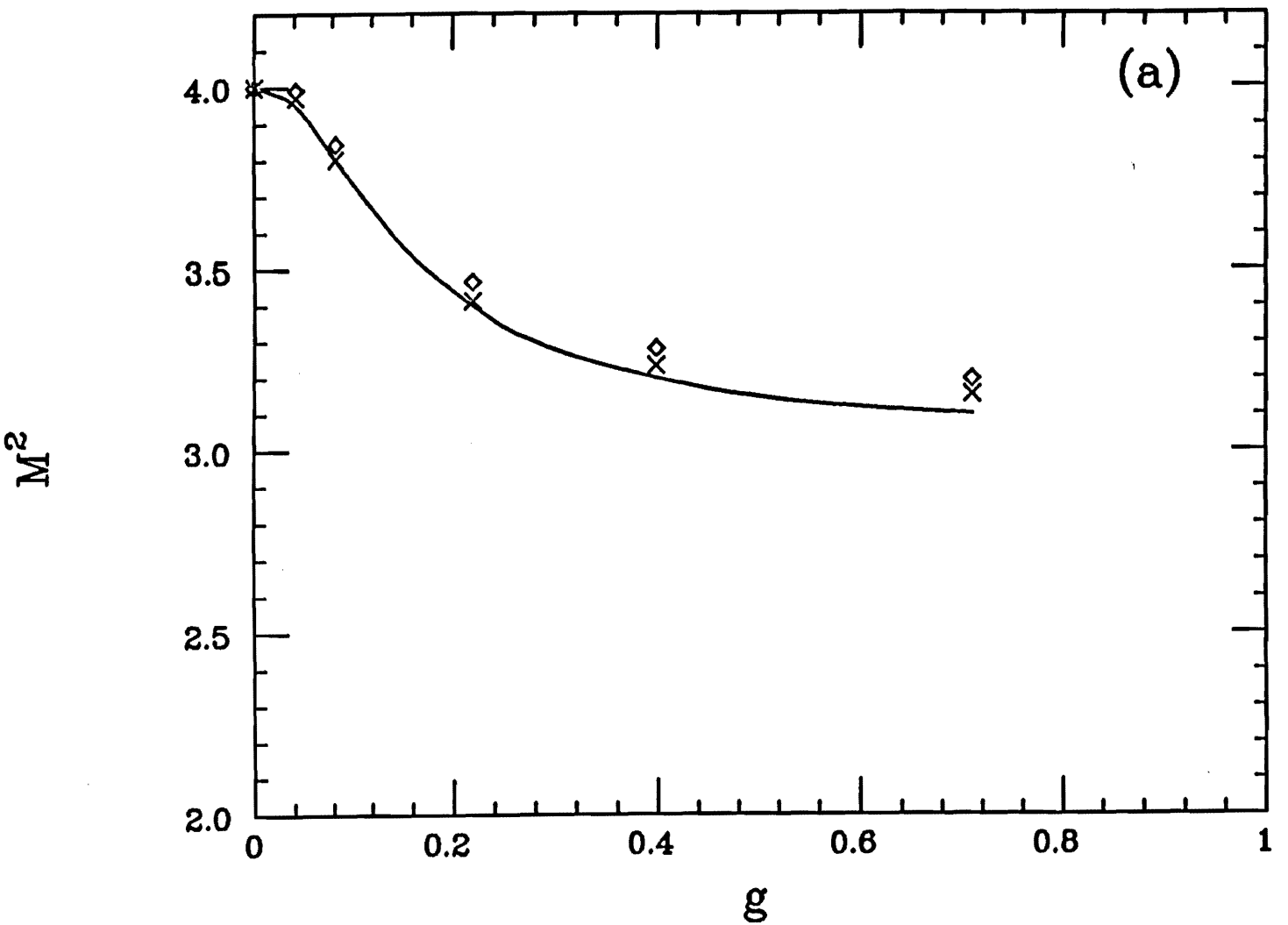

Figure 6b

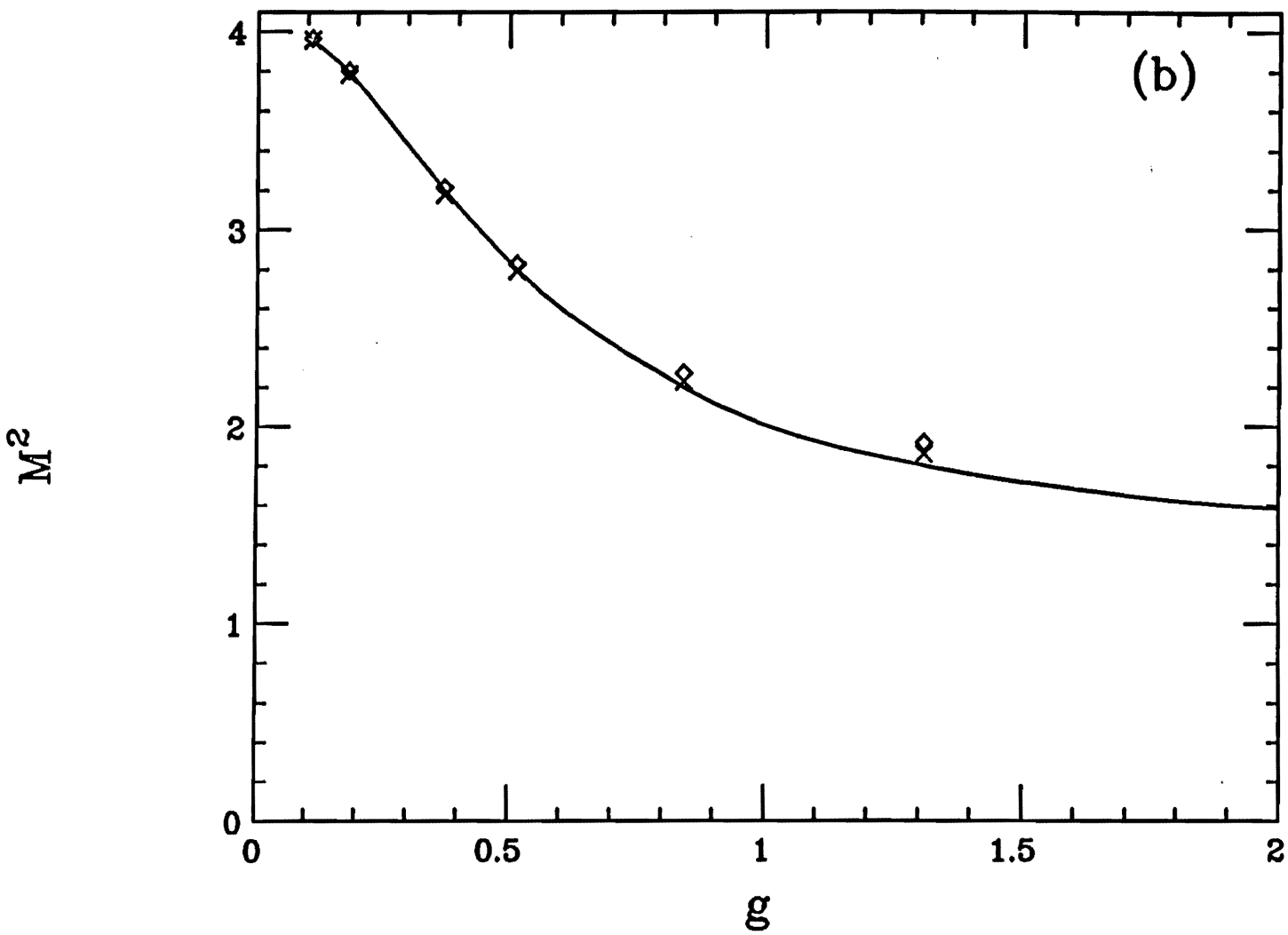

Figure 6c

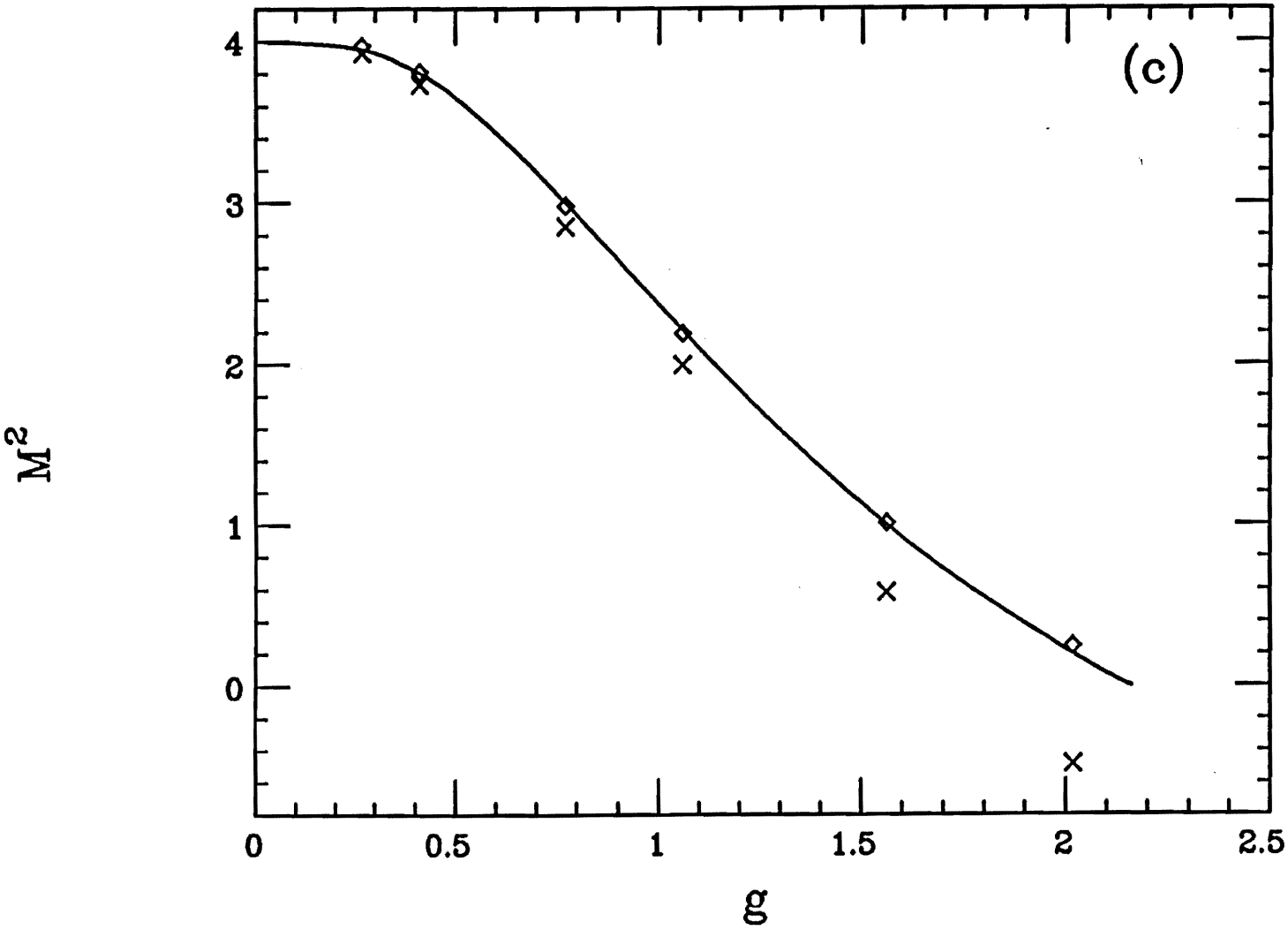

Figure 7

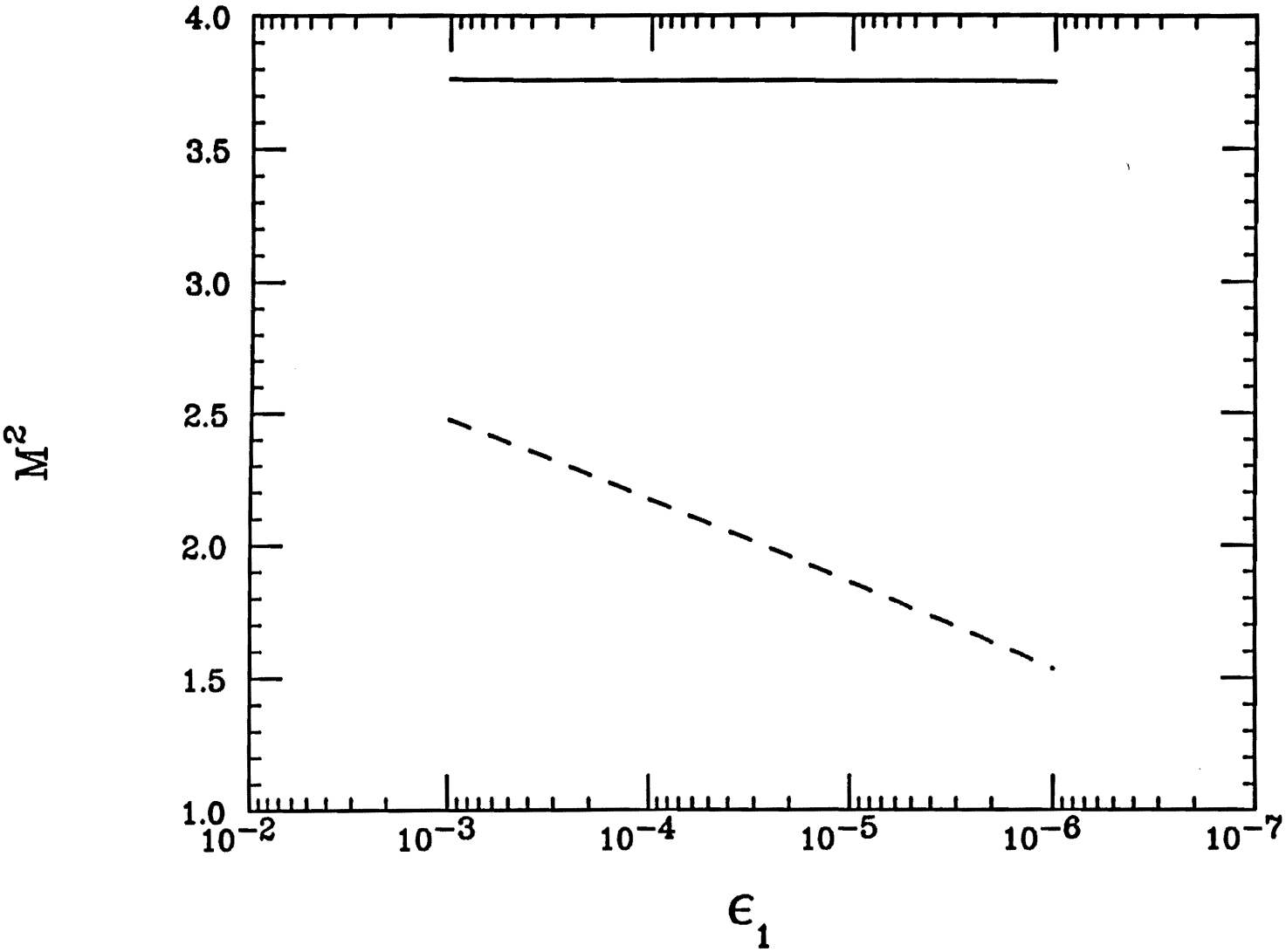

Figure 8a

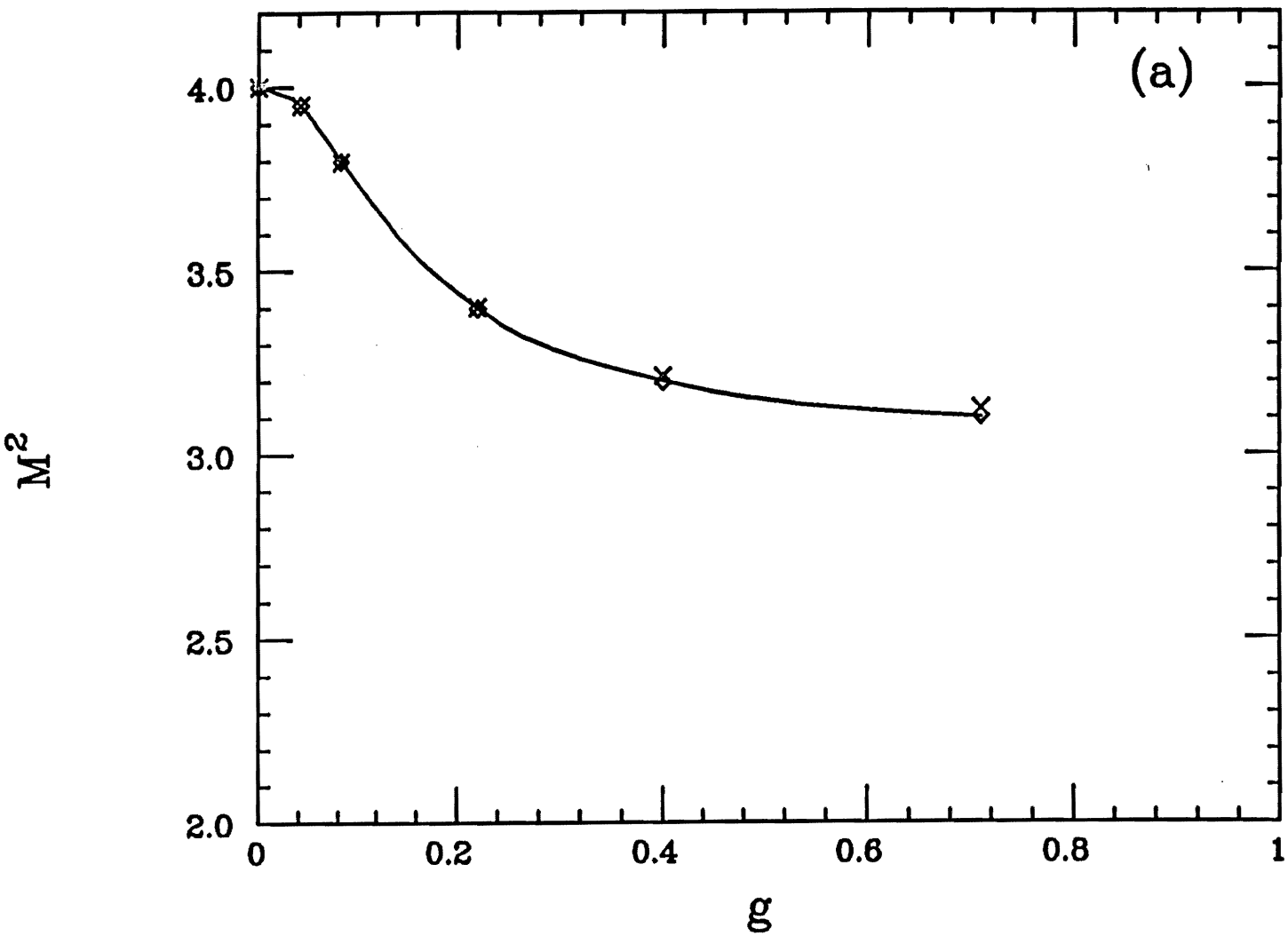

Figure 8b

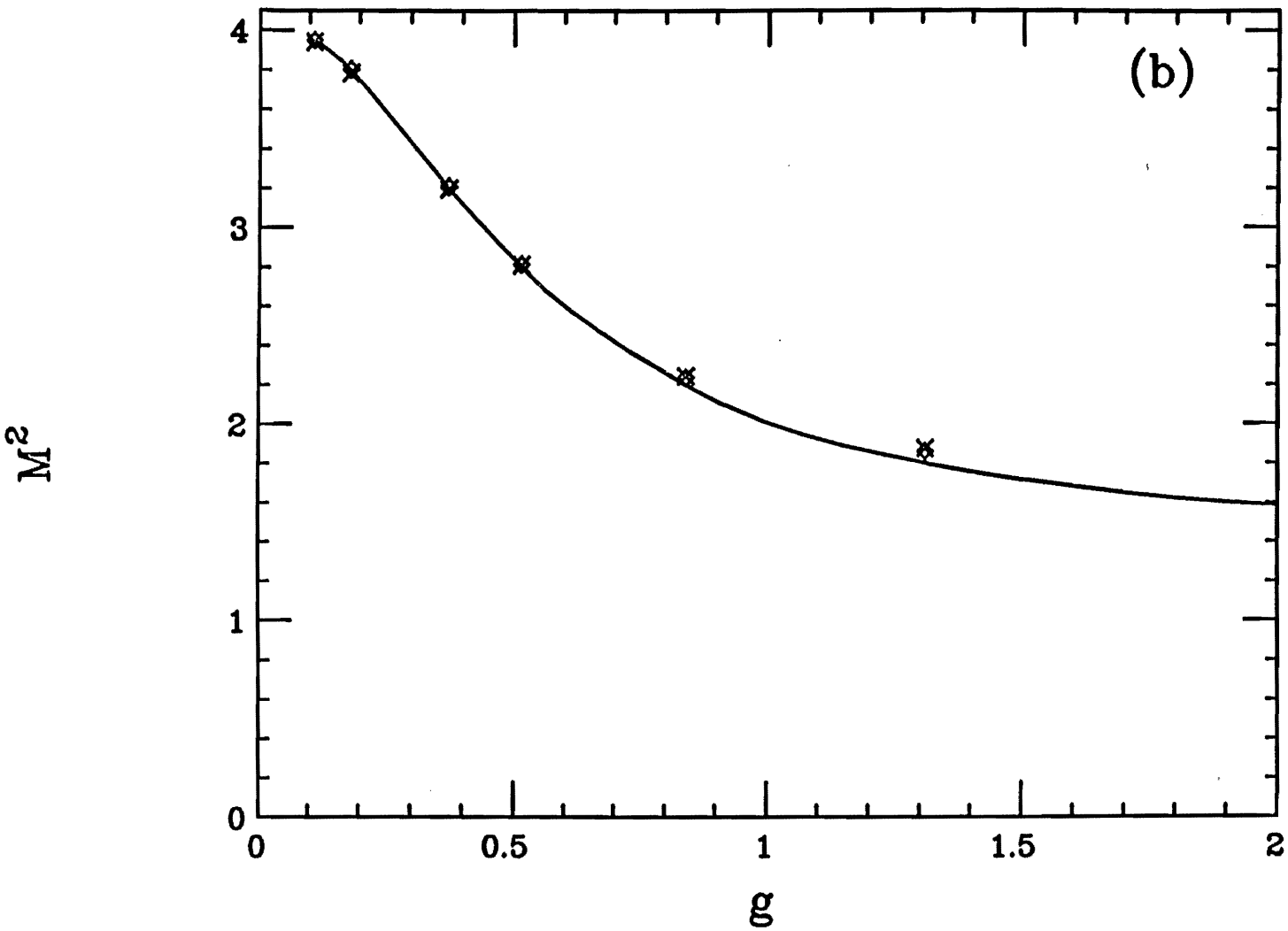

Figure 8c

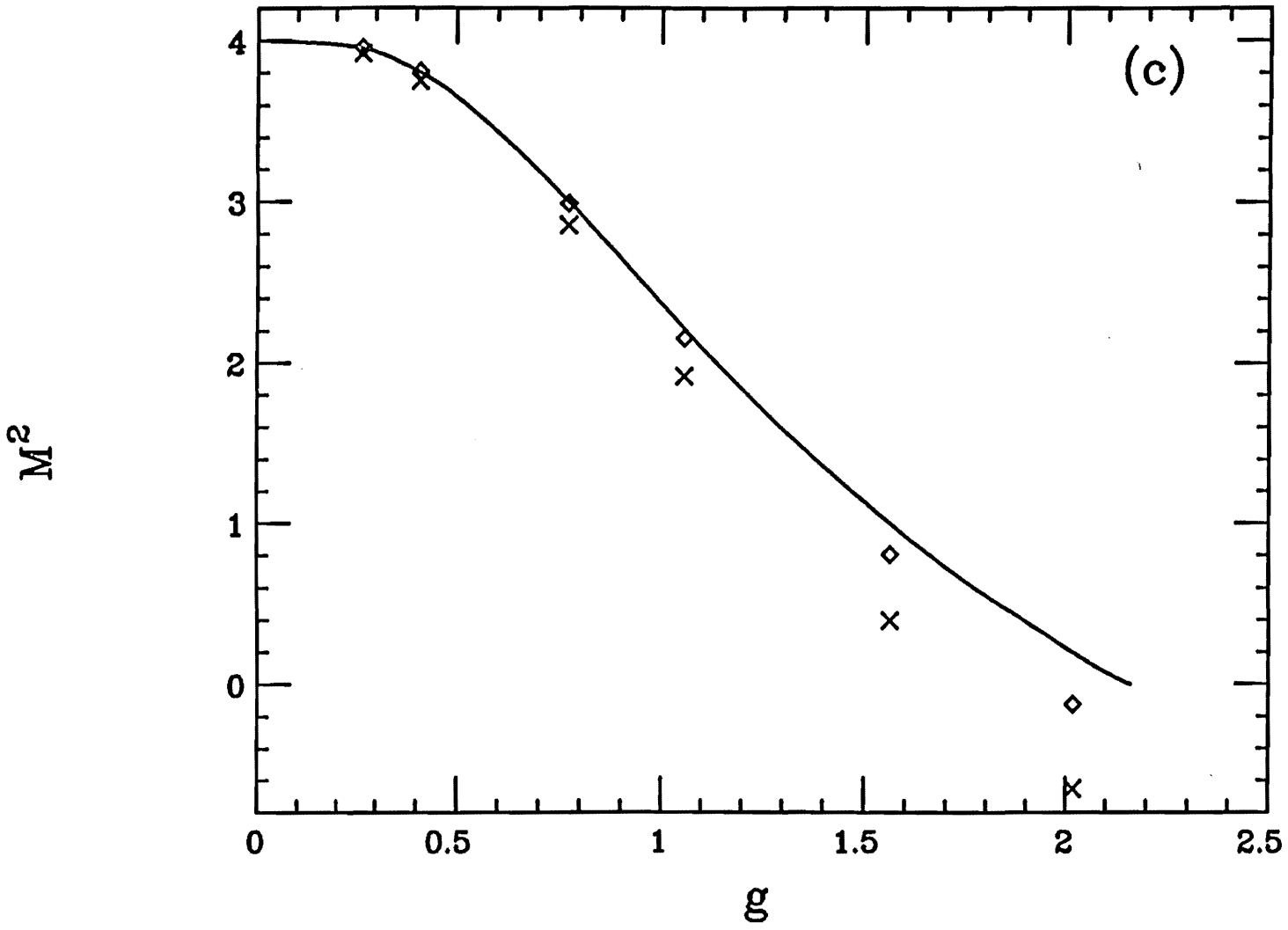

Figure 9a

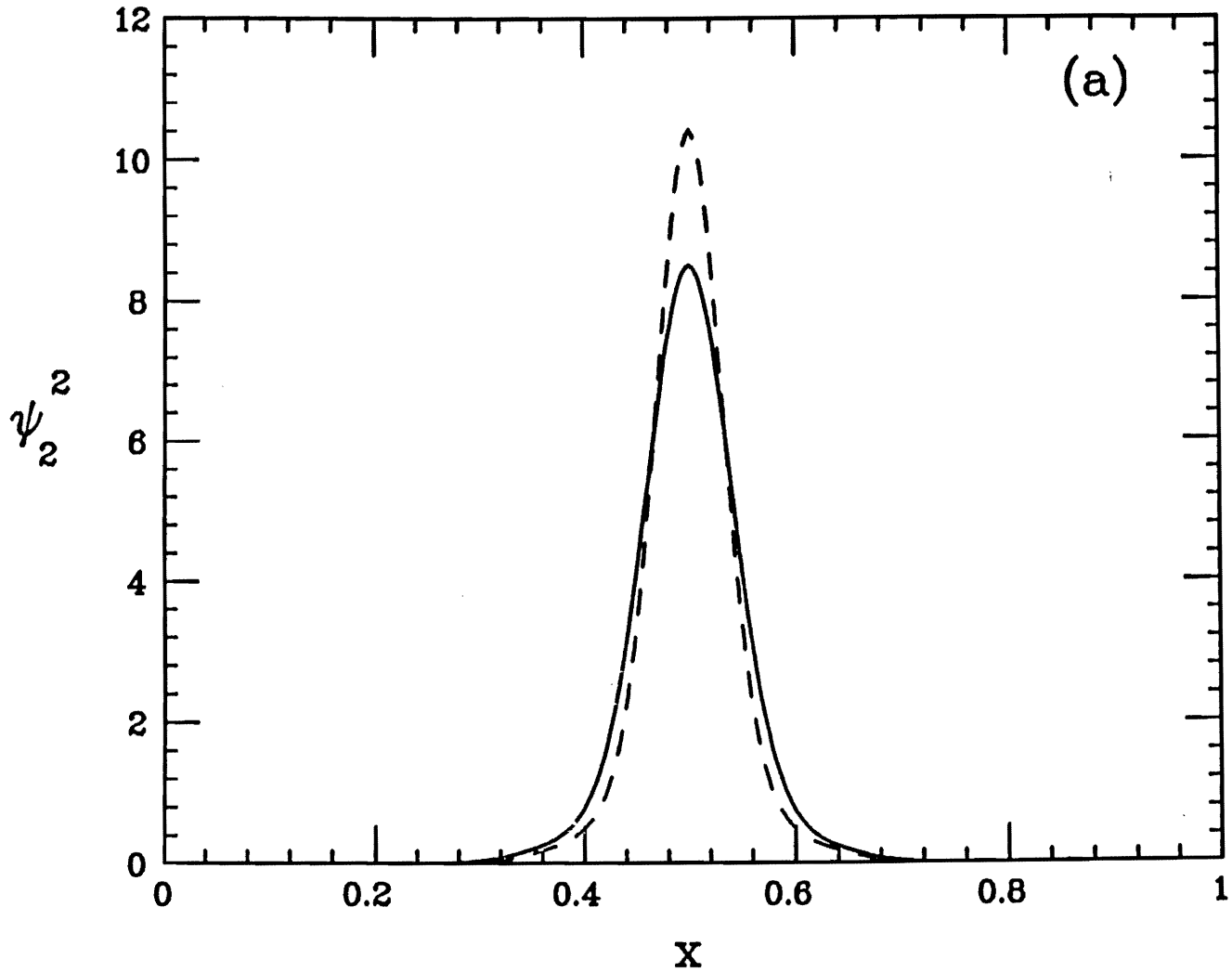

Figure 9b

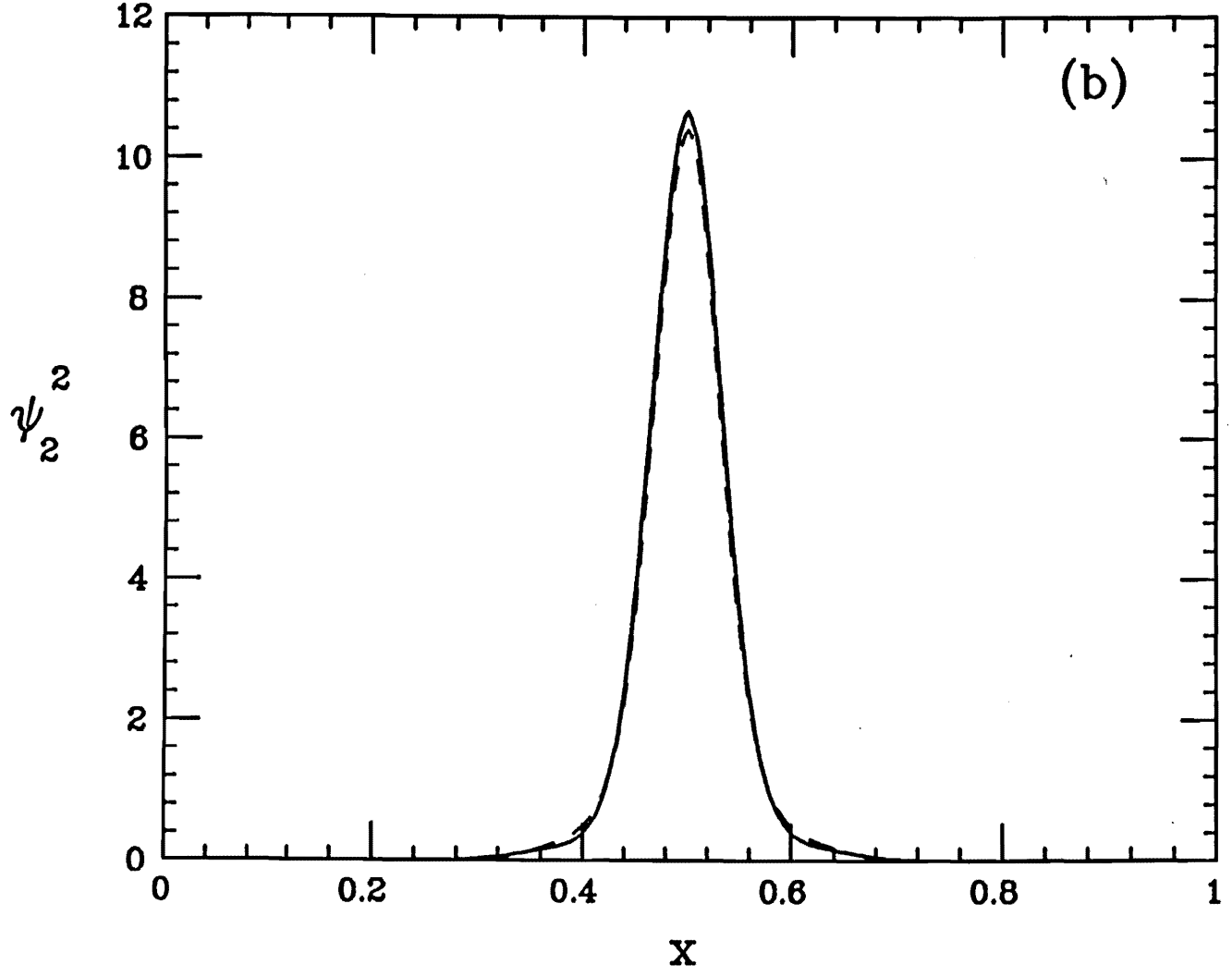

Figure 10a

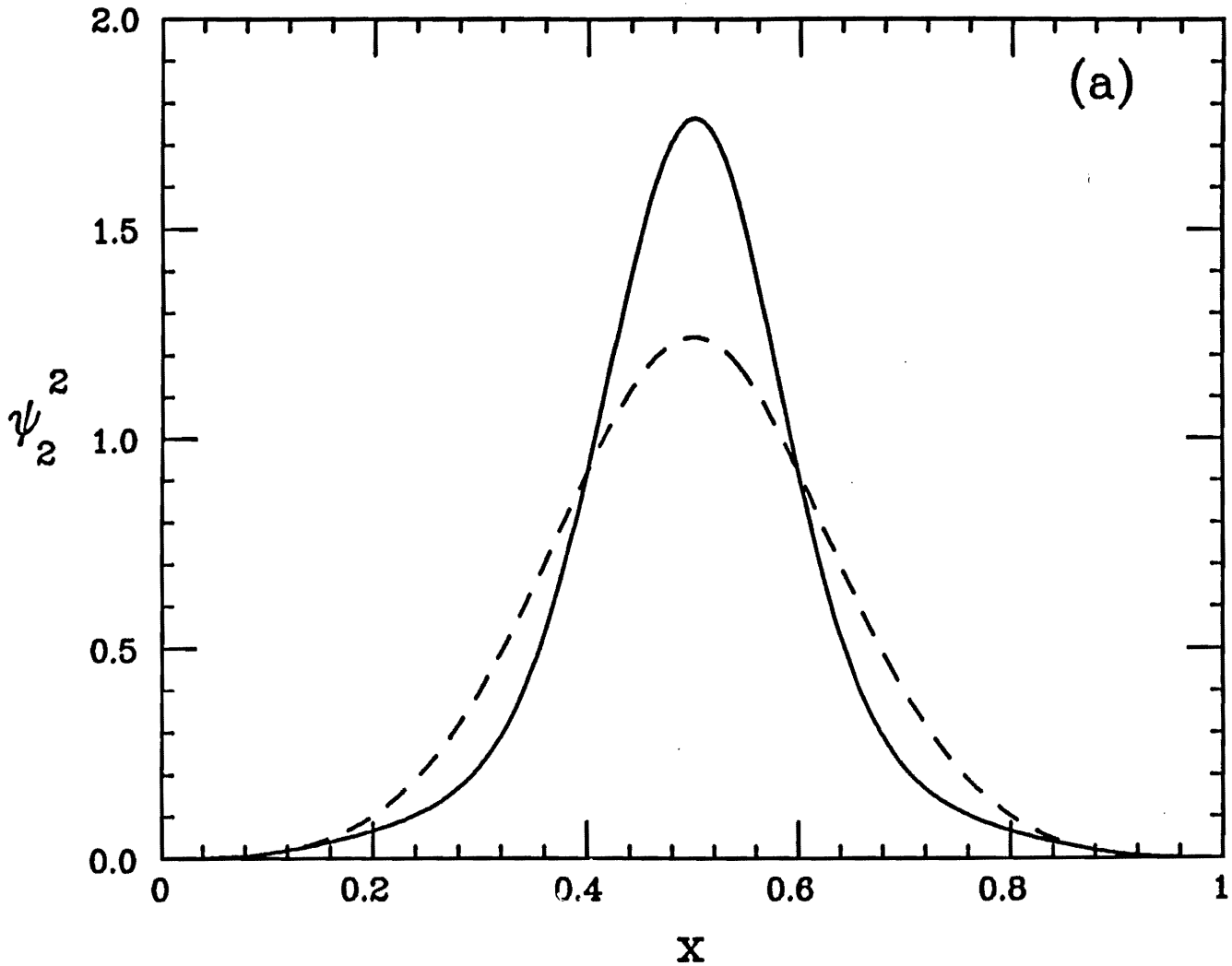

Figure 10b

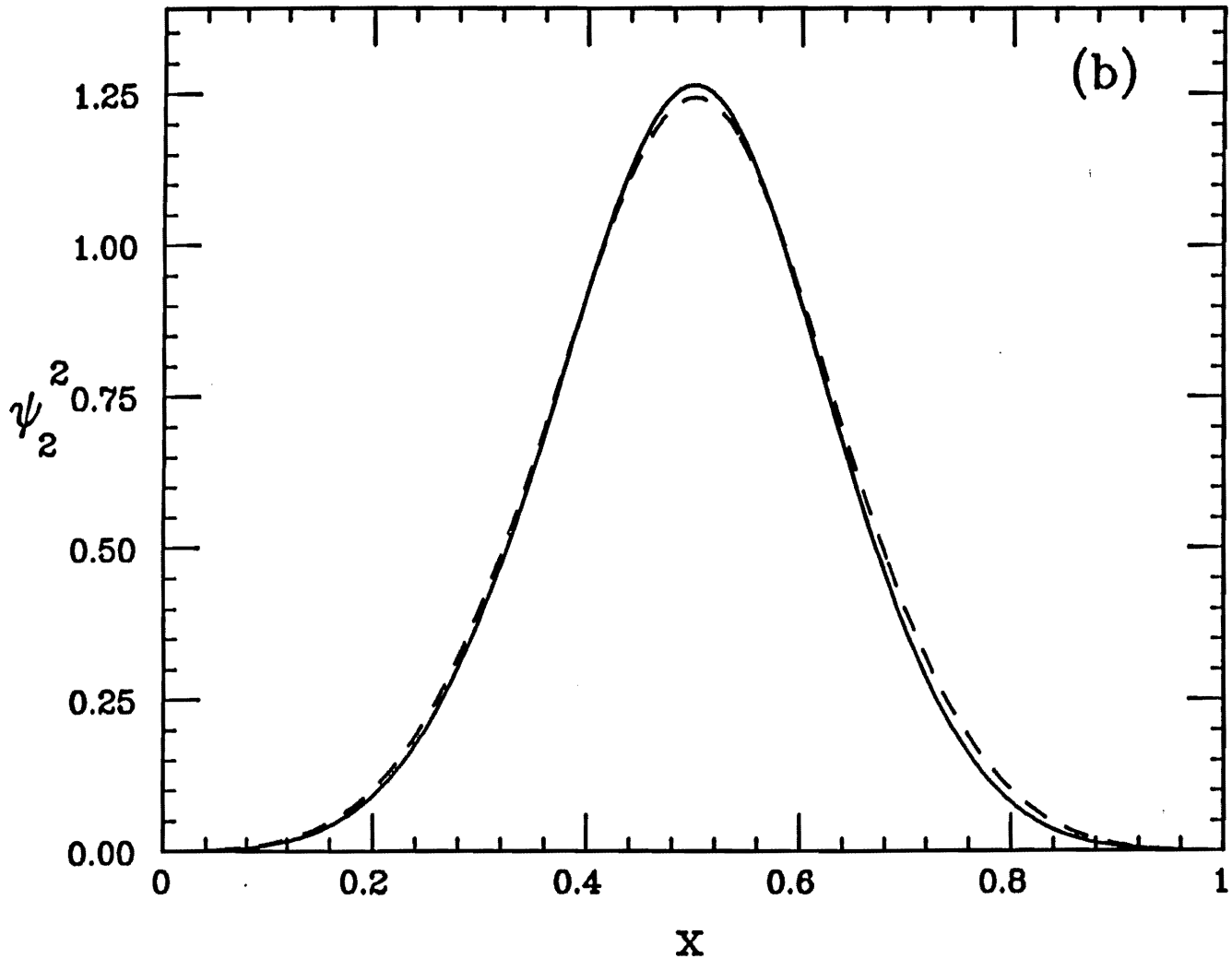

Figure 10c

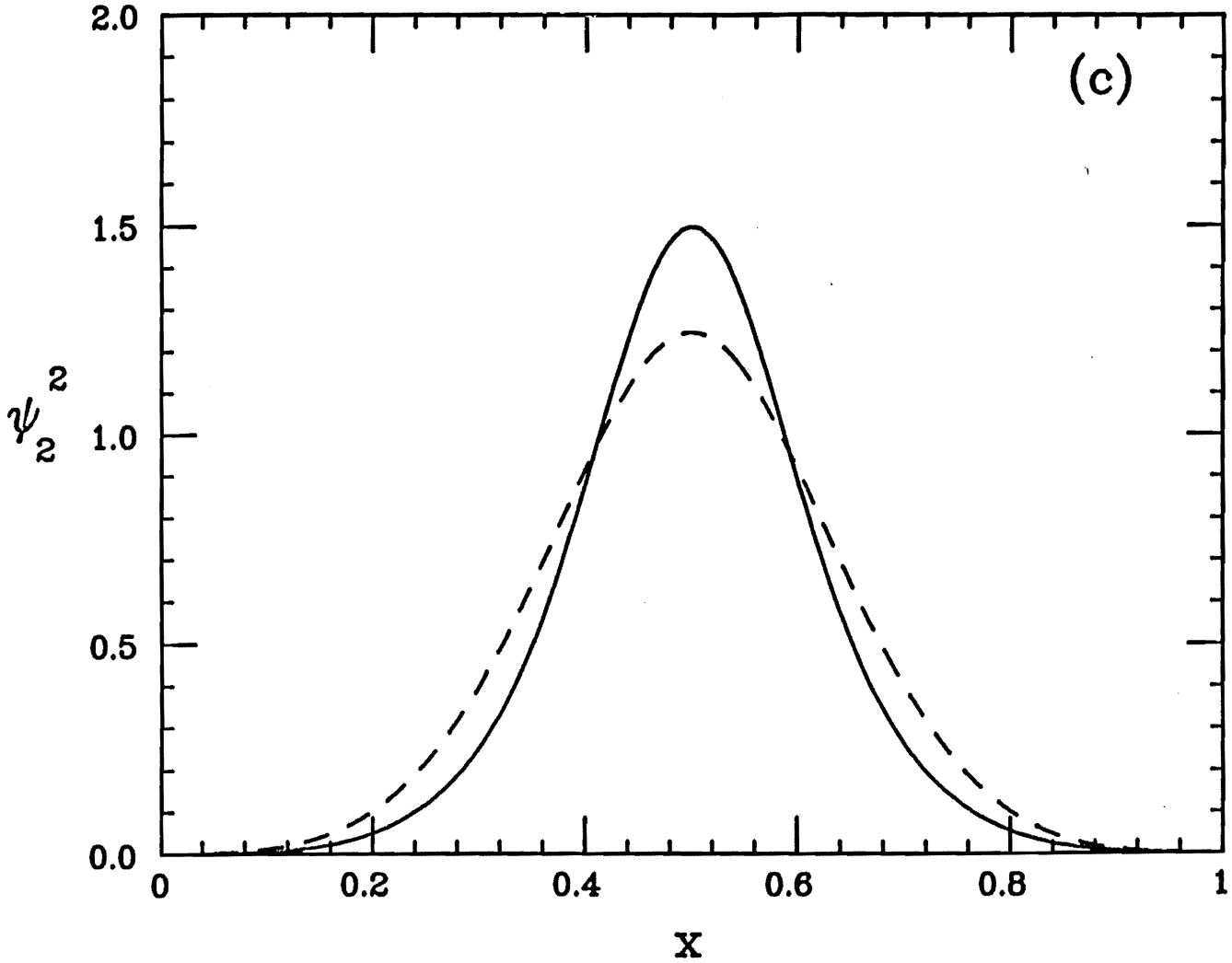

Figure 11a

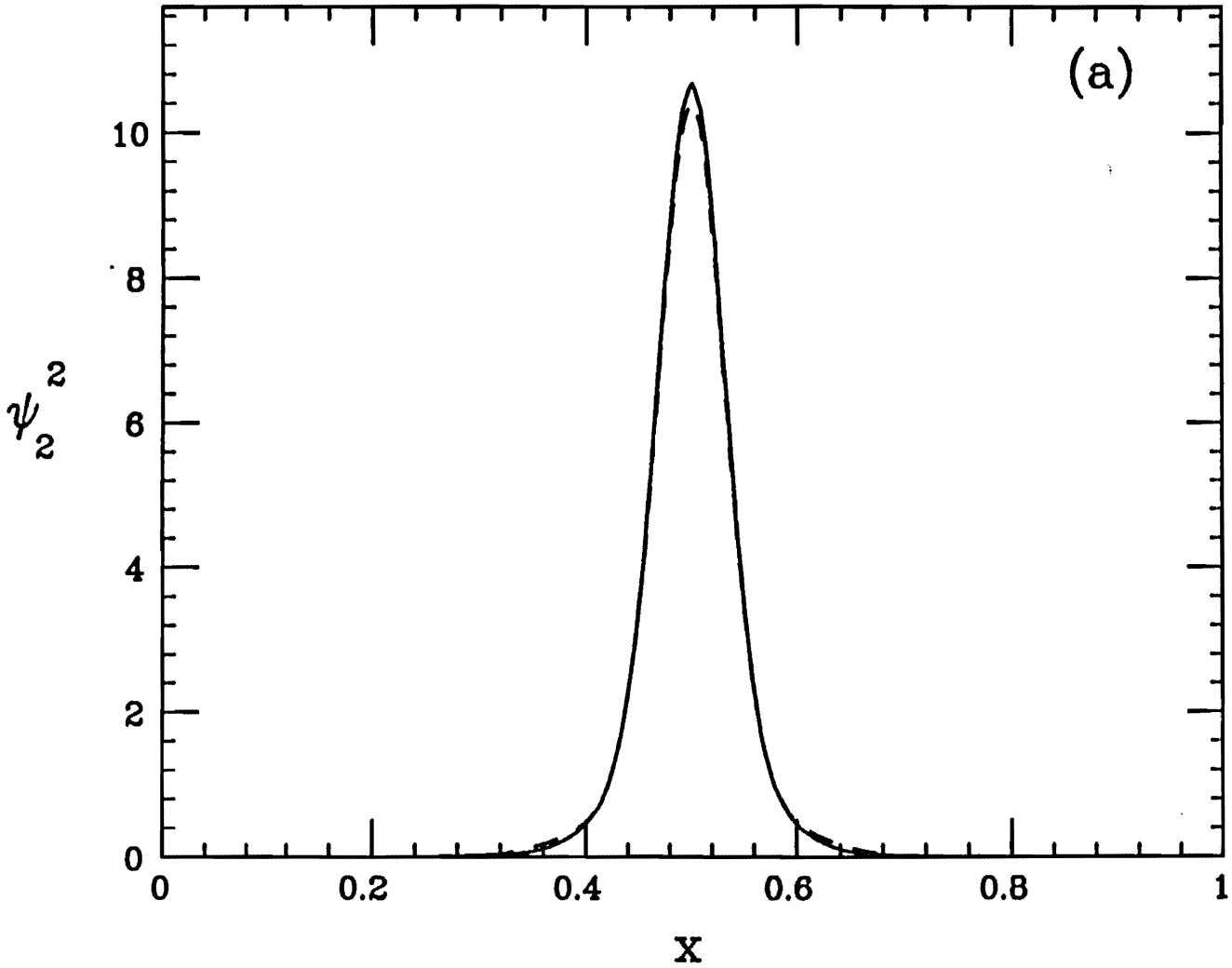

Figure 11b

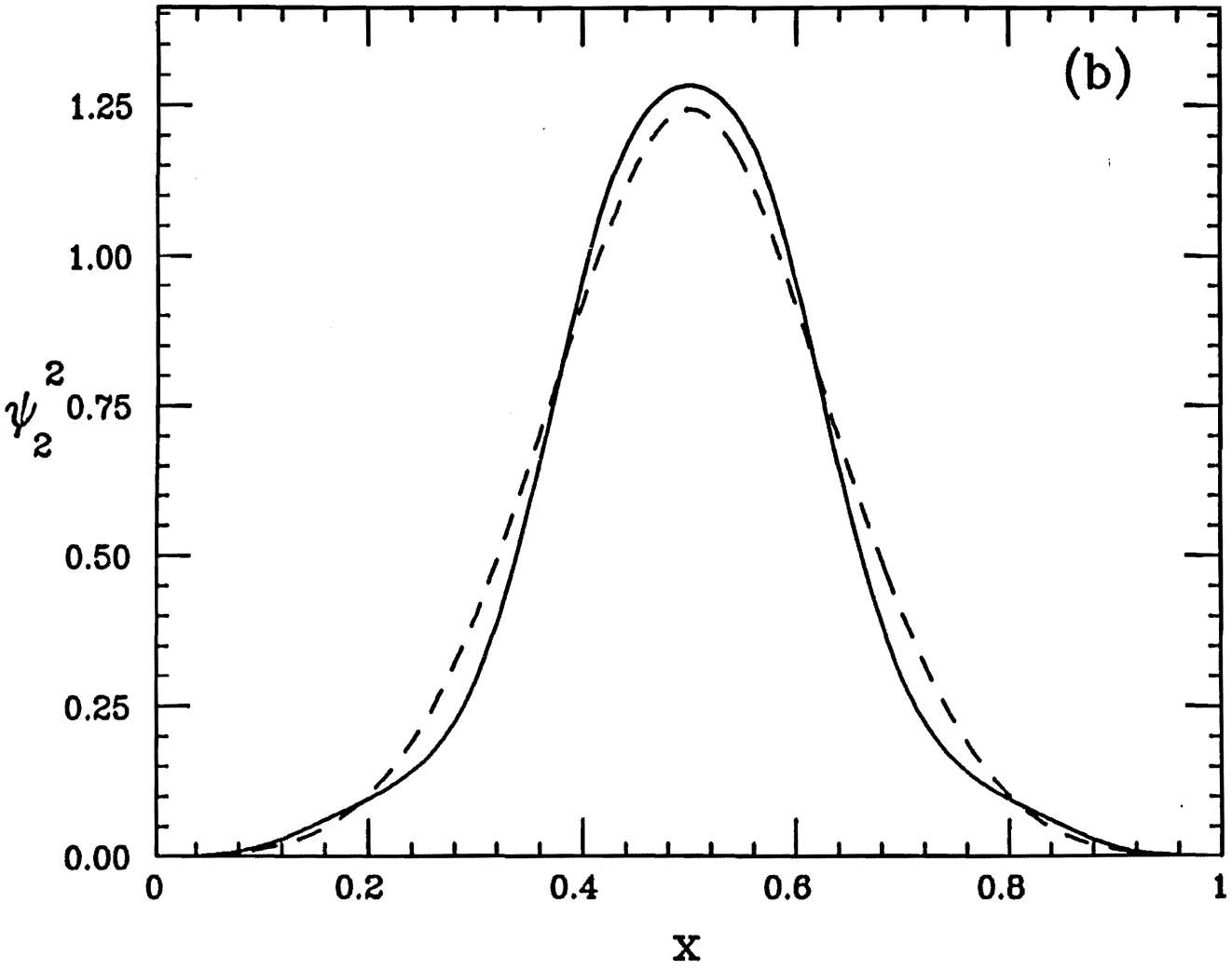

# Figure 12

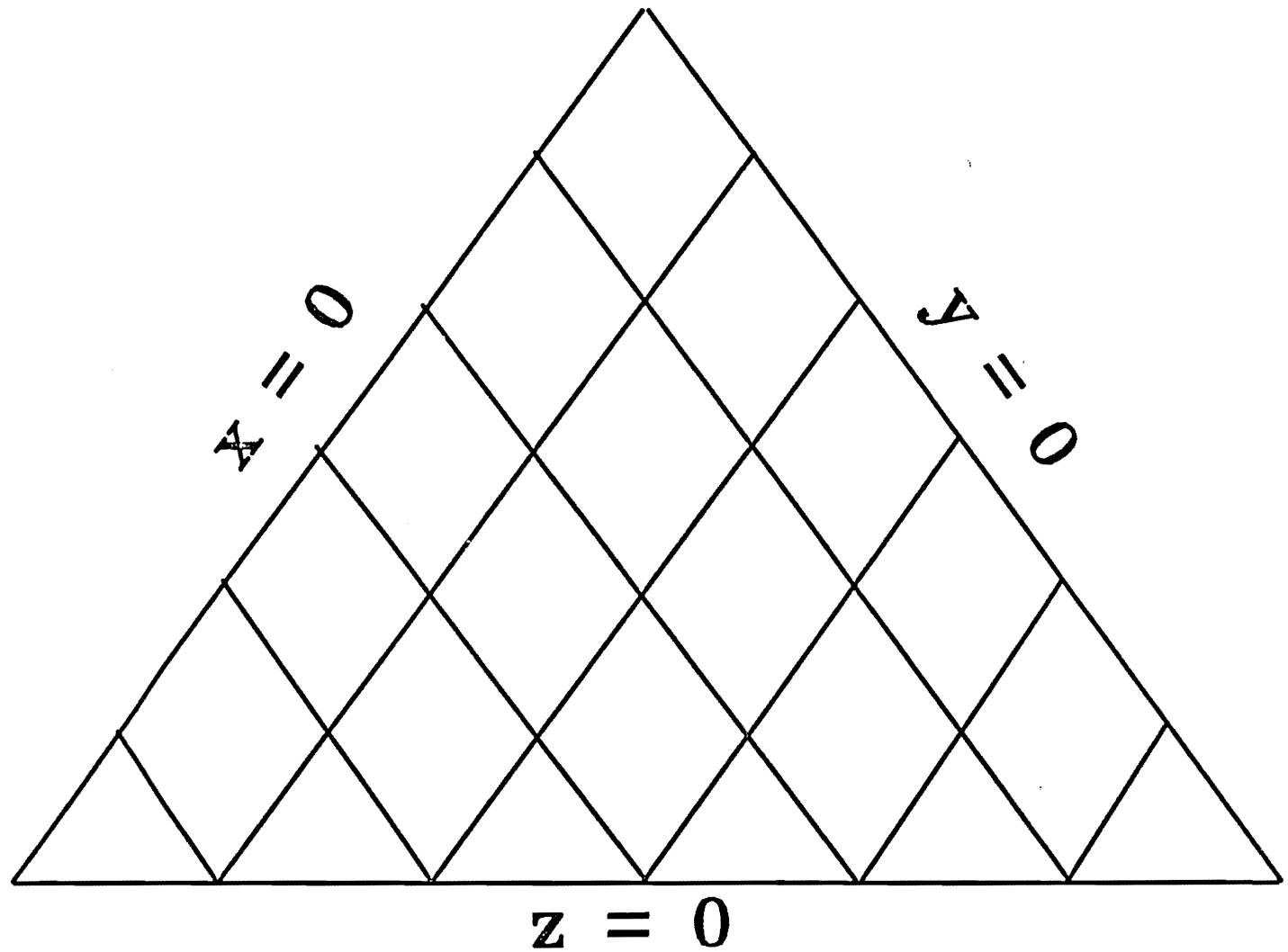

Figure 13a

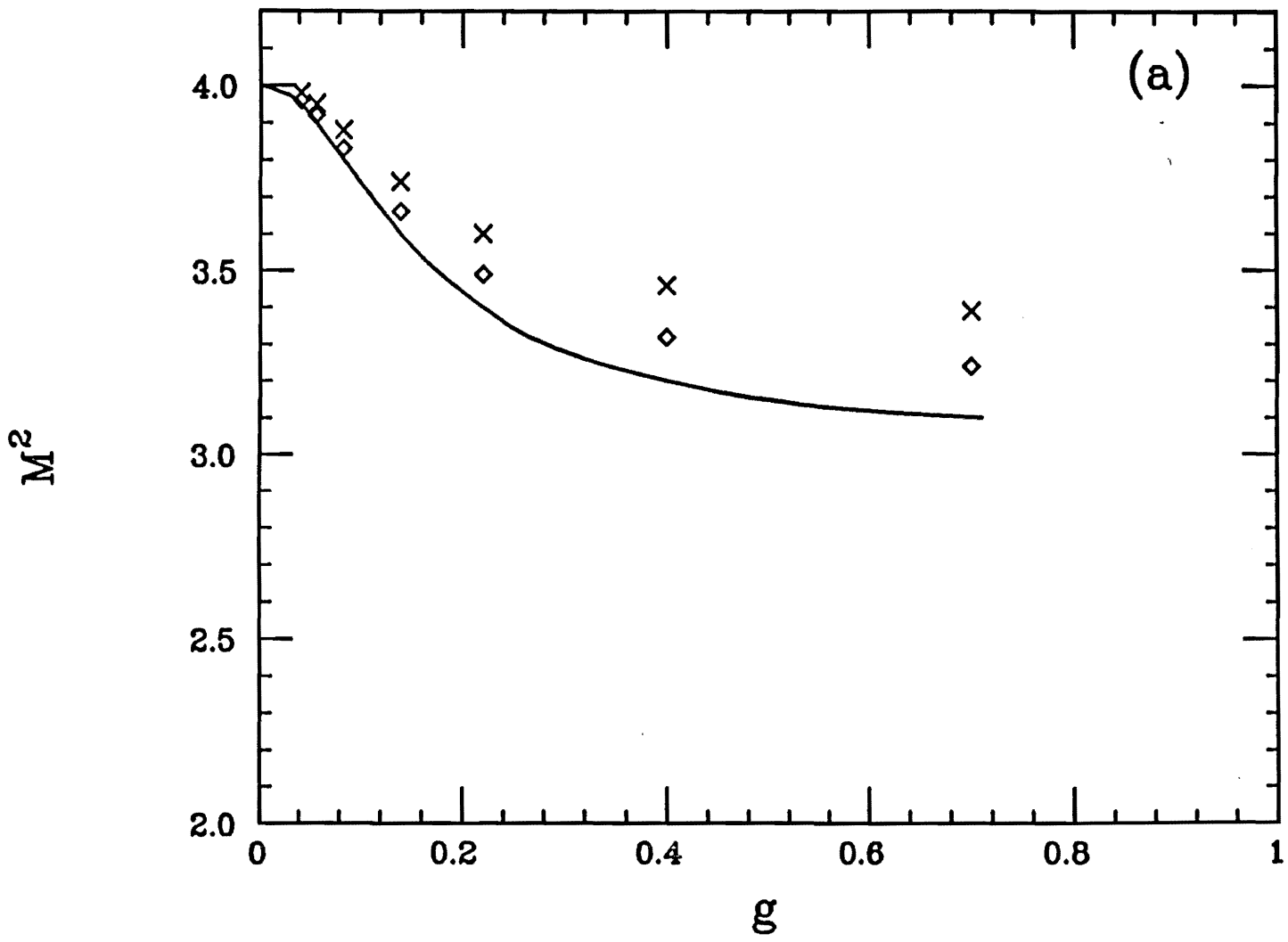

Figure 13b

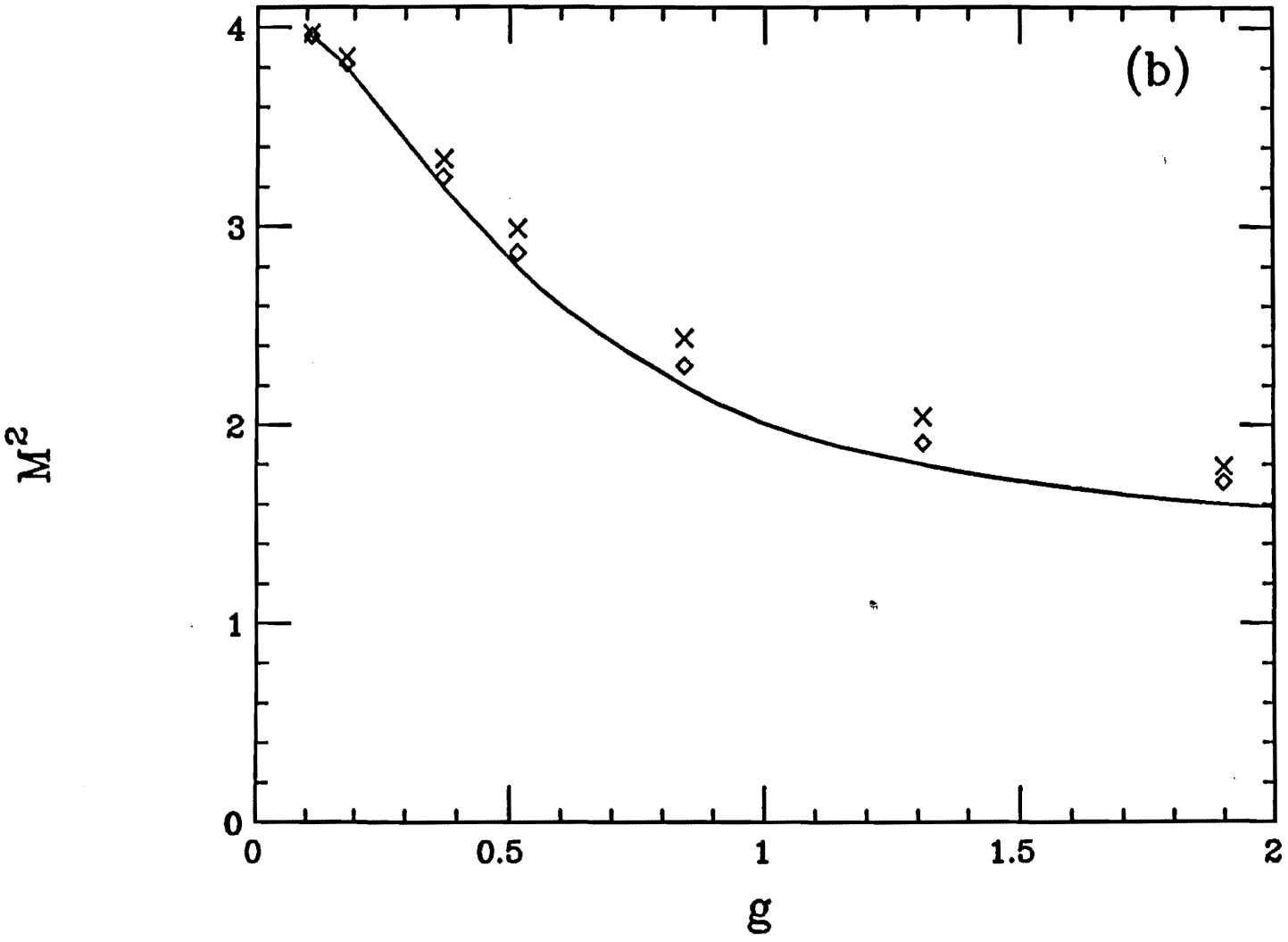

Figure 13c

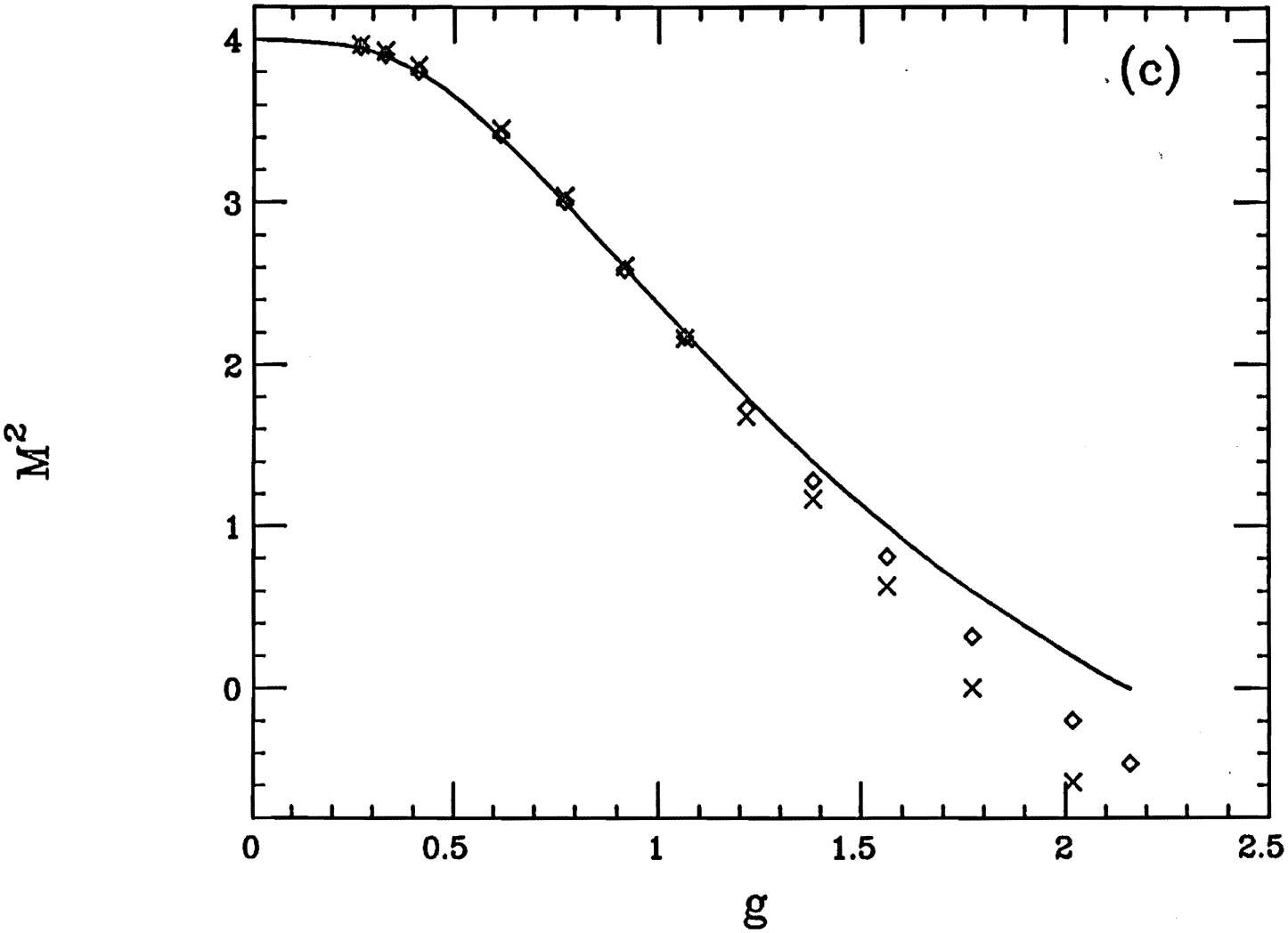

Figure 14a

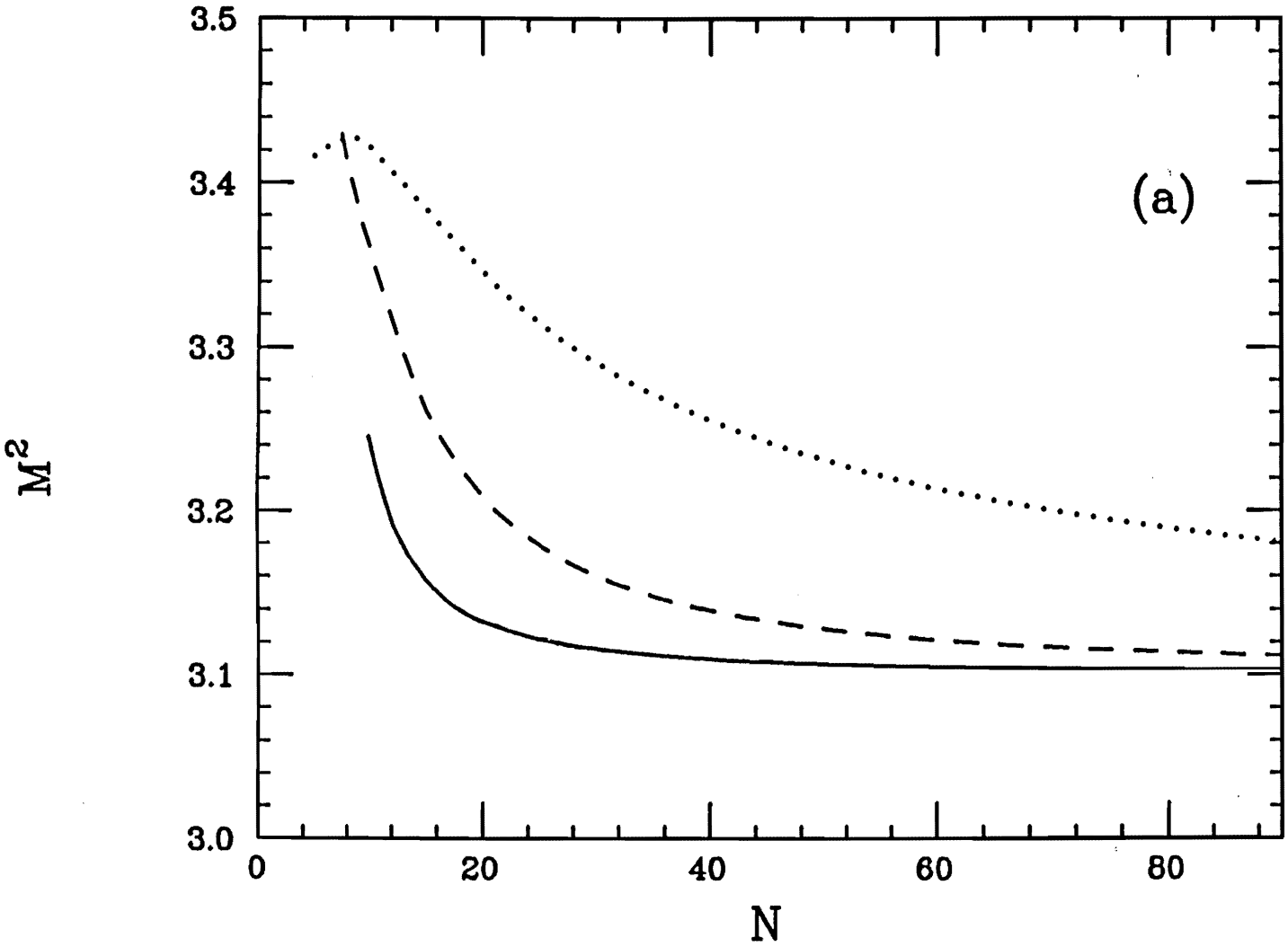

Figure 14b

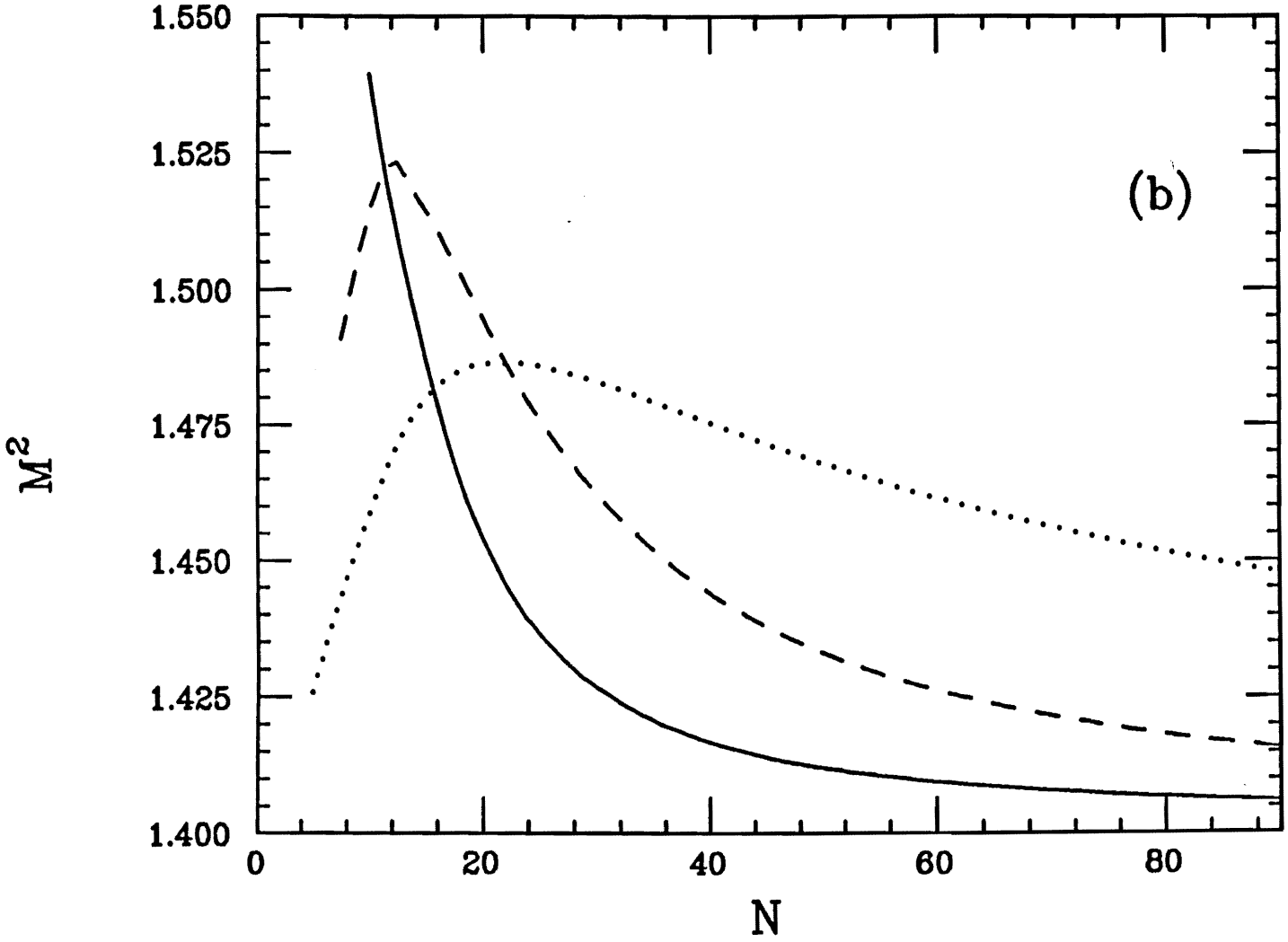

Figure 14c

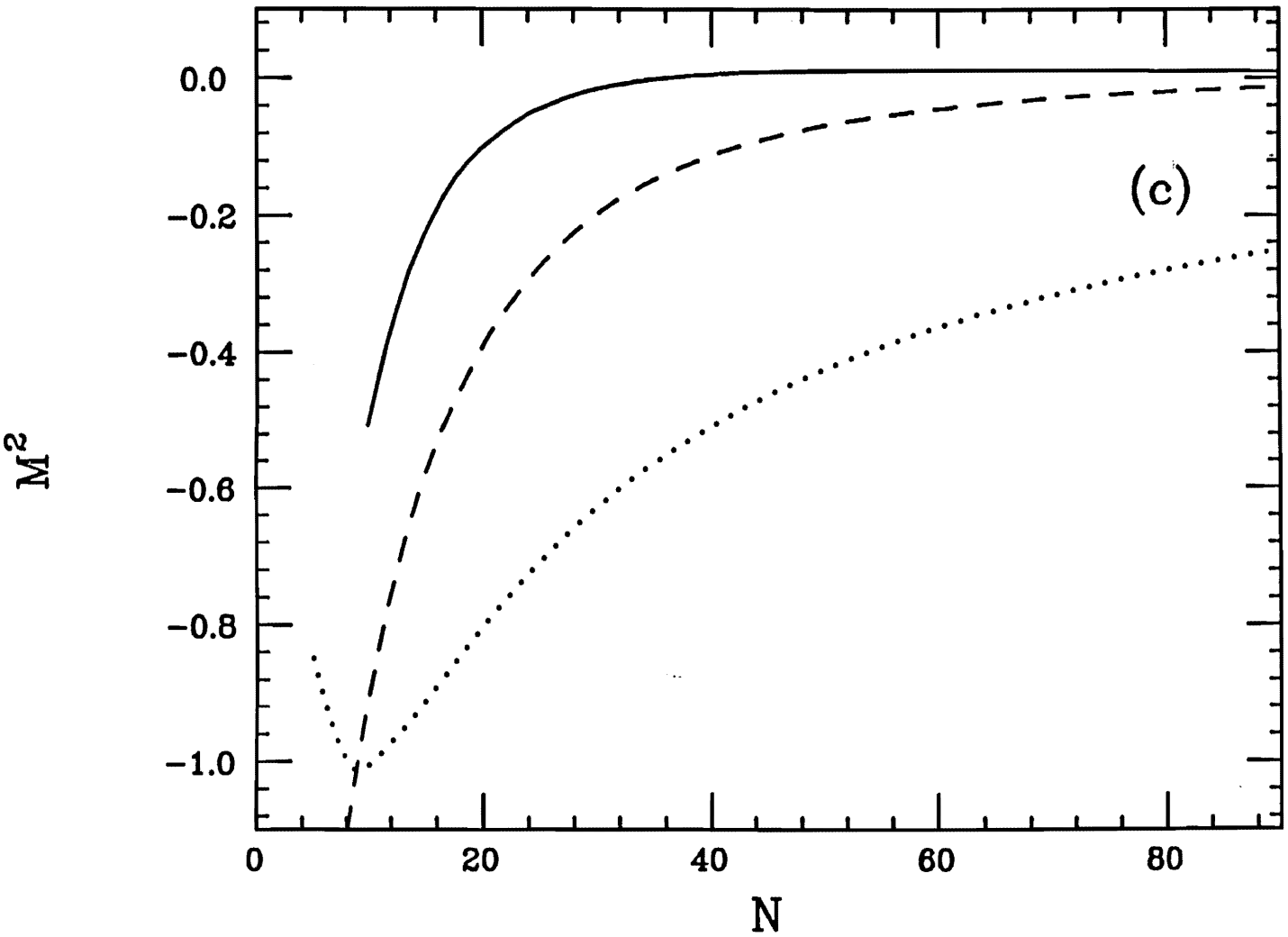

Figure 15a

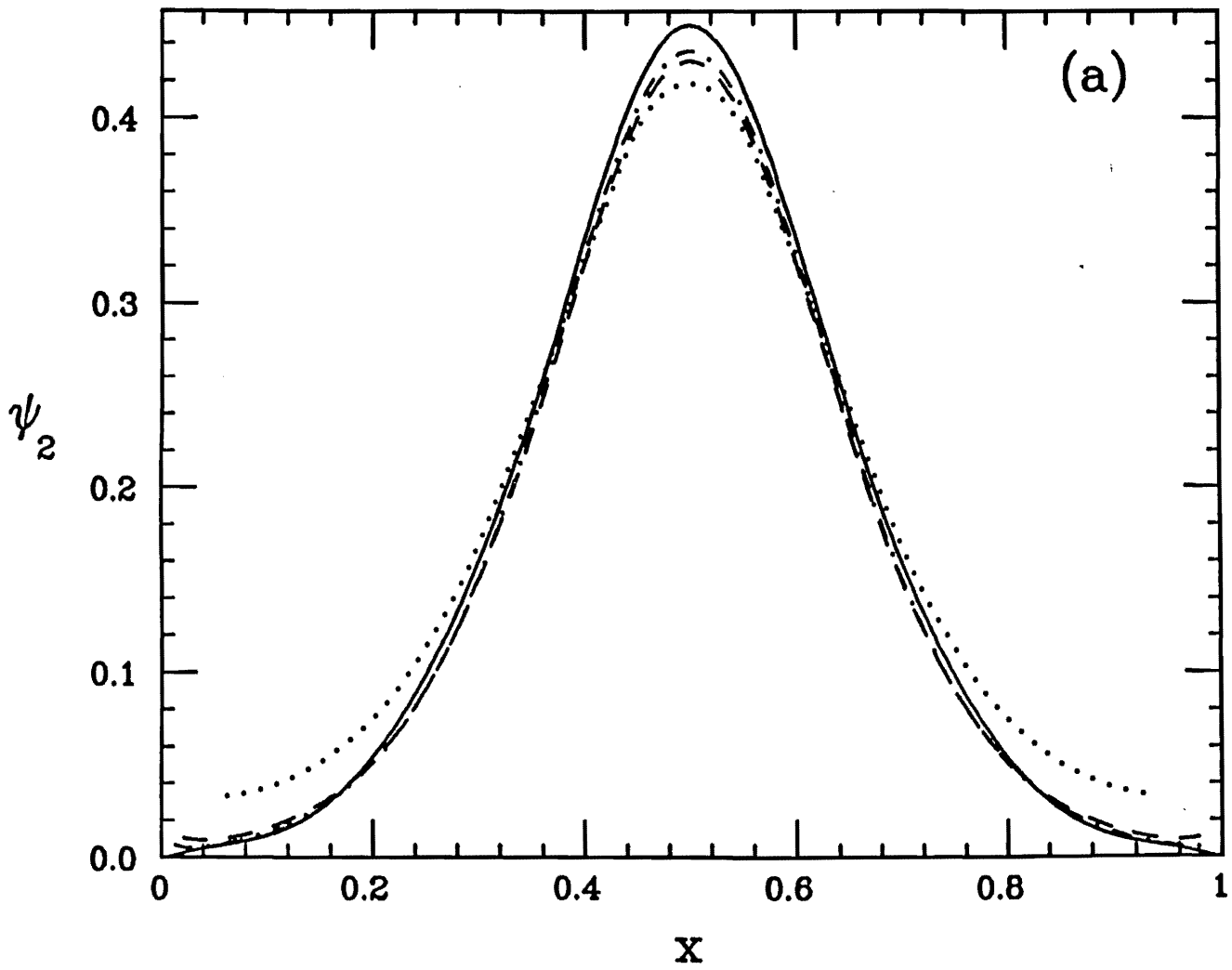

Figure 15b

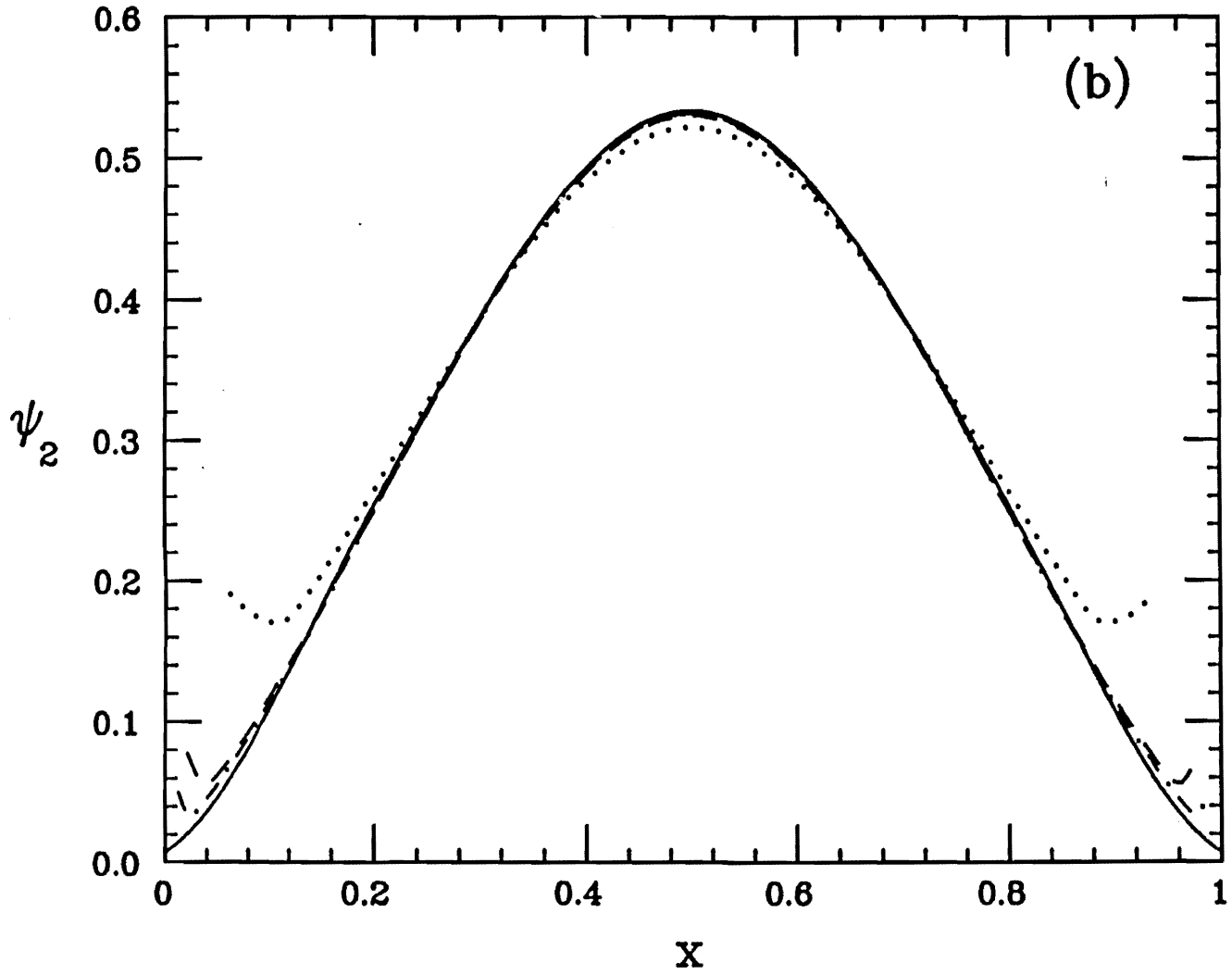

Figure 15c

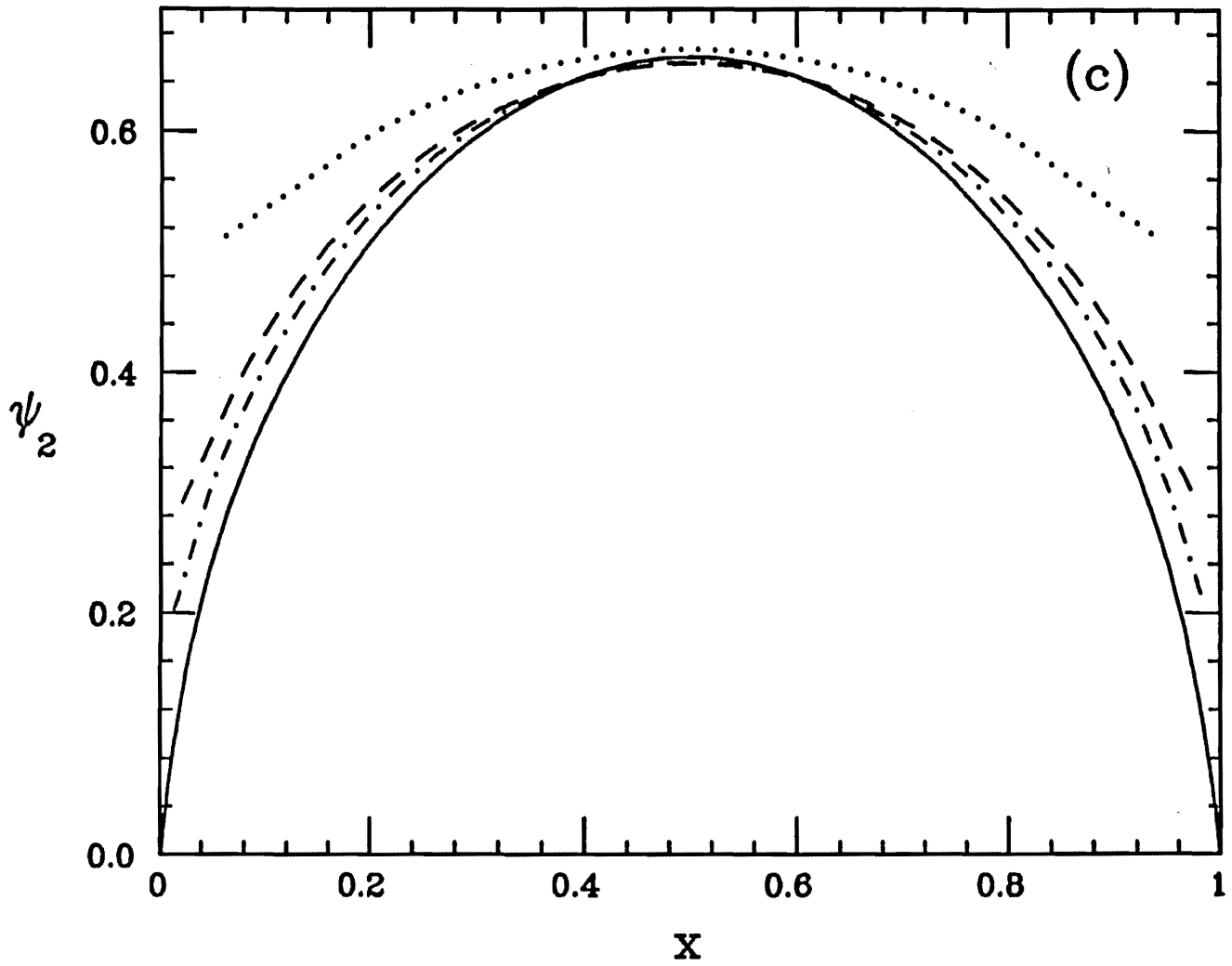

Figure 15d

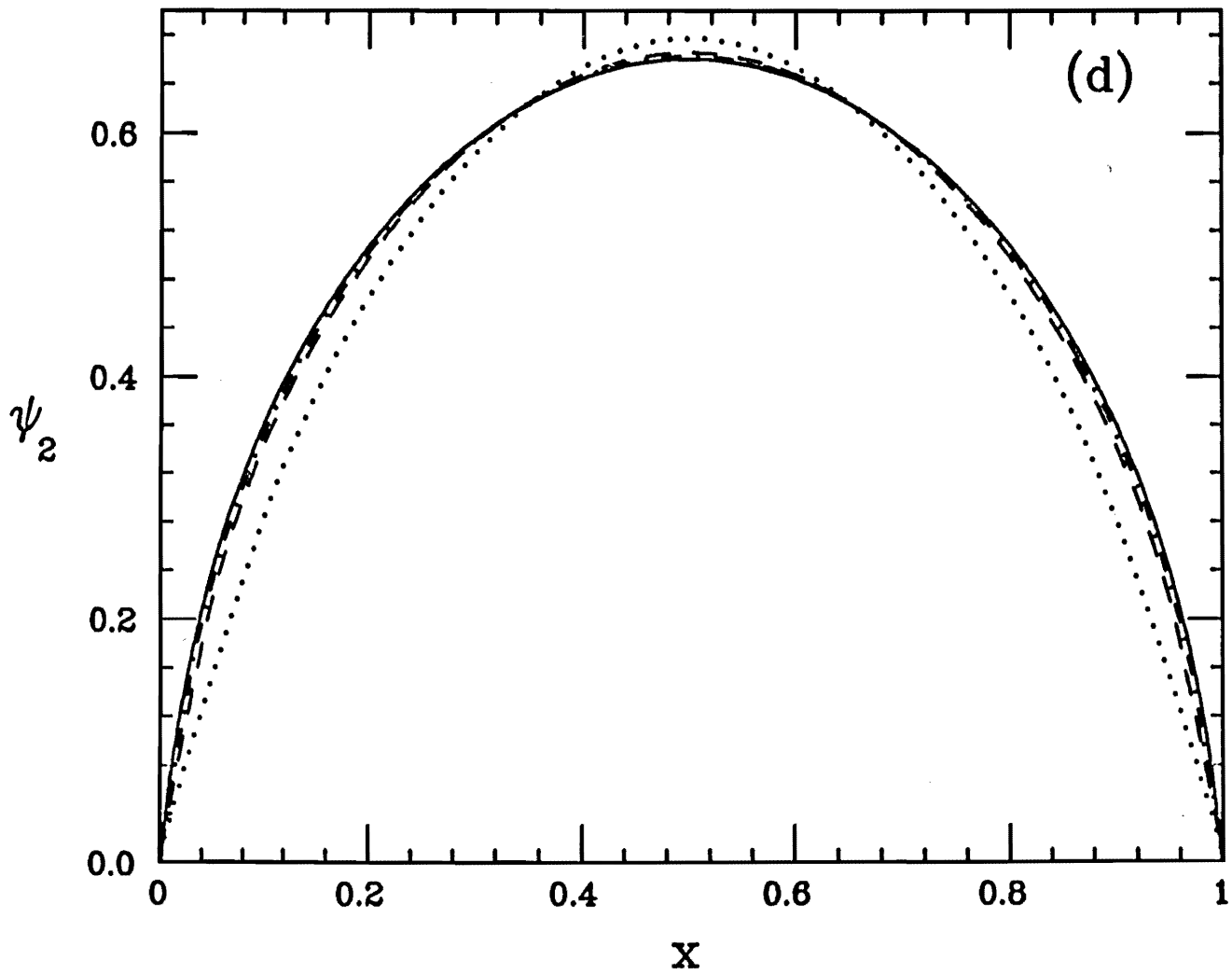

Figure 16a

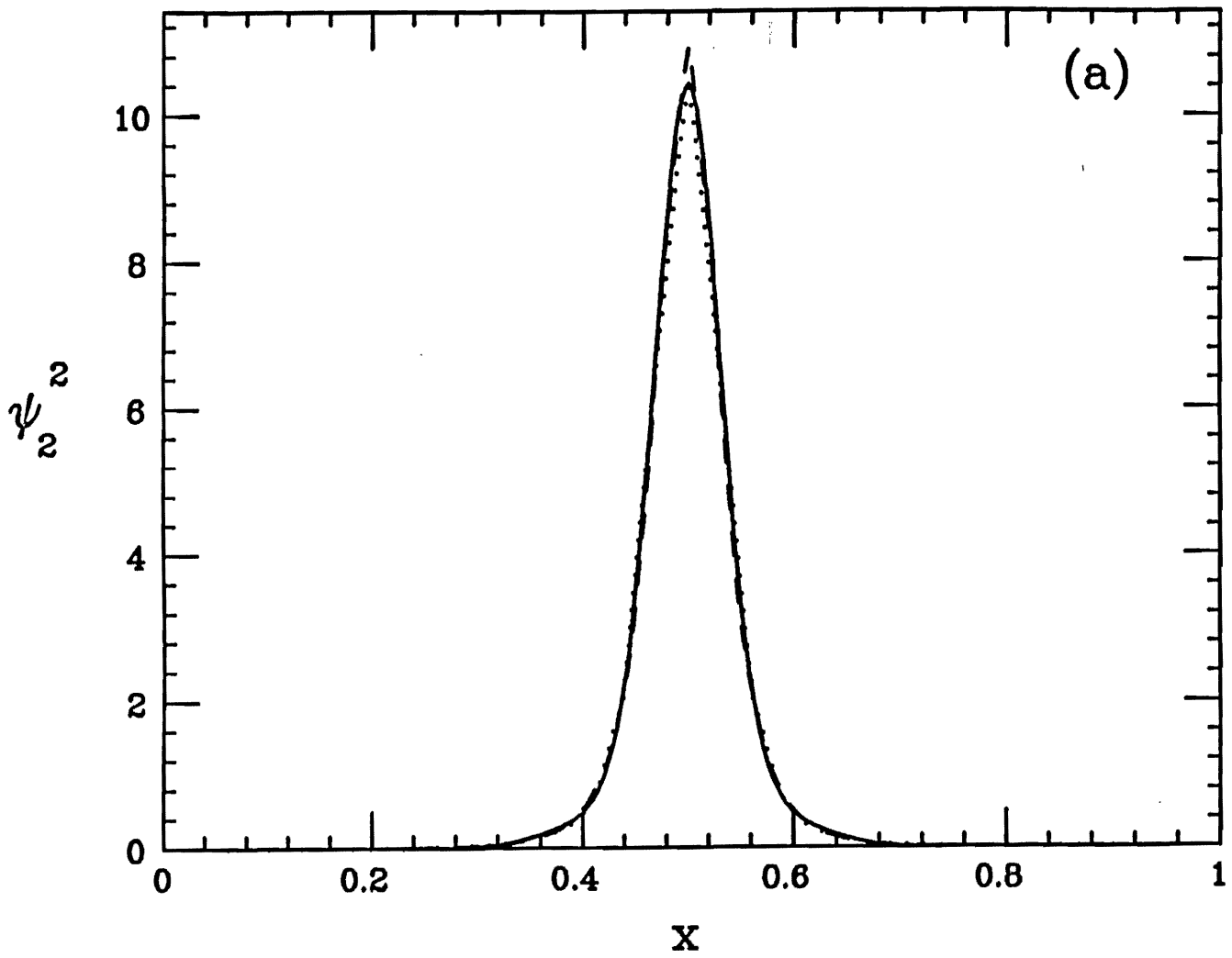
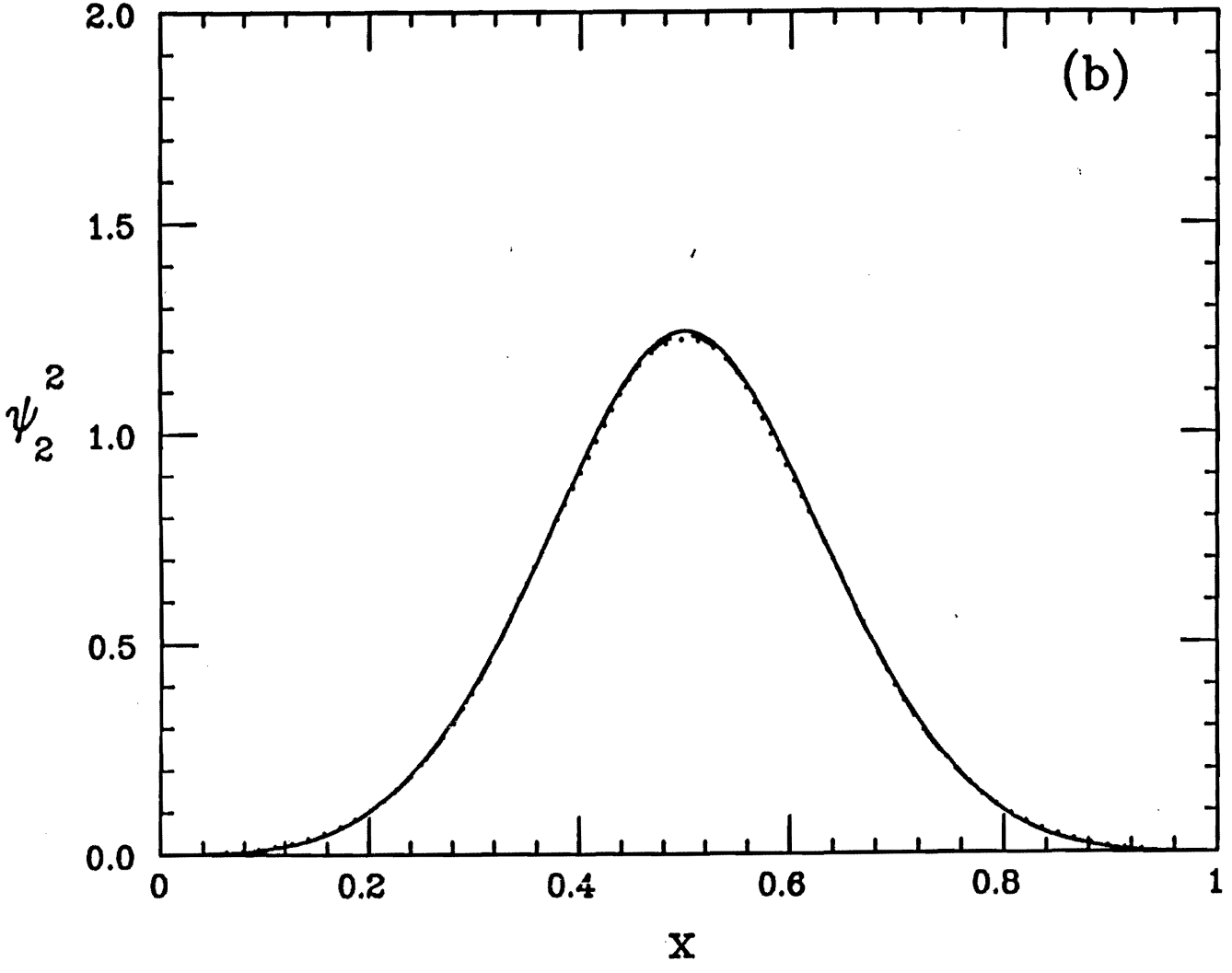
Figure 16b